DOI:10.15774/PPKE.ITK.2010.008

SELF-ORGANIZED CRITICALITY OF THE BRAIN: FRACTAL ANALYSIS OF THE HUMAN SLEEP EEG

Ph.D. dissertation

Béla Weiss

Supervisor:
Tamás Roska, D.Sc.
ordinary member of the Hungarian Academy of Sciences

Scientific advisers:
György Karmos, M.D., Ph.D.
emeritus professor
and
Zsuzsanna Vágó, Ph.D.
associate professor

Pázmány Péter Catholic University
Faculty of Information Technology
Interdisciplinary Technical Sciences Doctoral School

Budapest, 2010

DOI:10.15774/PPKE.ITK.2010.008

DOI:10.15774/PPKE.ITK.2010.008

To the memory of my Parents and Grandparents.

DOI:10.15774/PPKE.ITK.2010.008

DOI:10.15774/PPKE.ITK.2010.008

Acknowledgment

First and foremost, I would like to thank the consistent support of my supervisor and head of the doctoral school, *Prof. Tamás Roska*. The interdisciplinary environment that he provided turned out to be of a crucial importance for my research.

I would also like to express my gratitude to my advisers, *Prof. György Karmos* and *Zsuzsanna Vágó* for sharing their concerns and suggestions related to physiological and mathematical aspects of my work. I am indebted to *Prof. Ronald Tetzlaff* for his tutoring during my stay at the Institute of Applied Physics, Johann Wolfgang Goethe University in Frankfurt, Germany (IAP). During all these years my research was helped by *Prof. Péter Halász* and I appreciate this really much.

I am also thankful to my closest collaborators who contributed to my work. I am very grateful to *Zsófia Clemens* for all those discussions and her useful advices. I also acknowledge the contribution of *Róbert Bódizs*. Without the recordings acquired in his laboratory this research would not be possible. Although my work related to epilepsy did not become a part of the dissertation I thank the whole epilepsy monitoring and surgery team at the National Institute of Neuroscience. Special thanks go to *István Ulbert*, *Lóránd Erőss*, *László Entz, Rita Jakus* and *Dániel Fabó*.

I am also very grateful to my fellow PhD students, especially to *Éva Bankó*, *Csaba Benedek*, *Mária Ercsey-Ravasz*, *Gergely Feldhoffer*, *László Füredi*, *Gaurav Gandhi*, *András Kiss*, *Giovanni Pazienza*, *Tamás Pilissy*, *Gergely Soós*, *Ákos Tar*, *Róbert Tibold*, *Dávid Tisza*, *Gergely Treplán*, *József Vere*s and *Péter Vizi* for all their help, fruitful discussions and the time we spent together. I especially thank *György Cserey*, *Zoltán Fodróczi*, *Viktor Gál*, *Kristóf Iván*, *Kristóf Karacs*, *Attila Kis*, *András Oláh* and *Róbert Wagner* for their help at the beginning of my PhD studies.

I also say thank to all my colleagues at the IAP, but especially to *Denis Dzafic*, *Martin Eichler*, *Gunter Geis*, *Frank Gollas*, *Leonardo Nicolosi*, *Christian Niederhöfer* and *Hermine Reichau* for their friendship and help during my stay in Germany.

I acknowledge the kind help of *Anna Csókási*, *Lívia Adorján*, *Judit Tihanyi*, *Vida Tivadarné Katinka* and the personnel of the *Students' Office*, the *Dean's Office*, the *Warden's Office*, the *Financial Department*, the *IT Department*, the *Library*, the *Reception* and the *cleaning personnel*.

I thank all my friends for being so patient during my busy days.

DOI:10.15774/PPKE.ITK.2010.008

I am tremendously grateful to my *Parents* and *Grandparents* for all their love and support. Special thanks go to *Ómama* for her fostering and endless love and to my sister *Ági* and her family for their help during the toughest years.

Finally, I would like to thank my wife *Nóra* for her love, support, patient and understanding.

DOI:10.15774/PPKE.ITK.2010.008

TABLE OF CONTENTS

DOI:10.15774/PPKE.ITK.2010.008

DOI:10.15774/PPKE.ITK.2010.008

SUMMARY OF ABBREVIATIONS

Abbreviation	Concept
AN	adaptive neuro-fuzzy inference system
ANOVA	analysis of variance
ave	unweighted average distance (linkage method)
CCC	cophenet correlation coefficient
cen	centroid distance (linkage method)
che	Chebychev distance (similarity measure)
cit	city block metric (similarity measure)
CMS	selection of channel x measure features
com	furthest distance (linkage method)
cor	correlation distance (similarity measure)
cos	cosine distance (similarity measure)
CS	selection of channels considering a same measure
CVT	cross-validation time
DFA	detrended fluctuation analysis
ECG	electrocardiogram
EEG	electroencephalogram
EMG	electromyogram
EOG	electrooculogram
euc	Euclidean distance (similarity measure)
FF	feedforward neural network
FFT	fast Fourier transform
FST	feature selection time
IEEG	intracranial electroencephalogram
LD	linear discriminant analysis
LS	support vector machine with a linear kernel function
mah	Mahalanobis distance (similarity measure)
MANOVA	multivariate ANOVA
med	weighted center of mass distance (linkage method)

DOI:10.15774/PPKE.ITK.2010.008

min	Minkowski metric (similarity measure)
MLR	multiple linear regression
MS	selection of measures considering a same channel
NB	naïve Bayes classifier
OA	overall accuracy
PN	probabilistic neural network
PSM	power spectral measure
QD	quadratic discriminant analysis
RB	radial basis function neural network
RBP	relative band power
RS	support vector machine with a radial basis kernel function
seu	standardized Euclidean distance (similarity measure)
SFFS	sequential forward feature selection
sin	shortest distance (linkage method)
SO	slow oscillation
SOC	self-organized criticality
SVM	support vector machine
war	inner squared distance (linkage method)
wei	weighted average distance (linkage method)

DOI:10.15774/PPKE.ITK.2010.008

Chapter One

INTRODUCTION

1.1. Preface

Despite of the broad spectrum of electrophysiological and imaging methods available in the field of neurobiology still little is known about how exactly complex neural dynamics emerge. Hopefully, application of novel theoretical approaches and computational methods aimed for analysis and modeling of complex systems might provide a deeper insight into physiological and pathological mechanisms of the brain.

With advent of relatively cheap and high performance personal computers sophisticated and computation demanding time series analysis methods became available to a broad brain research community. Application of chaos theory and non-linear time series methods gave a deeper insight into brain dynamics reflected by EEG signals. For a comprehensive recent review on non-linear analysis of EEG I refer to [16]. This approach relies on a transition from the time domain to the phase space and generation of trajectories for EEG time series using different embedding techniques. Inferences about brain dynamics were drawn by estimating different characteristics of trajectory attractors using measures such as the correlation dimension D_2, the fractal dimension D_f, the largest Lyapunov exponent L_1, etc. Early results were promising and suggested a deterministic nature of brain dynamics with a rather low-dimensional chaotic behavior in physiological and pathological conditions that could not be revealed using simple linear methods such as the power spectral analyses. Filtered noise, however, can mimic the signatures of deterministic chaos [17]. This latter finding necessitated a revision of results obtained by non-linear techniques. Surrogate data analyses [18] did not entirely support early results on the low-dimensional chaotic behavior of the brain. This was in agreement with the finding that the relatively high complexity of the EEG signals does not allow a reliable dissociation of its waxing and waning oscillations exceeding 2-15 s from that of the filtered white noise [19-21]. As a consequence alternative approaches were developed including novel non-linear and stochastic time series analysis methods.

Unlike deterministic approaches aimed at finding low-dimensional chaos, the self-organized criticality (SOC) framework allows for describing the high-dimensional character of the dynamics and the presence of stochastic effects [22]. SOC is a

DOI:10.15774/PPKE.ITK.2010.008

phenomenon characterizing systems that might arrive at a critical state (phase transition) without any tuning of a specific parameter [23]. The proof of presence of SOC requires a demonstration of spatio-temporal long-range correlations and power-law scale-free (also called self-similar or fractal) fluctuations [24]. Scale-free behavior means that no characteristic scales dominate the dynamics of the underlying processes. It also reflects a tendency of complex systems to develop correlations that decay more slowly and extend over larger distances in time and space than the mechanisms of the underlying processes would suggest [24-26]. The long-range correlations build up through local interactions until they extend throughout the entire system. After this stage, the dynamics of the system exhibit power-law scaling behavior and the underlying process operates in a critical state [23, 27].

Several features of neural networks are consistent with SOC, such as a large number of elements (neurons) interacting with each other in a nonlinear way (e.g. presence of threshold for spiking), a possibility to change and save connectivity between the elements (e.g. via synaptic plasticity), absence of any special parameter tuning, and spatio-temporal dynamics obeying power-law statistics [22, 28]. A critical state is a regime of a system where opposing forces are balanced. In the nervous system such a balance might be represented by the relationship between excitation and inhibition, which is known to be important for the transfer of information [29] and for the sustained neuronal activity [30]. Neural network simulations demonstrated that the presence of long-range spatio-temporal correlations is beneficial for the optimal transfer of information since these correlations represent an optimal compromise between high susceptibility to perturbations and stability in the system [31, 32].

All these properties of the brain suggest that the SOC paradigm might be an appropriate tool to investigate and model of neural activities. In line with this fractal geometry of brain structures [33, 34] as well as power-law spatio-temporal properties of neuronal activities have been revealed. Although the spatial power spectral density (PSDx) of scalp EEG recordings might deviate from the ideal power-law scale-free behavior [35], the PSDx of epipial EEG conforms to it [36]. Temporal long-range correlations were observed at different levels of the brain electrical activity hierarchy in different species and during different conditions. For example, Lowen et al. revealed that the individual ion channel currents show long-term correlation and possess fractal properties [37]. Considering spike trains in extracellular recordings, long-term correlations were found among interspike intervals of the medullary sympathetic neurons in cats [38]. Spasic et

al. showed that the fractal dimension of local field potentials of anaesthetized rats changes significantly after unilateral discrete injury [39]. Fractal exponent of EEG activity in the Gallotia galloti lizard decreased with the increment of temperature from 25 °C to 35 °C [40].

1.2. Motivation and aims

Overall, the motivation of my research is two-fold and the work that I have done may be related to different general steps of brain research (Figure 1.1). From the theoretical point of view I am interested in how complex neural dynamics emerge across different scales and how are these dynamics related to different physiological and pathological mechanisms that thoroughly affect the information sensation, processing, storage and retrieval of the brain. On the other hand, I am interested in practical aspects of brain research as well. Namely, as an engineer I am also motivated to reveal how biologically-inspired information processing models can be transferred into technical applications, including the control of the brain itself. At the confluence of my general research interests I found the investigation of vigilance level and epilepsy to be of a crucial importance given the well-known influence of these basic mechanisms on the information processing properties of the brain. Thus, I devoted my PhD student years to explore the capability of the SOC paradigm to describe the information processing properties of the brain by fractal analyses of physiological sleep and epileptic neural activities. However, due to the size limitations of the dissertation and the difficulties related to the analyses of epileptic activities I will here concentrate on presentation of my results related to fractal analysis of the human sleep EEG only. To draw inferences about fractal properties of the brain activity I assessed topographic and sleep stage-wise distribution of monofractal and multifractal EEG features and the relation of these measures with power spectral properties. With a more practical motivation in the background I assessed whether a combination of fractal and power spectral EEG features

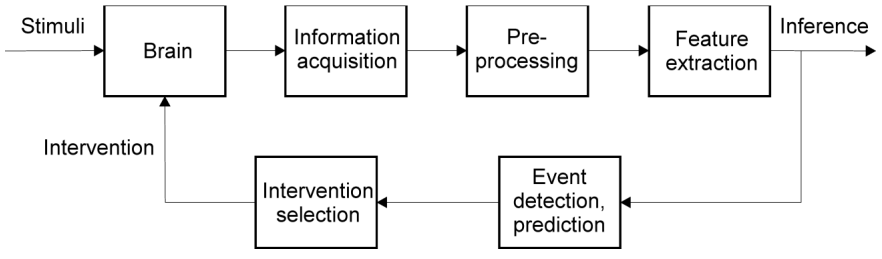

Figure 1.1. A possible process diagram of brain analyses and intervention.

DOI:10.15774/PPKE.ITK.2010.008

might improve the classification of the vigilance state.

1.3. Framework of the dissertation

In Chapter 2, a general description of materials and methods that have been used during the investigations is provided. Methods related to specific parts of the research will be provided in the corresponding chapters.

In Chapter 3, topographic and sleep stage-wise distribution of monofractal and multifractal sleep EEG measures and their relation to power spectral measures are assessed.

In Chapter 4, sleep stage discrimination capability of fractal and power spectral measures of EEG signals recorded at different topographic locations was analyzed with a special regard to combination of different features.

Conclusions are given in Chapter 5.

Summary of the new scientific results in form of thesis and delineation of possible applications can be found in Chapter 6.

Chapter 7 contains appendices.

1.3.1. General notes

From now on (except of Chapter 6) I will use “We/we” instead of “I” since most of the research was carried out in collaboration.
Although the notations used within a single chapter are unique, the same symbol may denote diverse quantities in two different chapters.

DOI:10.15774/PPKE.ITK.2010.008

Chapter Two

MATERIALS AND METHODS

2.1. Subjects and EEG recordings

Twenty-two healthy subjects with no sleep disturbances, free of drugs and medications as assessed by an interview and questionnaires on sleeping habits and health participated in the study (age: 17–55 years, mean±S.D.: 31±9 years, 11 males and 11 females). The study was approved by the ethical committee of the Semmelweis University and subjects gave written informed consent to participation. Sleep was recorded in the sleep laboratory for two consecutive nights. The present study was based on the second night. The timing of lights off was determined by the subjects, and morning awakenings were spontaneous. On average subjects spent 462.39±69.01 (mean±S.D.) minutes in sleep. Sleep was recorded by standard polysomnography, including electroencephalography (Fp1, Fp2, F3, F4, Fz, F7, F8, C3, C4, Cz, P3, P4, T3, T4, T5, T6, O1 and O2 electrodes), electrooculography (EOG), bipolar submental electromyography (EMG) and electrocardiography (ECG). EEG electrodes were referenced to the contralateral mastoid. Midline EEG electrodes were referenced to the right mastoid. Impedance of the EEG electrodes was kept below 5 kΩ. Signals were collected, pre-filtered, amplified and digitized at a sampling rate of $f_s = 249$ Hz using the 30 channel Flat Style SLEEP La Mont Headbox with implemented second order filters at 0.5 Hz (high pass) and 70 Hz (low pass) as well as the HBX32-SLP 32 channel preamplifier (La Mont Medical Inc., USA). Additionally, a 50 Hz digital notch filtering was performed by means of the DataLab acquisition software (Medcare, Iceland).

2.2. EEG processing

Pre-processing and feature estimation were accomplished in a self-developed EEG visualization and processing toolbox under Matlab2009b (MathWorks, Natick, MA, USA). This toolbox is freely available under GNU license upon request [41]. Calculations were performed on different hardware configurations and operating systems. Computation times presented later stand for the following configuration: Linux operating system; Intel Xeon 64 bit 3 GHz CPU with 8 cores, 2 MB cache memory; 2

DOI:10.15774/PPKE.ITK.2010.008

GB RAM memory. Statistical analyses were performed using STATISTICA (StatSoft, Inc., Tulsa, OK, USA) and Matlab2009b.

2.2.1. Pre-processing

Although hardware filtering had been applied during EEG recording, some artifacts remained. Thus, we first performed software filtering on the raw EEG recordings with Butterworth IIR filters (eight order 0.3 Hz-70 Hz band-pass and 50 Hz notch with a quality factor $Q = 45$). To avoid phase distortion, we used the built-in *filtfilt()* function of the Matlab for zero-phase digital filtering.

For all subjects a hypnogram was prepared according to the Rechtschaffen and Kales standard [15] using 20 s long epochs. To compare the analyzed EEG features during different sleep stages 90 epochs of 20 s length were selected from sleep stages NREM2, NREM4 and REM (30 minutes/stage) for all subjects. Selection included segments without artifact contamination only.

2.2.2. Fractal analysis

Monofractal and multifractal properties of the selected EEG epochs were evaluated by estimation of the self-similarity parameter H (also called Hurst exponent or Hurst parameter) [42, 43] and the range of fractal spectra (ΔD) [44], respectively. To estimate H, we applied the rescaled adjusted range based approach, while ΔD was approximated by estimation of generalized dimensions spectra. The brief description of the applied methods can be found in the following subsections.

2.2.2.1. Estimation of the Hurst exponent

The stochastic process $X(t)$ with continuous parameter t is self-similar with the self-similarity parameter H if the distribution of the rescaled process $c^{-H}X(ct)$ is the same as the distribution of $X(t)$, where $c > 0$ is arbitrary [43]. H is widely used to assess monofractality, scale-free properties and the degree of long-range temporal correlations of time series. When $0 < H < 0.5$, an increase in the process is more probably followed by a decrease (anti-persistence) and vice-versa, the process is considered to have short-range dependence. If $H = 0.5$, observations of the process are uncorrelated. When $0.5 < H < 1$, an increase in the process is more probably followed by an increase and a

DOI:10.15774/PPKE.ITK.2010.008

decrease is more probably followed by a decrease (persistence), the process is considered to have long-range dependence [42, 43, 45-47].

Basically two kinds of homogenous self-similar signals exist: fractional Gaussian noises (fGn) and fractional Brownian motions (fBm). fGn processes are considered to be stationary with a constant mean value and constant variance over time, while fBm's exhibit non-stationary property with a time-dependent variance. fGn and fBm signals are interconvertible. Taking the differences between neighboring elements of an fBm time series one might create an fGn signal, while by cumulative summation of fGn elements one can generate a motion process. The corresponding fBm and fGn signals are characterized by the same H. Self-similarity of a time series is also reflected in their power spectrum. The power versus frequency relationship is given by $P(f) \propto f^{-\kappa}$, where κ is called spectral or fractal exponent. Depending on the type of a fractal signal the relationship between H and κ is given by $H = (\kappa+1)/2,\ -1 < \kappa < 1$ for fGn and $H = (\kappa-1)/2,\ 1 < \kappa < 3$ for fBm. Similarly, H is linearly related to the detrended fluctuation analysis (DFA) exponent λ [48, 49] as $H = \lambda$ for fGn signals and $H = \lambda - 1$ in case of fBm processes. Additionally, the Hurst exponent is also related to the widely used fractal dimension as $H = 2 - D_f$ for fBm time series [50, 51]. Although many approaches are available for the estimation of H none of these can be generally considered as an ideal one because of differences of fGn and fBm signals [50, 52-54] and doubts related to the estimation of non-linear parameters from time series of finite length [47, 55-59]. For the estimation of H we used the rescaled adjusted range or R/S statistics based method [42, 43, 45]. We implemented this method keeping in mind the stationarity properties of the analyzed EEG segments and the fact that this method is applicable to stationary fGn processes or to differenced fBm signals only.

Here we provide a short description of this approach. Let $X(n)$ be a discrete time series. The partial sum process is defined as

$$Y(n) = \sum_{i=1}^{n} X(i), \qquad n \in \mathbb{N}. \tag{2.1}$$

The sample variance of the process X can be obtained using

$$S^2(n) = \frac{1}{n} \sum_{i=1}^{n} \left(X(i) - \frac{1}{n} Y(n) \right)^2. \tag{2.2}$$

DOI:10.15774/PPKE.ITK.2010.008

The adjusted range is given by

$$R(n) = \max_{1 \le i \le n} \Delta(i) - \min_{1 \le i \le n} \Delta(i), \tag{2.3}$$

where

$$\Delta(i) = Y(i) - \frac{i}{n} Y(n). \tag{2.4}$$

The R/S statistics or the rescaled adjusted range is defined by

$$R/S(n) = R(n)/S(n). \tag{2.5}$$

In [43] it was proven that for self-similar processes the expected value of $R/S(n)$ is proportional to n^H, i.e.

$$E[R/S(n)] \sim \mathrm{C_H} n^H, \tag{2.6}$$

as $n \to \infty$, where C_H is a positive constant and H is the self-similarity parameter of the process. Using this power-law relationship the Hurst exponent can be estimated by:

$$H \sim \log(E[R/S(n)])/\log(n). \tag{2.7}$$

To estimate H, the N sample point long data segments ($N = 20 * 249 = 4980$) were subdivided into K blocks ($K = 20$). Blocks of length N/K corresponded to duration of 1 second. $R/S(n)$ was computed starting at points $k_l = lN/K + 1$, $l = 0,1,...,K-1$. These values can be denoted by $R(k_l, n)/S(k_l, n)$. Overlapping of blocks was avoided, the upper boundary, i.e., the high cut-off point ($hcf = 249$) of n was limited to N/K. This resulted K different estimates of $R(n)/S(n)$ for each value of lag n. By plotting $\log[R(k_l, n)/S(k_l, n)]$ versus $\log(n)$ we got the so-called pox plot for the R/S statistics. H can be estimated by fitting a straight line to the points in this plot. H is equal to the slope of the fitted line. Pox plots for 20s long representative brain electrical activities recorded from subject #16 (channel Cz) during sleep stages NREM4, NREM2 and REM can be seen in Figure 2.1. Due to the transient zone at the low end of the plot we set a low cut-off point as well. The low cut-off point ($lcf = 50$) was ~20% of N/K. Thus, we used only values of n that lie between the low and high cut-off points to estimate H. This range of n ($lcf \sim 0.2\ s$, $hcf \sim 1\ s$) was in agreement with the scaling range [0.2 s 1 s] used for estimation of DFA λ-exponents in [60]. Hereby our estimations

DOI:10.15774/PPKE.ITK.2010.008

were not influenced by the frequency cut-offs of the applied 0.3Hz-70Hz or $(3.333s)^{-1}$-$(0.014s)^{-1}$ band-pass filter. The computation of a single *H* value took about 1.8 s with these particular settings.

2.2.2.2. Estimation of multifractal spectra

Homogenous self-similar time series can be described by a single scale-free exponent. These signals are also called monofractal time series. Additionally, heterogeneous multifractal time series showing self-similarity only in local ranges of the structure also exist. Their scale-free property varies in time. Hence they should be decomposed into many sub-sets and characterized by different exponents. This can be carried out by estimation of fractal spectra. Using the Alfréd Rényi's generalized entropy, a continuous spectrum of generalized dimensions (also called Rényi dimensions or fractal spectrum)

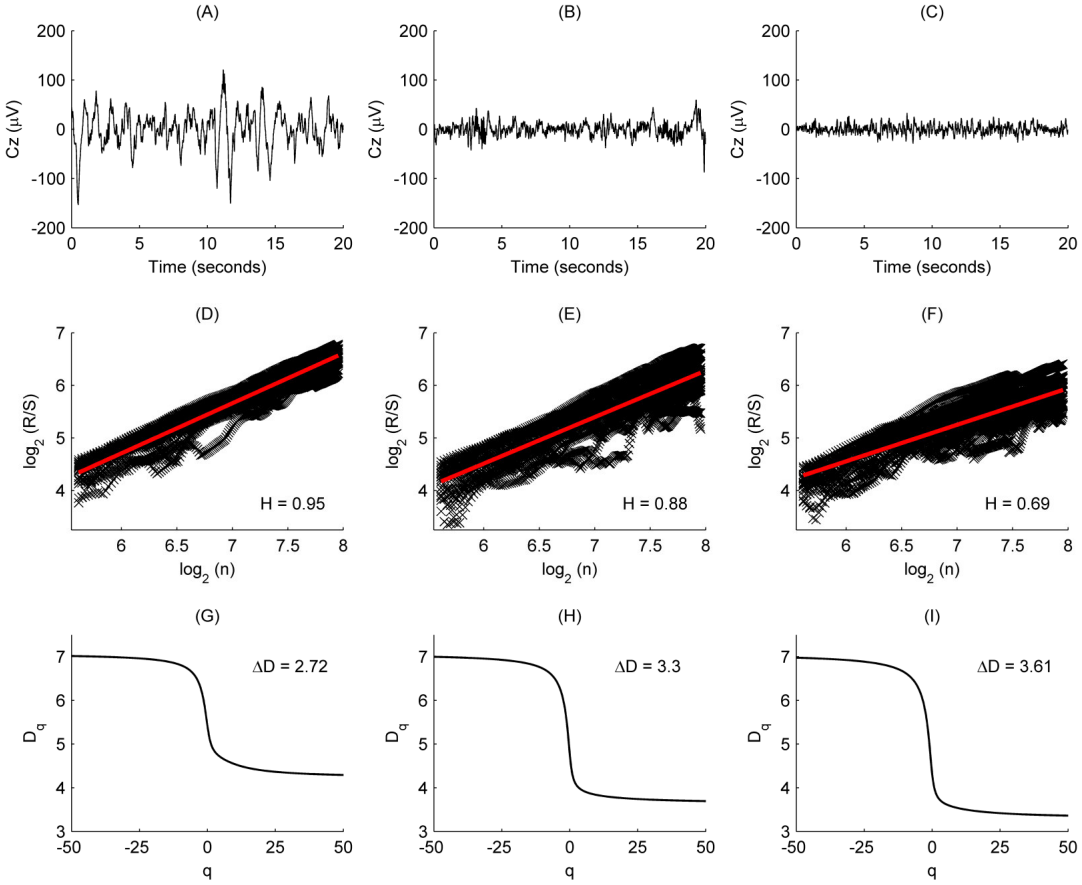

Figure 2.1. (A-C) Examples of EEG segments recorded from subject #16 during sleep stages NREM4 (A), NREM2 (B) and REM (C). (D-F) Pox plots of the R/S statistics and the estimated H values for the EEG segments presented in the top row (D: NREM4; E: NREM2; F: REM). (G-I) Generalized dimension spectra and the estimated ΔD values for the EEG segments presented in the top row (G: NREM4; H: NREM2; I: REM).

DOI:10.15774/PPKE.ITK.2010.008

D_q can be defined, where $-\infty \le q \le \infty$ [61]. A common method for estimation of fractal spectra is the box-counting technique. In this study we applied a box-counting approach that is based on estimation of the moments of signal amplitude distribution and was also used in [44]. One reason for choosing this method is that a previous study [62] revealed a promising sleep stage classification performance based on the entropy of amplitudes (ENA), a measure that is closely related to the amplitude distribution of time series. In our case D_q is defined as follows:

$$D_q = \lim_{\delta V \to 0} \frac{\log\left[\chi(q, \delta V)\right]}{(q-1)\log \delta V}, \; q \neq 1. \tag{2.8}$$

δV is the bin width or box length (set to 0.3μV in this case based on the conversion range and the resolution of the analogue to digital converter). The partition function can be obtained using

$$\chi(q, \delta V) = \sum_{i=1}^{b(\delta V)} \chi_i(q, \delta V), \tag{2.9}$$

where $b(\delta V)$ denotes the number of non-overlapping bins

$$b(\delta V) = \frac{V_{\max} - V_{\min}}{\delta V}. \tag{2.10}$$

$V_{\max}$ and $V_{\min}$ are the maximum and minimum values of EEG signals recorded during measurements, respectively. $\chi_i(q, \delta V) = p_i^q$ is a weighted measure that represents the percentage of EEG values that falls into the *i*th bin, and *q* is the moment or weight of the measure. If n_i is the number of EEG values in the *i*th bin and *N* is the total number of the samples, than the probability that the signal falls into the *i*th bin of length δV is:

$$p_i = \frac{n_i}{N}. \tag{2.11}$$

Some of the D_q values are known under different names and widely used in the field of time series analysis. D_0 is the Hausdorff-Besicovitch or fractal dimension. For $q = 1$ one should use

$$D_1 = \lim_{\delta V \to 0} \frac{-\sum_{i=1}^{b(\delta V)} p_i \log p_i}{\log(1/\delta V)}, \tag{2.12}$$

DOI:10.15774/PPKE.ITK.2010.008

where the numerator is the well-known Shannon's entropy and can be related to ENA applied in [62]. D_2 is called correlation dimension.

The range of fractal spectra is defined as $\Delta D = \max\left(D_q\right) - \min\left(D_q\right)$, where $\max\left(D_q\right) = D_{-\infty}$, $\min\left(D_q\right) = D_{\infty}$, i.e., $\Delta D = D_{-\infty} - D_{\infty}$, since D_q is a monotonically decreasing function. ΔD is a measure of multifractality, indicates deviation from monofractal. Larger ΔD indicates multifractality, while smaller ΔD indicates that the analyzed system tends to possess the monofractal property. We estimated the range values by $\Delta D = D_{-50} - D_{50}$ based on preliminary analysis (Fig. 2). The approximation of a single ΔD value took about 2.4 ms with these particular settings.

2.2.3. Power spectral measures (PSMs)

To assess the relationship between fractal measures and power spectral properties of sleep EEG signals, we estimated the relative power of widely used frequency bands (RBPs). Relative powers were used instead of absolute ones in order to avoid the effect of variation of total power across subjects. To describe spectral properties in a more compact way, we calculated the spectral edge frequency (f_{se}) since this measure can be considered as a clinically well-established EEG measure for monitoring sleep cycles and depth of anesthesia [62-65].

Before estimation of power spectral EEG features, Hanning windowing was applied to the selected epochs to damp out the frequency leakage, i.e. the Gibbs phenomenon that originates from truncation of time series. From these windowed time series the power spectra $P\left(f\right)$ were obtained using the Fast Fourier Transformation (FFT) with frequency resolution $\Delta f = 0.152$ Hz and range $\left[0 \text{ Hz}, f_s/2 \text{ Hz}\right]$. The relative power of the B frequency band can be calculated from a power spectrum as follows:

$$P_{Br} = \frac{P_B}{P_T} = \frac{\sum_{i=B_{lb}}^{B_{ub}} P\left(f_i\right)}{\sum_{i=1}^{N} P\left(f_i\right)}, \tag{2.13}$$

where P_T is the total power of the time series, P_B is the total power of the B frequency band, $f_i = \left(i-1\right)\Delta f$ with a maximal value of $f_s/2$ when $i = N$, B_{ub} and B_{lb} are indices corresponding to the upper and lower boundary frequencies of the B band, respectively. The analyzed bands were as follows: SO: (0.5-1] Hz, δ: (1-4] Hz, θ: (4-8] Hz, α: (8-11]

DOI:10.15774/PPKE.ITK.2010.008

Hz, σ: (11-16] Hz, β: (16-30] Hz, γ: (30-70] Hz. These frequency bands are thought to represent specific EEG patterns. Slow oscillations (SOs) were assessed separately from delta band activity given their distinct characteristics [66, 67].

The spectral edge frequency was defined as the frequency up to which *SEP* % of the total power of the $[0\text{ Hz}, f_{cse}\text{ Hz}]$ frequency range is accumulated:

$$\int_0^{f_{se}} P(f)\,df = \frac{SEP}{100}\int_0^{f_{cse}} P(f)\,df. \tag{2.14}$$

In this study *SEP* and cut-off f_{cse} frequency parameters were set to 95 % and 70 Hz, respectively. According to Eq. (2.14) and the nature of sleep EEG, lower f_{se} values can be predicted for deeper sleep stages since during these states the power spectrum is biased towards lower frequencies.

Calculation of power spectra and their parameters can be realized almost real-time using the FFT algorithm with appropriate settings and hardware architecture.

DOI:10.15774/PPKE.ITK.2010.008

Chapter Three

FRACTAL PROPERTIES OF THE HUMAN SLEEP EEG AND THEIR RELATIONS TO POWER SPECTRAL MEASURES

3.1. Introduction

The exact values of fractal measures may be related to biophysical mechanisms and the neural architecture underlying oscillations [22], however, given the uncertainties related to the estimation of these measures [47, 55-59] it might be more reasonable to compare the variances of features for different conditions. In line with this, a series of human studies revealed differences in the fractal measures between specific conditions. For example Linkenkaer-Hansen et al. showed that mu and alpha oscillations scale similarly, but beta oscillations have a significantly smaller scaling exponent compared to these two latter oscillations during eyes-closed state [22]. Another study showed that long-range temporal correlations are stronger in the eyes-closed condition as compared with the eyes-open condition [68]. In the study of Nikulin and Brismar largest exponent values for alpha and beta oscillations were found during the eyes-closed condition in the occipital and parietal areas [28]. Fractal dimension was found to be significantly higher for drowsy EEG compared to the wake state [69]. Increased sensory input [70] or high level of alertness [71] was shown to disrupt long-range temporal correlations. Several studies also addressed self-similarity of sleep EEG [46, 60, 72-76]. Generally, most of these studies reported higher scaling exponents and thus stronger long-range temporal correlations for deeper sleep stages. However, these studies were limited by a low sampling rate (100Hz in [46, 73-75]; 128Hz in [60]) or a low number of EEG channels (Fpz-Cz and Pz-Cz in [46, 75]; Cz in [73, 74]; C3 in [60, 76]; C4 in [72]). Furthermore, in contrast to the general opinion that the EEG is more regular and synchronized during deeper sleep stages, the only study that assessed multifractality of the sleep EEG found that the EEG is most multifractal during NREM3 and NREM4. It is to be noted that none of the abovementioned sleep studies assessed topographic aspects of the temporal fractal properties. Moreover, as far as we know, no previous study carried out a joint analysis of monofractal and multifractal properties, neither the relationship between fractal and power spectral measures was assessed yet. Therefore, in this study we attempted to address these theoretical controversies and shortcomings by estimation of spatial and

DOI:10.15774/PPKE.ITK.2010.008

sleep stage-wise distributions of temporal monofractal and multifractal properties of the human sleep EEG and by assessing the relation of fractal measures with power spectral properties. Our analyses included: comparison of inter-site correlations, estimations of cross-correlations between monofractal and multifractal measures as well as between fractal and power spectral measures, multiple linear regression analysis, hierarchical clustering of the EEG channels and measures, assessment of gender-related differences of particular measures.

3.2. Methods

3.2.1. Recordings and estimated measures

All analyses except of the assessment of gender-related differences were carried out using the recordings of 22 subjects introduced in the previous chapter. Gender analysis was carried out using recordings of 17 subjects only. Nine female (age: 25–37 years, mean±S.D.: 29.1±3.9 years) and eight male (age: 24–37 years, mean±S.D.: 30.5±4.2 years) healthy young adults were selected from the database to form male and female groups with similar case numbers and similar age characteristics (mean, range and S.D.). Monofractal and multifractal properties of the selected EEG epochs were evaluated by estimation of the self-similarity parameter H and the range of fractal spectra (ΔD), respectively. Power spectral properties of the human sleep EEG were assessed by calculating relative band powers and the spectral edge frequency. Detailed description of estimation settings can be found in the previous chapter. Additionally, we estimated the multifractal measures for the whole-night EEG recording with 19 s overlap of the 20 s long epochs to reveal general tendencies of the measures across different sleep stages. To emphasize slower dynamics and suppress promiscuous perturbations that can occur due to artefacts we applied moving average to the whole-night courses of the measures. Moving average of the $X(i)$ discrete time series with a $2a+1$, $a=1,2,...$ long sliding window was defined as:

$$MA(i)=\frac{1}{2a+1}\sum_{j=i-a}^{i+a}X(j)\,. \tag{3.1}$$

The value of parameter a was set to 45 for visualization purposes, depicting this way averages of 91 estimated values of H and ΔD.

DOI:10.15774/PPKE.ITK.2010.008

3.2.2. Statistical analysis

3.2.2.1. Topographic distribution of EEG measures across different sleep stages

At the individual level comparisons between sleep stages relied on the selected 3x90 epochs of 20 s length. To test whether the fractal variables H and ΔD are both together affected by the sleep stages, first we performed one-way multivariate analysis of variance (MANOVA). The independent variable "STAGE" contained groups NREM4, NREM2 and REM. Afterwards, to identify the specific dependent variables that contributed to the significant overall effect, one-way ANOVA test was applied to both dependent variables (H and ΔD). Since ANOVA revealed significant main effects for both H and ΔD, Tukey HSD post-hoc test was used for pair-wise comparison of group means. All statistical tests were carried out for all channels separately.

At the group level statistical analyses were carried out using individual medians of fractal and power spectral measures. Normality of the estimated features was tested using the Shapiro-Wilk W test, while the homogeneity of variances was evaluated with the Levene test. Since not all of the estimated measures matched normality and homogeneity in each channel we evaluated the effect of sleep stages using the non-parametric one-way Kruskal-Wallis ANOVA. Individual medians of the estimated measures were grouped using the independent variable "STAGE" having the same factors levels as in the case of individual-level analyses (NREM4, NREM2 and REM). Pair-wise comparison of sleep stages was carried out with rank post-hoc test. To test differences between bilateral symmetric scalp locations we used the Wilcoxon matched pairs test for each measure and sleep stage. For this purpose eight symmetrical channel pairs (Fp1-Fp2, F7-F8, F3-F4, C3-C4, T3-T4, T5-T6, P3-P4, O1-O2) and an additional midline channel pair (Fz-Cz) were formed.

3.2.2.2. Cross-correlation analysis

Cross-correlations were calculated between locations for all estimated measures (inter-site correlations) and between the measures at each location. Specifically, cross-correlations were carried out between monofractal and multifractal measures as well as between fractal and power spectral features. Spearman's correlation coefficients were calculated in all cases using individual medians of particular EEG measures. Sleep stages were considered separately as well as together. To assess the contribution of specific frequency band activities to the compact measures (H, ΔD and f_{se}) we used multiple linear regression analysis.

DOI:10.15774/PPKE.ITK.2010.008

3.2.2.3. Hierarchical clustering

Effect of topography was analyzed by hierarchical clustering of channels for all three sleep stages. Z-score standardization of the individual medians was carried out for all measures and channels separately. Hierarchical channel cluster trees were generated by pairing eight similarity measures (Euclidean distance (euc); standardized Euclidean distance (seu); Mahalanobis distance (mah); city block metric (cit); Minkowski metric (min); cosine distance (cos); correlation distance (cor); Chebychev distance (che)) with seven linkage methods (unweighted average distance (ave); centroid distance (cen); furthest distance (com); weighted center of mass distance (med); shortest distance (sin); inner squared distance (war); weighted average distance (wei)). Performance of each combination was assessed by calculation of the cophenet correlation coefficient (CCC). We selected the similarity-linkage pair with highest CCC value to cluster the channels into four and nine clusters. The 4-cluster analysis was aimed to reveal possible groupings of neighbor EEG channels and thus forming e.g. anterior, posterior, central, lateral or similar clusters. The 9-cluster analysis was applied to assess whether symmetrical EEG channels (see section 3.2.2.1) also cluster together.

Clustergrams were generated for measure and channel clustering using group-level medians (medians of individual medians) of all measures in all channels. Standardization of features was performed across channels. Clustergrams, enclosing heat maps and dendrograms were examined for sleep stages separately. Hierarchical channel cluster trees were generated using the cosine similarity metric and the unweighted average linkage method. Measure dendrograms were constructed applying the Euclidean distance as a similarity measure and the unweighted average method for linkage. Channel clustering was also carried out based on the two fractal measures as well as combining the seven relative band powers.

3.2.2.4. Effects of gender

Normality of the estimated features was tested using the Shapiro-Wilk W test. Since not all of the estimated measures matched normality in each channel the effect of gender was assessed by the Mann-Whitney U test. Individual medians of all features in all channels and during all three sleep stages were compared separately according to the “GENDER” factor.

DOI:10.15774/PPKE.ITK.2010.008

3.3. Results

3.3.1. Distribution of EEG measures across vigilance states and topographic locations

Since results found at the individual level were near similar across subjects here we restrict presentation of individual data to a representative subject (#16). Inspection of individual whole-night H and ΔD profiles and corresponding hypnograms in this subject indicated a visually striking correlation with the succession of sleep cycles. As can be seen in Figure 3.1, as sleep deepens H increases and ΔD decreases while with sleep shallowing H and ΔD exhibit an inverse course. In Figure 3.2 H and ΔD measures are shown with an expanded time scale for a single sleep cycle that contains a typical sequence of sleep stages and for three EEG channels to picture the variation of H and ΔD across brain regions and vigilance states.

One-way MANOVA analysis yielded a statistically significant overall effect for all

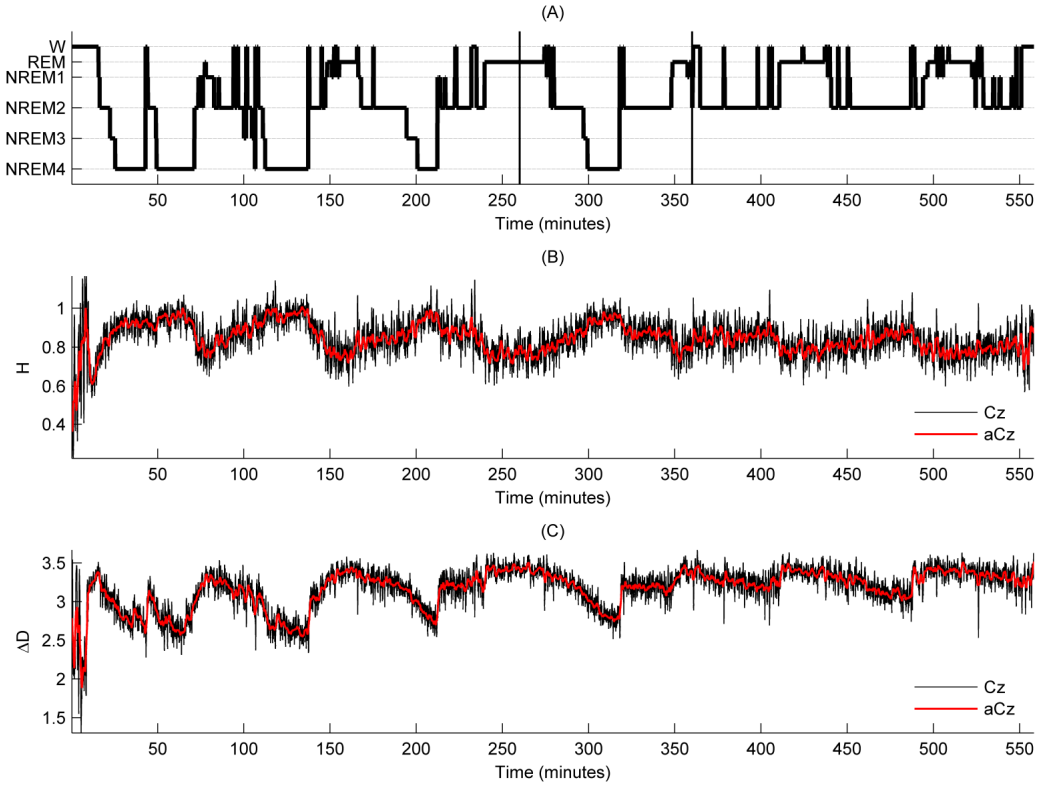

Figure 3.1. Hypnogram and whole-night courses of H and ΔD in subject #16. (A) Hypnogram prepared according to the Rechtschaffen and Kales standard [15] using 20 s long epochs. Time period between the vertical black lines is expanded in Figure 3.1. (B) Estimated H values for channel Cz and their moving average (aCz) using a=45. (C) Estimated ΔD values for channel Cz and their moving average (aCz) using $a = 45$. *A sudden increase of H (B) and drop of ΔD (C) occurring at the beginning of the recording are due to immense artefacts before falling asleep.*

DOI:10.15774/PPKE.ITK.2010.008

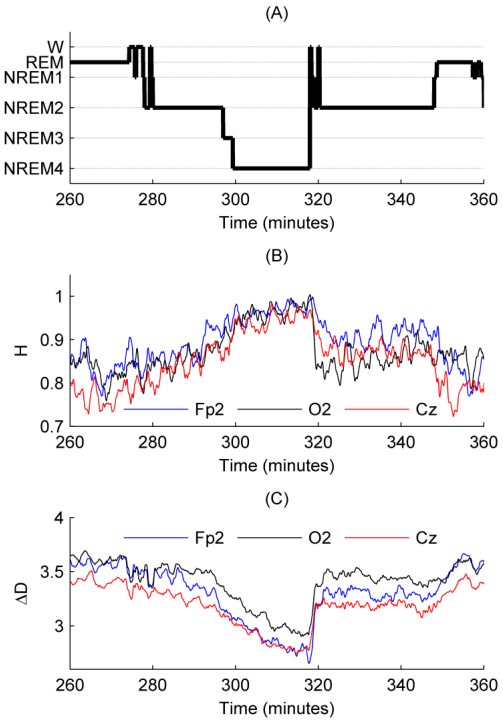

Figure 3.2. Subject #16, expanded hypnogram, H and ΔD courses corresponding to the interval denoted by the vertical black lines in Fig. 3A. (A) Hypnogram prepared according to the Rechtschaffen and Kales standard [15] using 20 s long epochs. (B) Moving average of the estimated H values for channels Fp2, Cz and O2 using $a = 45$. *(C) Moving average of the estimated ΔD values for channels Fp2, Cz and O2 using* $a = 45$.

channels (Wilks' $\lambda = 0.05 - 0.08$; $F_{4,\,532} = 340.04 - 437.82$; $p < 0.00001$). Subsequent one-way ANOVA tests revealed statistically significant main effects for both measures in all channels ($p < 0.00001$).

Figure 3.3 depicts the topography of average *H* (for the selected 90 segments) for the three vigilance states. Highest average *H* values emerged in the frontal region during all

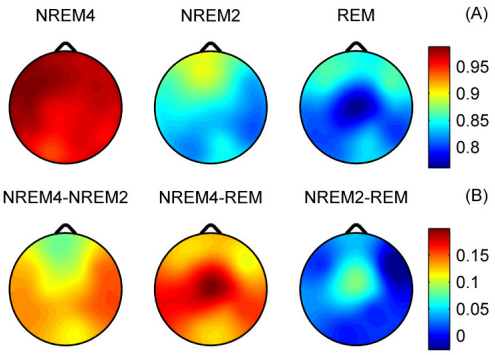

Figure 3.3. (A) Subject #16, topographic maps of H averages (for the 90 selected segments of 20 s length) for sleep stages NREM4, NREM2 and REM. (B) Topographic maps for differences of the H averages between sleep stages.

DOI:10.15774/PPKE.ITK.2010.008

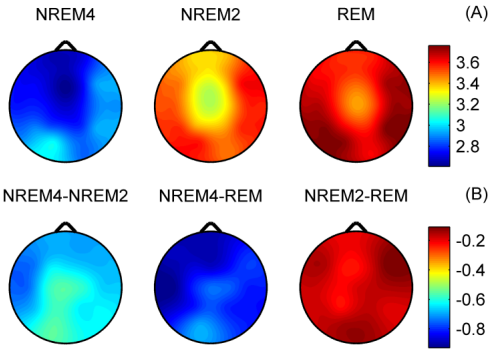

Figure 3.4. (A) Subject #8, topographic maps of ΔD averages (for the 90 selected segments of 20s length) for sleep stages NREM4, NREM2 and REM. (B) Topographic maps for differences of the ΔD averages between sleep stages.

vigilance states, while the minimum was found during REM in the central zone. A $H_{\mathrm{NREM4}} > H_{\mathrm{NREM2}} > H_{\mathrm{REM}}$ trend could be observed across the whole head surface. Post-hoc tests revealed significant differences between stages NREM4 and NREM2 as well as between NREM4 and REM in all channels ($p < 0.0001$). Comparison of NREM2 and REM stages reached significancy at the following recording sites only: Fp1, Fp2, F3, Fz, F4, C3, Cz, C4 and P3 ($p < 0.0001$); T3 ($p < 0.001$); T5 ($p < 0.01$). Difference between NREM4 and REM as well as between NREM2 and REM reached maxima in Cz electrode (Figure 3.3B).

Measure ΔD, as expected based on the inverse course of H and ΔD, showed an opposite trend between sleep stages: $\Delta D_{\mathrm{REM}} > \Delta D_{\mathrm{NREM2}} > \Delta D_{\mathrm{NREM4}}$ (Figure 3.4A). During all sleep stages minima of ΔD could be found in the fronto-central region. The central difference peak that was present for H (Figure 3.3B) disappeared in the ΔD difference maps (Figure 3.4B). Multiple comparisons revealed significant ΔD differences ($p < 0.0001$) for all sleep stage pairs in all channels.

Topographic distributions of group-level medians for the three sleep stages as well as their differences are shown in Figure 3.5. Results obtained for the fractal measures were in agreement with those obtained at the individual level. Namely, highest H values emerged frontally during all sleep stages, while the minimum was found during REM in the central zone. A $H_{\mathrm{NREM4}} > H_{\mathrm{NREM2}} > H_{\mathrm{REM}}$ trend was present across the whole head surface. Measure ΔD, showed an opposite trend: $\Delta D_{\mathrm{REM}} > \Delta D_{\mathrm{NREM2}} > \Delta D_{\mathrm{NREM4}}$. Minima of ΔD could be found in the fronto-central region during all sleep stages, while higher values were observed in the posterior circumferential channels. Salient H difference peaks that occurred for sleep stage pairs NREM4-REM and NREM2-REM could not be

DOI:10.15774/PPKE.ITK.2010.008

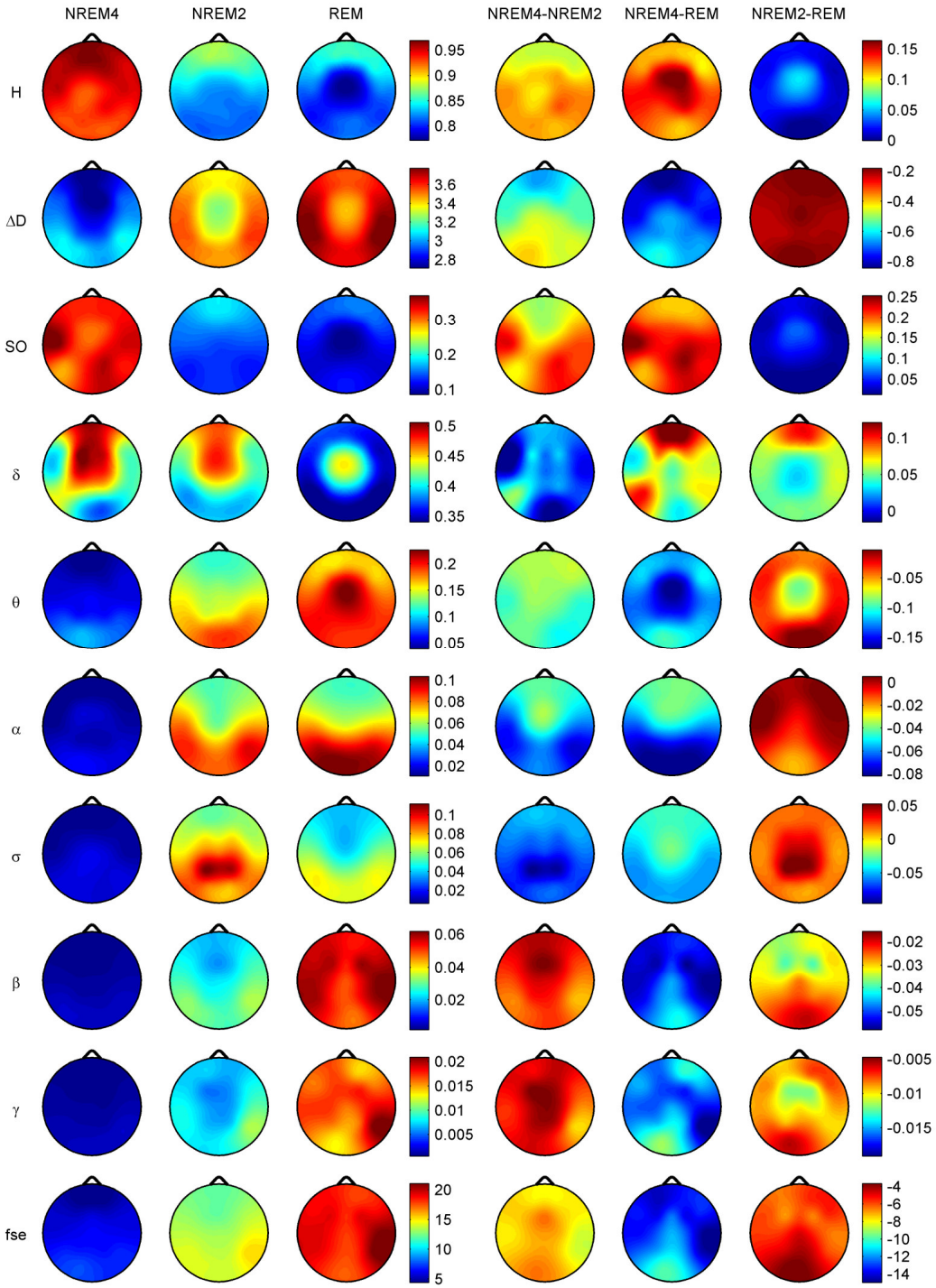

Figure 3.5. Topographic distribution of group-level medians (medians of individual medians) for the analyzed sleep stages and differences of these medians between sleep stages. Relative band powers are denoted by the labels of the corresponding frequency bands.

observed in the case of ΔD. Power spectral measures also exhibited expected topography. Relative band powers of slow activities (SO and δ bands) were higher for NREM4 than NREM2 as well as for NREM2 than REM. Generally, P_{SOr} showed a more even topographic distribution when compared to $P_{\delta r}$ in all sleep stages. Across all sleep stages

DOI:10.15774/PPKE.ITK.2010.008

the minimum of P_{SOr} occurred at the vertex during REM sleep. Frontal regions exhibited slightly higher values of P_{SOr} compared to other regions during NREM2 and REM. During NREM4 higher P_{SOr} values occurred bilaterally in the fronto-temporal region and in C4, P4, O2 channels. $P_{\delta r}$ exhibited higher values in the fronto-central channels during NREM4 and NREM2 and in the central region during REM sleep. Generally, faster activities (above 4 Hz) showed an opposite trend with lower relative band power values for deeper sleep stages. During NREM4 relatively even topographic distributions were found for faster activities. During NREM2 higher values appeared in the posterior region, showing maxima in the parietal channels for $P_{\sigma r}$. REM sleep revealed a more diverse topography of faster activities. Maximum of theta activity was found centrally. Highest values in the α and σ bands occurred in posterior channels. Finally, relative power of β and γ frequency bands peaked in temporal channels. Spectral edge frequency showed lower values for deeper sleep stages as it was conjectured from Eq. (2.14). Slightly higher values of f_{se} were present in posterior channels during NREM4 and NREM2, while during REM higher values were located in temporal channels.

Comparing sleep stages using one-way Kruskal-Wallis ANOVA revealed highly significant ($p < 0.00001$) differences for all measures in all channels except for the relative power of the δ band (Table 3.I). The level of significance for $P_{\delta r}$ varied across channels between $p < 0.01$ and $p < 0.00001$. Pair-wise comparison of sleep stages using the rank post-hoc test resulted in most significant differences between sleep stages NREM4 and REM for all measures and channels with the exception of $P_{\sigma r}$. This latter measure exhibited highest significance values between NREM4 and NREM2 in fronto-centro-parietal channels (F3, Fz, F4, C3, Cz, C4, P3 and P4). In general, least or non-significant differences were observed between sleep stages NREM2 and REM. Comparison between NREM4 and NREM2 revealed significant values for all measures with the exception of the relative δ band power which reached significancy in F3, C3, P3 and P4 channels only.

3.3.1.1. Interhemispheric comparisons

As expected, Wilcoxon matched pairs test revealed (Table 3.II) more significant differences for the non-symmetric Fz-Cz channel pair as compared with the other symmetric channel pairs. Out of the 30 cases (10 measures × 3 stages) the Fz-Cz channel

DOI:10.15774/PPKE.ITK.2010.008

TABLE 3.I. RESULTS OF THE KRUSKAL-WALLIS ANOVA AND RANK POST-HOC TESTS.

Measure	Test	Channel																	
		Fp2	F8	T4	T6	O2	Fp1	F7	T3	T5	O1	F4	C4	P4	F3	C3	P3	Fz	Cz
H	KW	5	5	5	5	5	5	5	5	5	5	5	5	5	5	5	5	5	5
	N4 - N2	>5	>5	>5	>5	>5	>5	>5	>4	>5	>5	>4	>4	>5	>4	>4	>5	>4	>3
	N4 - R	>5	>5	>5	>5	>5	>5	>5	>5	>5	>5	>5	>5	>5	>5	>5	>5	>5	>5
	N2 - R	>x	>x	>x	>x	<x	>x	>x	>x	>x	>x	>1	>x	>x	>1	>2	>x	>2	>2
ΔD	KW	5	5	5	5	5	5	5	5	5	5	5	5	5	5	5	5	5	5
	N4 - N2	<3	<3	<3	<3	<4	<4	<3	<3	<3	<4	<4	<3	<3	<3	<3	<4	<4	<4
	N4 - R	<5	<5	<5	<5	<5	<5	<5	<5	<5	<5	<5	<5	<5	<5	<5	<5	<5	<5
	N2 - R	<2	<2	<2	<2	<x	<2	<2	<2	<2	<x	<2	<2	<2	<2	<2	<2	<2	<2
SO	KW	5	5	5	5	5	5	5	5	5	5	5	5	5	5	5	5	5	5
	N4 - N2	>4	>5	>5	>5	>5	>4	>5	>4	>5	>5	>3	>4	>5	>3	>3	>4	>3	>3
	N4 - R	>5	>5	>5	>5	>5	>5	>5	>5	>5	>5	>5	>5	>5	>5	>5	>5	>5	>5
	N2 - R	>x	>x	>x	>x	>x	>x	>x	>x	>x	>x	>1	>1	>x	>2	>2	>x	>2	>2
δ	KW	5	3	3	5	2	5	2	2	5	2	3	3	3	3	3	5	3	2
	N4 - N2	>x	>x	>x	>x	>x	>x	<x	>x	>x	>x	>x	>x	>1	>1	>1	>2	>x	>x
	N4 - R	>5	>3	>4	>5	>x	>5	>1	>2	>4	>2	>3	>3	>4	>4	>4	>5	>3	>2
	N2 - R	>3	>1	>2	>2	>2	>3	>1	>2	>1	>1	>x	>x	>x	>x	>x	>x	>x	>x
θ	KW	5	5	5	5	5	5	5	5	5	5	5	5	5	5	5	5	5	5
	N4 - N2	<4	<4	<5	<5	<5	<4	<4	<5	<4	<5	<3	<3	<4	<3	<3	<3	<3	<3
	N4 - R	<5	<5	<5	<5	<5	<5	<5	<5	<5	<5	<5	<5	<5	<5	<5	<5	<5	<5
	N2 - R	<1	<x	<x	<x	<x	<1	<x	<x	<1	<x	<2	<2	<2	<2	<2	<2	<2	<3
α	KW	5	5	5	5	5	5	5	5	5	5	5	5	5	5	5	5	5	5
	N4 - N2	<5	<5	<5	<5	<4	<5	<5	<5	<5	<5	<5	<5	<5	<5	<5	<5	<4	<4
	N4 - R	<5	<5	<5	<5	<5	<5	<5	<5	<5	<5	<5	<5	<5	<5	<5	<5	<5	<5
	N2 - R	>x	>x	<x	<x	<x	<x	>x	<x	<x	<x	<x	<x	<x	<x	<x	<x	<x	<x
σ	KW	5	5	5	5	5	5	5	5	5	5	5	5	5	5	5	5	5	5
	N4 - N2	<5	<5	<5	<5	<5	<5	<5	<5	<5	<5	<5	<5	<5	<5	<5	<5	<5	<5
	N4 - R	<5	<5	<5	<5	<5	<5	<5	<5	<5	<5	<3	<3	<4	<3	<3	<3	<3	<2
	N2 - R	>x	>x	>x	>x	>x	>x	>x	>x	>x	>x	>x	>1	>1	>x	>1	>1	>x	>2
β	KW	5	5	5	5	5	5	5	5	5	5	5	5	5	5	5	5	5	5
	N4 - N2	<3	<3	<3	<3	<3	<3	<3	<3	<3	<3	<3	<3	<3	<3	<3	<3	<3	<3
	N4 - R	<5	<5	<5	<5	<5	<5	<5	<5	<5	<5	<5	<5	<5	<5	<5	<5	<5	<5
	N2 - R	<3	<3	<2	<2	<2	<3	<3	<3	<3	<2	<3	<3	<3	<3	<3	<3	<3	<3
γ	KW	5	5	5	5	5	5	5	5	5	5	5	5	5	5	5	5	5	5
	N4 - N2	<3	<3	<3	<3	<3	<3	<2	<2	<2	<2	<3	<3	<3	<2	<2	<2	<2	<2
	N4 - R	<5	<5	<5	<5	<5	<5	<5	<5	<5	<5	<5	<5	<5	<5	<5	<5	<5	<5
	N2 - R	<2	<2	<2	<1	<1	<2	<2	<2	<2	<2	<2	<2	<2	<3	<2	<2	<3	<2
fse	KW	5	5	5	5	5	5	5	5	5	5	5	5	5	5	5	5	5	5
	N4 - N2	<3	<3	<3	<4	<4	<3	<3	<3	<3	<3	<3	<3	<3	<3	<3	<3	<3	<3
	N4 - R	<5	<5	<5	<5	<5	<5	<5	<5	<5	<5	<5	<5	<5	<5	<5	<5	<5	<5
	N2 - R	<2	<2	<2	<2	<1	<2	<3	<2	<2	<2	<3	<2	<2	<3	<2	<2	<2	<2

Results of the Kruskal-Wallis ANOVA test are presented for each measure and channel separately in rows denoted by KW. Similarly, pair-wise post-hoc comparison of sleep stages can be found in rows denoted by N4-N2, N4-R and N2-R (N4: NREM4, N2: NREM2, R: REM). The > (<) sign denotes greater (smaller) group-level medians for sleep stages denoted by first codes. Significance level notation are as follows: x (not significant), 1 ($p<0.05$), 2 ($p<0.01$), 3 ($p<0.001$), 4 ($p<0.0001$), 5 ($p<0.00001$). Relative band powers are denoted by the labels of the corresponding frequency bands.

pair exhibited 19 significant values. Regarding the symmetric channel pairs most

DOI:10.15774/PPKE.ITK.2010.008

TABLE 3.II. RESULTS OF THE WILCOXON MATCHED PAIRS TEST.

M	S	Channel pair									SC
		Fp1 Fp2	F7 F8	T3 T4	T5 T6	O1 O2	F3 F4	C3 C4	P3 P4	Fz Cz	
H	N4	>x	>x	>1	<x	>x	<x	<x	<1	>3	2
	N2	>x	>x	>x	>x	<x	<x	>x	>x	>3	0
	R	>x	<x	<x	<x	<x	<x	<x	<x	>3	0
ΔD	N4	<x	<x	<x	<x	>x	>1	>x	>x	<3	1
	N2	>x	>x	<x	<1	>x	>x	<x	<1	>x	2
	R	>x	>x	>x	<x	>x	>x	<x	<x	>x	0
SO	N4	<x	>1	>x	<x	<3	>x	<3	<2	<x	4
	N2	>x	<x	>x	>x	>x	>x	>x	>x	>3	0
	R	<x	<x	<x	<x	>x	<x	<x	<x	>3	0
δ	N4	>x	<x	<x	>x	>x	>x	>1	>1	>x	2
	N2	>x	>x	<x	<x	>x	>2	>1	<x	>x	2
	R	>1	>2	>x	>x	>x	>1	>x	>x	<1	3
θ	N4	<x	<x	<1	>x	>x	>x	>x	>x	<3	1
	N2	<x	>x	<x	<x	<x	>x	<1	<3	<2	2
	R	<x	>x	>x	>1	>x	>x	>x	<x	<x	1
α	N4	<x	<x	<1	>x	>1	>x	>x	>x	>x	2
	N2	<x	>x	>x	<x	<x	<x	<2	<2	<x	2
	R	>x	>x	>x	>x	>x	>x	<x	>x	<4	0
σ	N4	<x	<x	<x	<x	>2	>x	>x	>2	<3	2
	N2	<1	>x	>x	>x	>1	<x	<x	>x	<4	2
	R	<x	>x	<x	>x	>x	<x	<x	<1	<2	1
β	N4	>x	<x	<x	>x	>1	>x	<x	<x	<4	1
	N2	<x	<1	<2	<x	>x	<1	<1	<1	<4	5
	R	>x	>x	<x	<x	>1	<x	<x	<x	>x	1
γ	N4	>x	<x	<x	<x	<x	>x	>x	>x	<4	0
	N2	>x	<1	<x	<2	<x	<x	>x	<1	<2	3
	R	>x	>x	<x	<2	<1	<x	<x	<x	>x	2
fse	N4	<x	<x	<x	<x	>2	<x	<1	>x	<2	2
	N2	<x	<x	<1	<1	>x	<x	<x	<x	<3	2
	R	>x	>x	<x	<x	<x	<x	<x	<x	>x	0
All	N4	0	1	3	0	5	1	3	4	7	17
	N2	1	2	2	3	1	2	4	5	7	20
	R	1	1	0	2	2	1	0	1	5	8
	AS	2	4	5	5	8	4	7	10	19	45

M: measure, relative band powers are denoted by the labels of the corresponding frequency bands; S: sleep stage; SC: number of symmetrical channel pairs (the midline Fz-Cz channel pair not included) that resulted significant differences; All: number of measures that revealed significant differences summed for sleep stages NREM4 (N4), NREM2 (N2) and REM (R) separately as well as considering all sleep stages (AS) together. The > (<) sign denotes greater (smaller) group-level medians in the upper row channels (electrodes above the left hemisphere and Fz) and it is followed by the significance level sign: x (not significant), 1 ($p<0.05$), 2 ($p<0.01$), 3 ($p<0.001$), 4 ($p<0.0001$).

significant differences were found for channel pairs P3-P4 (10 cases) and O1-O2 (8 cases), while least significant differences appeared for the frontal channel pairs Fp1-Fp2 (2 cases), F7-F8 (4 cases) and F3-F4 (4 cases). In posterior channel pairs more significant results occurred during deeper sleep stages while in frontal channel pairs the least

DOI:10.15774/PPKE.ITK.2010.008

significant differences were found during sleep stage NREM4. Most significant interhemispheric differences occurred for relative powers of delta and beta frequency bands (7 cases for both out of total 24 = 3 sleep stages × 8 symmetrical channel pairs). For $P_{\delta r}$ significant cases were distributed similarly across sleep stages, while $P_{\beta r}$ revealed the most (5 cases) significant differences for NREM2 sleep. P_{SOr} resulted in 4 significant cases, all during NREM4. By contrast, no significant interhemispheric differences were found for $P_{\gamma r}$ in this sleep stage. No gross tendencies were observed for $P_{\alpha r}$ and $P_{\sigma r}$ across sleep stages and locations, however, there were some significant results. Compact EEG features (H, ΔD and f_{se}) altogether revealed smaller number of significant results: 5, 4 and 0 significant cases for NREM4, NREM2 and REM, respectively.

Considering all 10 measures NREM2 (20 cases) and NREM4 (17 cases) revealed twice more significant differences as compared to REM sleep (8 cases out of total 80 = 10 measures × 8 symmetrical channel pairs).

3.3.2. Cross-correlation analysis

3.3.2.1. Inter-site correlations

In Figure 3.6 the 35 strongest inter-site correlations ($p < 0.05$) are denoted by black lines drawn between the appropriate locations for all 10 EEG measures and for each sleep stage separately as well as together. Considering all sleep stages together highest inter-site correlations were observed centrally (F3, Fz, F4, C3, Cz, C4, P3, P4) for all features except for the relative power of the γ band where highest correlations were found intrahemispherically. Sleep stages were characterized by different topography in inter-site correlation maps. In general, power spectral measures (except for $P_{\gamma r}$) showed strongest correlations between anterior channels during NREM4. During NREM2 and REM highest correlations were observed more posteriorly. $P_{\gamma r}$ exhibited higher correlations within than between hemispheres during NREM4 and NREM2, a tendency which was not true for REM. Compared to the topographic properties of the above spectral measures, H exhibited an opposite trend with higher posterior correlations during NREM4 and higher anterior correlations during NREM2 and REM. At the same time ΔD did not reveal such differences between sleep stages. In agreement with previous results

DOI:10.15774/PPKE.ITK.2010.008

presented in ΔD showed higher inter-site correlations compared to H.

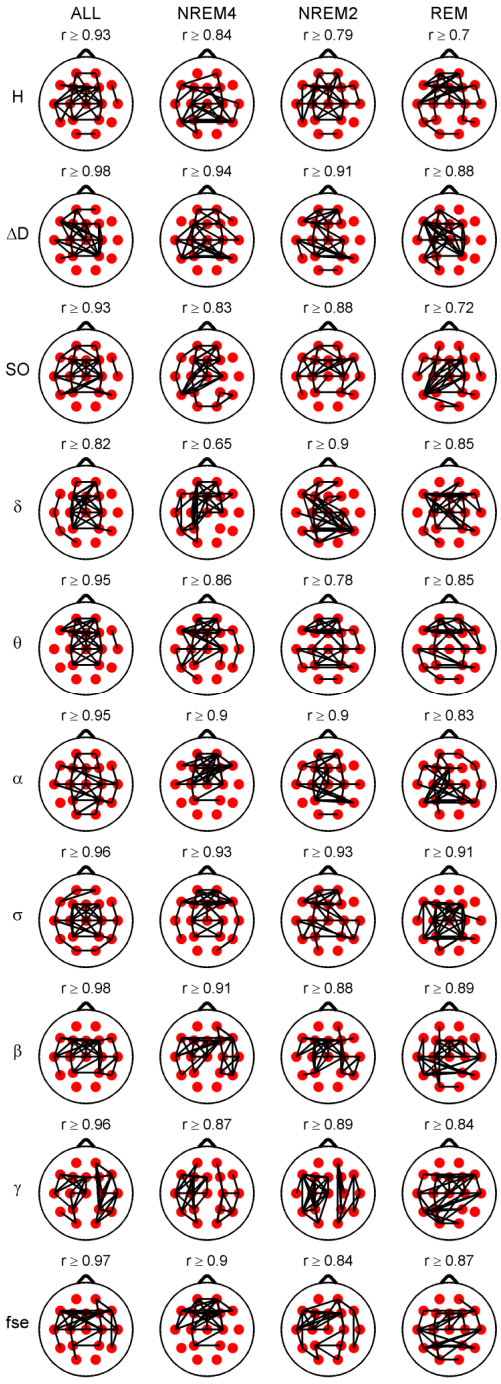

Figure 3.6. Highest 35 inter-site correlations denoted by black lines drawn between the appropriate locations. Spearman's correlation coefficients were calculated considering all sleep stages together (column ALL) as well as separately. Only significant ($p < 0.05$) correlations are depicted. Lowest presented correlation values can be found above the topographic maps. Relative band powers are denoted by the labels of the corresponding frequency bands.

3.3.2.2. Cross-correlation of measures

3.3.2.2.1. Cross-correlation between the fractal measures

When all sleep stages were considered together strong negative cross-correlations ($p < 0.00001$) between H and ΔD were found with weakest correlations in the occipital zone (Figure 3.7). Evaluating sleep stages separately one could observe stronger and more significant correlation values for deeper sleep stages. During NREM4 lower values were found in the occipital and the fronto-polar regions. During NREM2 weakest correlations were found posteriorly. REM sleep showed non-significant negative correlations in the circumferential channels and non-significant but positive correlation in the F3, Fz, and F4 channels.

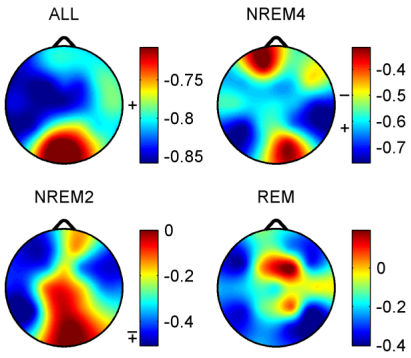

Figure 3.7. Spearman cross-correlations between H and ΔD considering all sleep stages together as well as separately. Significant values ($p < 0.05$) are denoted on the left side of the color bars using the following notations: no sign (none of the values are significant); only + (all values are significant); + with a dash (only values below the dash are significant).

3.3.2.2.2. Cross-correlation between fractal and power spectral measures

Results of cross-correlation analyses between fractal and power spectral measures are summarized in Figure 3.8. Generally, a positive cross-correlation was observed between H and slower brain activities (SO and δ bands), while faster activities (above 4 Hz) were negatively correlated with the monofractal measure H. Higher and more significant correlations were found for deeper sleep stages. Overall, the strongest positive correlation was revealed for the relative power of the SO band, while the strongest negative correlation was found for the relative power of the theta band. Generally, weaker correlations appeared in the anterior channels during NREM4. During NREM2 stronger correlations (positive for the SO and negative for the θ band) were found in the anterior

DOI:10.15774/PPKE.ITK.2010.008

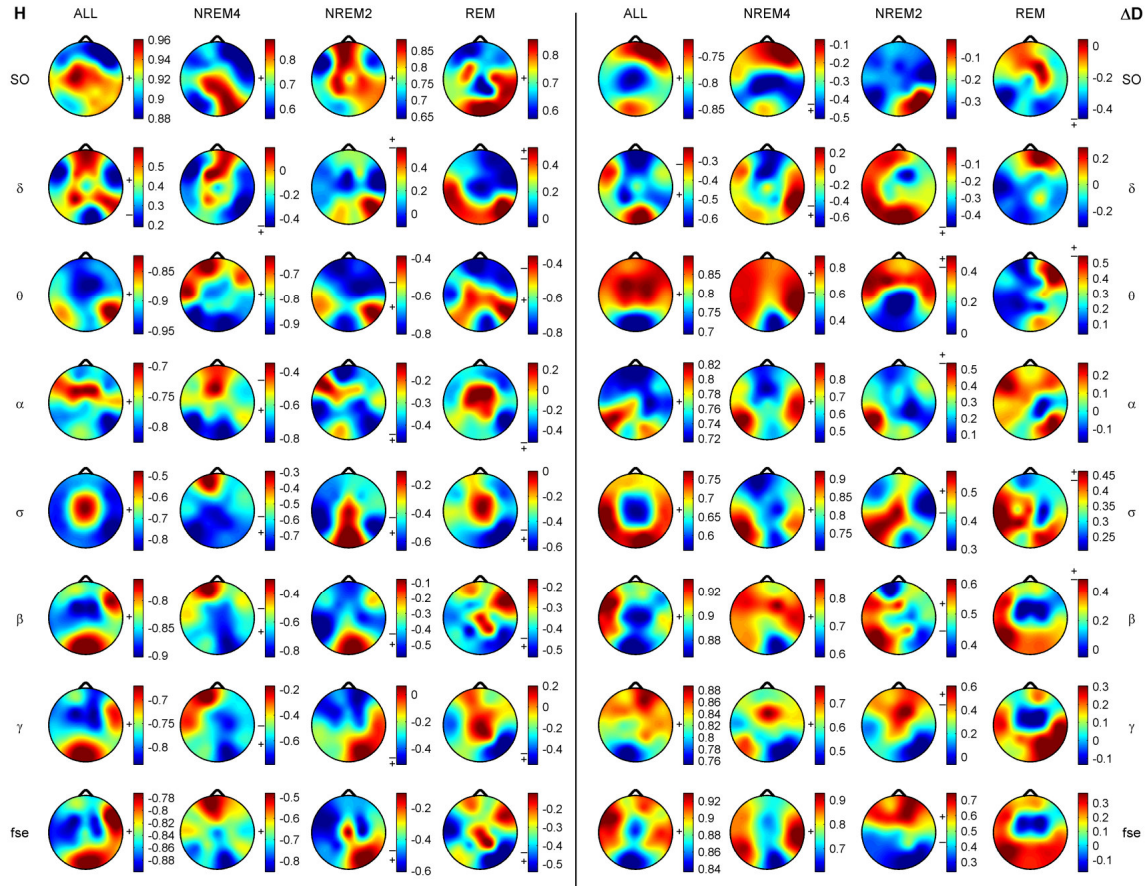

Figure 3.8. Spearman cross-correlations between fractal and power spectral measures (PSMs). The left panel depicts results obtained for H. Cross-correlations between ΔD and PSMs are presented in the right panel. Sleep stages were considered together (columns denoted by ALL) as well as separately. Significant values ($p < 0.05$) are marked on the left side of the color bars using the following notations: no sign (none of the values are significant); only + (all values are significant); + with a dash (only values above/below the dash are significant). Relative band powers are denoted by the labels of the corresponding frequency bands.

region while faster activities (σ, β, and γ bands) exhibited weakest correlations with *H* in posterior channels. During REM stronger positive correlation between slow activities (SO and δ bands) and *H* was found in the temporal and occipital channels while faster activities were negatively correlated with the monofractal measure *H*. Above the θ band stronger negative correlations were present in the circumferential channels decreasing around the vertex and even switching to positive correlation values in the case of α and γ bands.

Generally, correlations between Δ*D* and RBPs exhibited relationships with a sign opposite to that found for measure *H*. Namely, Δ*D* was negatively correlated with slow (SO and δ) while positively correlated with faster (above 4 Hz) activities. Similarly to *H*, more significant values appeared for deeper sleep stages. Compared to *H*, correlations of

DOI:10.15774/PPKE.ITK.2010.008

ΔD with slow activities were weaker and less significant. Highest positive correlation values between ΔD and $P_{\theta r}$ were found in the anterior channels regardless of sleep depth. Relative power of alpha and sigma bands exhibited strongest positive correlations with ΔD in the temporal channels. $P_{\beta r}$ and $P_{\gamma r}$ showed strongest positive correlations with ΔD around the Fz channel during NREM4, while the nadirs of these correlations were found during REM sleep in the same region.

Inspection of cross-correlation maps between spectral edge frequency and the fractal measures indicated that these correlations reflect contribution of certain frequency bands in a compact way, such as in the case of the correlation between f_{se} and H during NREM4 where the minimum of correlations was found frontally.

To estimate the contribution of single frequency bands to the overall variation of compact measures, one must bear in mind that certain band powers are also correlated [77]. To control for this effect, we performed multiple linear regression (MLR) analyses with relative band powers as predictors and compact EEG measures as response variables. At this point we analyzed sleep stages together and only in those channels where best classifications were predicted based on results presented in previous sections. Thus, for H MLR was carried out in channel Cz with a result

$$H = \overset{**}{0.52}(\pm 0.15)P_{SOr} + 0.04(\pm 0.07)P_{\delta r} - \overset{***}{0.47}(\pm 0.11)P_{\theta r} + 0.03(\pm 0.05)P_{\alpha r}$$
$$-0.04(\pm 0.07)P_{\sigma r} - 0.07(\pm 0.06)P_{\beta r} + 0.08(\pm 0.04)P_{\gamma r} + \overset{*****}{0.82}(\pm 0.08)$$

and statistics $F(7,58) = 200.99$, $p < 0.00001$, $Std.\,Err.\,Est. = 0.01$, $R = 0.98$, $R^2 = 0.96$, $Adjusted\ R^2 = 0.96$. For ΔD MLR was performed considering the T4 channel. The obtained result was

$$\Delta D = -0.08(\pm 0.12)P_{SOr} - 0.07(\pm 0.05)P_{\delta r} + \overset{*****}{0.55}(\pm 0.09)P_{\theta r} + 0.17(\pm 0.11)P_{\alpha r}$$
$$+0.005(\pm 0.09)P_{\sigma r} + 0.14(\pm 0.08)P_{\beta r} + 0.09(\pm 0.06)P_{\gamma r} + \overset{*****}{2.99}(\pm 0.24)$$

with statistics $F(7,58) = 77.54$, $p < 0.00001$, $Std.\,Err.\,Est. = 0.12$, $R = 0.95$, $R^2 = 0.9$, $Adjusted\ R^2 = 0.89$. Finally, contribution of different frequency bands to the spectral edge frequency was tested in channel T6 with the

$$f_{se} = -0.08(\pm 0.07)P_{SOr} - 0.05(\pm 0.03)P_{\delta r} + 0.08(\pm 0.05)P_{\theta r} - 0.04(\pm 0.04)P_{\alpha r}$$
$$+0.06(\pm 0.04)P_{\sigma r} + \overset{****}{0.17}(\pm 0.04)P_{\beta r} + \overset{*****}{0.73}(\pm 0.03)P_{\gamma r} + \overset{**}{9.62}(\pm 3.12)$$

DOI:10.15774/PPKE.ITK.2010.008

result and the following statistics $F(7,58)=360$, $p<0.00001$, $Std.\,Err.\,Est.=1.23$, $R=0.99$, $R^2=0.98$, $Adjusted\ R^2=0.97$. Coefficients of relative band powers were standardized and their standard errors were provided in brackets. Only coefficients with stars above them were significant with notation: ** $(p<0.01)$, *** $(p<0.001)$, **** $(p<0.0001)$ and ***** $(p<0.00001)$.

3.3.3. Clustering of channels and measures

Hierarchical channel cluster trees were generated for all three sleep stages and EEG features separately using the best similarity and linkage combinations. Visual inspection of the dendrograms revealed both common and distinct channel clusters across sleep stages (see e.g. Figure 3.9 for measure ΔD). For statistical evaluation channels were

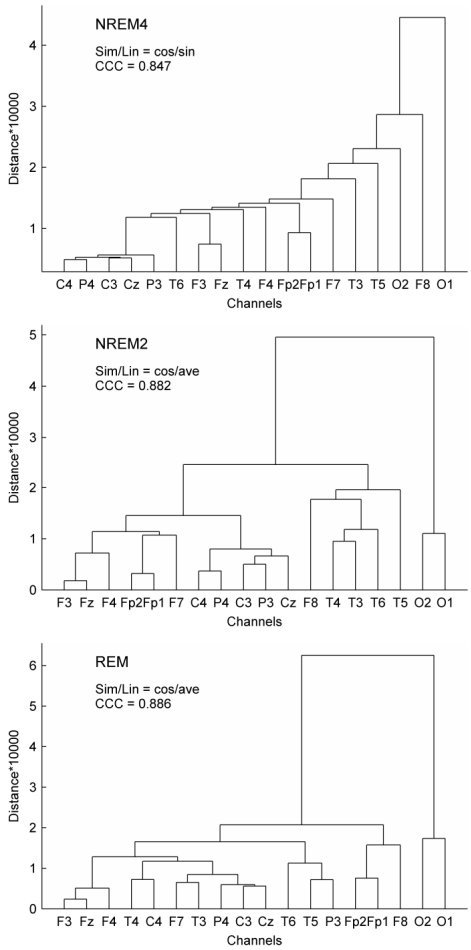

*Figure 3.9. Dendrograms of EEG channels obtained using the multifractal measure Δ*D*. Hierarchical cluster trees were generated applying the best similarity/linkage (Sim/Lin) methods according to the cophenet correlation coefficient (CCC). For the abbreviation of Sim/Lin methods see the section 3.2.2.3.*

DOI:10.15774/PPKE.ITK.2010.008

clustered into 4 and 9 clusters, respectively (Table 3.III).

As can be seen in Table 3.III and Table 3.IV, the 9-cluster analysis showed that most EEG features revealed proximity of symmetrical channels in the frontal region and during NREM4. During REM most of the symmetric channels were clustered together posteriorly. Regardless of the sleep stage most of the measures (6-9 out of 10) indicated the proximity of F3-F4, C3-C4 and P3-P4 channels. The non-symmetrical Fz and Cz

TABLE 3.III. HIERARCHICAL CLUSTERING OF EEG CHANNELS USING ALL MEASURES SEPARATELY.

M	Sleep stage	Channel																		SC	Sim/Lin	CCC
		Fp2	F8	T4	T6	O2	Fp1	F7	T3	T5	O1	F4	C4	P4	F3	C3	P3	Fz	Cz			
H	N4	1|7	2|6	2|4	2|2	3|8	4|9	2|5	2|3	2|1	2|2	**2|2**	**2|2**	**2|2**	**2|2**	**2|2**	**2|2**	**2|2**	3	seu/cen	0.803
	N2	1|2	2|6	2|7	4|9	**3|8**	1|1	1|3	1|5	1|5	**3|8**	1|2	1|4	1|4	1|2	1|4	1|4	1|2	1|4	4	seu/ave	0.859
	R	3|**1**	4|5	4|6	1|9	2|7	3|**1**	3|2	3|2	2|8	2|8	3|**2**	3|**4**	3|3	3|**2**	3|**4**	3|4	3|2	3|4	3	cit/ave	0.775
ΔD	N4	4|**5**	3|9	4|3	4|6	1|7	4|**5**	4|4	4|1	4|2	2|8	4|**5**	4|**6**	4|**6**	4|**5**	4|**6**	4|**6**	4|5	4|6	4	euc/ave	0.840
	N2	3|**1**	2|6	2|7	1|3	4|**9**	3|**1**	3|5	1|4	1|4	4|**9**	3|**2**	3|**8**	3|**8**	3|**2**	3|**8**	3|**8**	3|2	3|8	5	euc/ave	0.835
	R	3|8	4|9	1|7	2|5	2|**2**	2|6	2|4	2|4	2|1	2|**2**	2|**3**	2|**4**	2|**4**	2|**3**	2|**4**	2|**4**	2|3	2|4	4	euc/cen	0.759
SO	N4	3|**9**	4|5	4|6	2|1	2|2	3|**9**	4|7	4|7	2|3	1|8	3|**9**	2|**4**	2|2	3|**9**	2|**4**	2|4	3|9	2|4	3	euc/ave	0.746
	N2	1|2	1|2	2|7	2|4	3|8	1|5	1|5	1|5	1|6	4|9	1|2	1|2	2|4	1|5	1|1	2|3	1|5	1|1	0	seu/ave	0.814
	R	2|5	4|9	4|9	1|6	2|**8**	2|3	3|1	3|2	2|4	2|**8**	2|**4**	1|7	1|**7**	2|**4**	2|4	1|**7**	2|4	1|7	3	euc/ave	0.706
δ	N4	4|**4**	2|**2**	1|8	1|8	4|7	4|**4**	2|**2**	4|5	2|1	3|9	4|**4**	4|**3**	4|6	4|**4**	4|**3**	4|3	4|4	4|3	4	euc/ave	0.812
	N2	2|**8**	3|5	3|6	2|4	4|9	2|**8**	1|2	1|2	1|1	1|7	2|**4**	2|**4**	2|4	2|**4**	2|**4**	2|3	2|**4**	2|**4**	3	seu/ave	0.792
	R	2|6	3|1	3|**4**	3|5	4|9	2|7	3|2	3|**4**	1|8	1|8	3|**3**	3|**3**	3|**5**	3|**3**	3|**3**	3|**5**	3|**3**	3|**3**	4	seu/ave	0.787
θ	N4	2|**4**	1|5	1|6	1|6	4|9	2|**4**	2|3	2|1	2|2	3|8	2|**4**	2|**7**	2|**7**	2|**4**	2|**7**	2|**7**	2|4	2|7	4	euc/ave	0.826
	N2	3|**6**	2|1	2|2	1|9	4|7	3|**6**	3|6	2|3	2|4	4|8	3|**6**	3|**5**	3|**5**	3|**6**	3|**5**	3|**5**	3|6	3|5	4	seu/ave	0.844
	R	1|1	1|2	1|2	2|3	4|**9**	3|5	3|6	3|6	2|4	4|**9**	3|**5**	3|**8**	3|**8**	3|**5**	3|**8**	3|**8**	3|5	3|7	4	seu/ave	0.777
α	N4	2|**2**	2|1	1|4	1|4	4|9	2|**2**	2|5	2|6	1|7	3|8	2|**2**	2|**2**	1|**3**	2|**2**	2|**2**	1|**3**	2|**2**	2|**2**	4	seu/cen	0.826
	N2	1|**6**	4|1	4|2	2|7	2|3	1|**6**	1|5	4|8	3|9	2|4	1|**6**	2|**7**	2|**7**	1|**6**	2|**7**	2|**7**	1|6	2|7	4	euc/ave	0.848
	R	3|8	1|2	1|2	1|1	2|5	2|3	2|7	2|7	1|6	4|9	2|**4**	2|**4**	2|**4**	2|**4**	2|**4**	2|**4**	2|**4**	2|**4**	3	che/ave	0.900
σ	N4	1|3	2|7	3|9	3|9	4|8	2|5	2|6	4|2	4|2	4|1	1|**3**	1|**4**	4|**8**	1|**3**	1|**4**	4|**8**	1|3	1|4	3	euc/ave	0.766
	N2	4|**1**	4|5	4|4	4|3	2|6	4|**1**	4|1	4|3	3|9	2|7	4|**1**	4|**2**	1|**8**	4|**1**	4|**2**	1|**8**	4|1	4|2	4	seu/med	0.763
	R	4|7	4|8	2|**2**	2|1	3|3	1|9	2|2	2|**2**	2|6	3|4	2|**6**	2|**6**	2|**6**	2|**6**	2|**6**	2|**6**	2|6	2|5	4	euc/ave	0.836
β	N4	2|2	1|6	1|6	1|5	2|3	4|9	2|7	2|1	2|1	3|8	2|**2**	2|**2**	2|2	2|**2**	2|**2**	2|4	2|2	2|4	2	che/cen	0.898
	N2	2|6	1|7	2|3	2|4	3|8	4|9	2|2	2|2	2|1	2|5	2|**3**	2|**3**	2|**3**	2|**3**	2|**3**	2|**3**	2|**3**	2|**3**	3	che/sin	0.841
	R	2|8	1|7	1|7	1|**6**	3|1	4|9	2|8	2|3	1|**6**	3|2	2|**4**	2|**4**	1|6	2|**4**	2|**4**	1|5	2|**4**	2|**4**	3	euc/ave	0.814
γ	N4	3|8	1|3	1|4	1|4	1|4	4|9	2|5	2|5	2|6	2|1	1|4	1|4	1|4	2|5	2|7	2|2	2|**2**	2|**2**	0	che/ave	0.902
	N2	3|5	3|1	3|1	3|2	3|1	4|9	3|3	3|3	2|6	2|7	3|1	3|2	3|2	3|3	1|8	3|4	3|**4**	3|**4**	0	che/ave	0.927
	R	2|4	2|**3**	2|3	2|5	2|3	4|9	2|**3**	2|2	3|8	1|7	2|**3**	2|3	2|1	2|**3**	2|6	2|2	2|**3**	2|**3**	2	che/ave	0.993
fse	N4	1|**7**	1|**6**	2|8	4|4	4|3	1|**7**	1|**6**	3|1	3|2	4|5	1|**7**	2|**9**	4|**4**	1|**7**	2|**9**	4|**4**	1|7	2|9	5	cit/ave	0.712
	N2	2|5	3|3	3|4	3|3	3|4	4|9	2|6	2|6	1|8	2|7	2|6	2|6	2|**6**	2|1	2|2	2|**6**	2|1	2|2	1	che/ave	0.775
	R	2|4	2|1	2|6	2|6	2|3	4|9	2|2	2|2	3|8	1|7	2|3	2|**3**	2|**2**	2|5	2|**3**	2|**2**	2|**3**	2|**3**	2	che/ave	0.949

For all the 3 analyzed sleep stages (N4: NREM4, N2: NREM2, R: REM) channels were clustered into 4 (denoted by first numbers) and 9 (indicated by second numbers) clusters. Number of symmetrical channel pairs (the midline Fz-Cz channel pair not included) that fell into same clusters considering the 9-cluster analysis (designated by bold numbers) is presented in column SC. Abbreviation of best similarity (Sim) and linkage (Lin) combinations used for clustering can be found in the second last column. Performance of these best combinations is described by the cophenet correlation coefficient (CCC). For the definition of symmetrical channel pairs as well as for abbreviation of similarity and linkage methods see sections 3.2.2.1 and 3.2.2.3 Relative band powers are denoted by the labels of the corresponding frequency bands.

DOI:10.15774/PPKE.ITK.2010.008

TABLE 3.IV. NUMBER OF MEASURES THAT INDICATED COMMON CLUSTERS FOR CHANNEL PAIRS BASED ON RESULTS OF THE 9-CLUSTER ANALYSIS PRESENTED IN TABLE 3.III.

Sleep stage	Channel pair									
	Fp1 Fp2	F7 F8	T3 T4	T5 T6	O1 O2	F3 F4	C3 C4	P3 P4	Fz Cz	SC
NREM4	6	2	0	0	0	9	9	6	3	32
NREM2	5	0	0	0	2	7	7	7	3	28
REM	1	1	2	1	3	9	8	7	5	32
Alls	12	3	2	1	5	25	24	20	11	92

SC denotes sums across symmetrical channel pairs (the midline Fz-Cz channel pair not included), while Alls indicates sums across sleep stages.

channels clustered together in much less cases. A more detailed examination of data in Table 3.III unveiled that Fz tended to cluster with frontal F3 and F4 channels, while Cz mostly formed common clusters with the central channels C3 and C4. With regard to $P_{\gamma r}$ symmetric channels did not cluster together during NREM4 and NREM2 sleep stages but did so in REM sleep.

In the 4-cluster analysis, where all measures were considered separately, a rather uneven clustering of channels was found. Notably, in almost all cases there were channels (typically the circumferential ones such as: Fp1, Fp2, O1, O2, T5, T6) that formed individual clusters because of their large distance from the remaining EEG derivations. At the same time, several topographic features revealed by the above analyses could be verified. For example, highest $P_{\sigma r}$ values in parietal channels during NREM2 (Figure 3.5) were reflected in a separate cluster formed by P3 and P4 channels. As another example disconnection of the hemispheres during NREM4 with regard to the relative power of the γ band (Figure 3.6) was also supported by forming separate clusters over left and right hemispheres.

Hierarchical clustering of channels was also carried out using all measures together to minimize the effect of "outlier" channels and to assess topography of overall brain dynamics. Performing 4-cluster analysis of hierarchical channel cluster trees (Figure 3.10) revealed symmetric channel clusters for all sleep stages (Table 3.V). In general, separate clusters were formed by anterior, central, temporal and posterior channels. Topographic boundaries of these clusters slightly varied across sleep stages.

DOI:10.15774/PPKE.ITK.2010.008

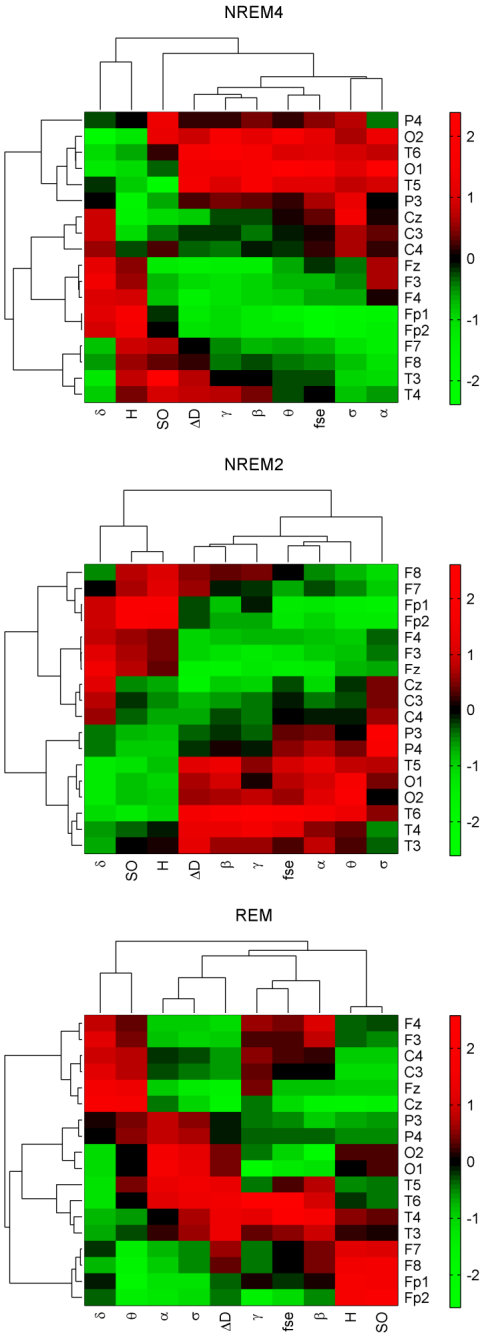

Figure 3.10. Clustergrams generated for sleep stages NREM4, NREM2 and REM using group-level medians of all measures in all channels. Heat maps and hereby the dendrograms were generated after z-standardization of the measures across the channels. Hierarchical channel cluster trees were generated using the cosine similarity metric and the unweighted average linkage method. The corresponding cophenet correlation coefficients (CCCs) were as follows: 0.749 (NREM4), 0.843 (NREM2) and 0.826 (REM). Measure dendrograms were constructed applying the Euclidean distance as a similarity measure and the unweighted average method for linkage (CCC: 0.959 (NREM4), 0974 (NREM2) and 0.886 (REM)). Relative band powers are denoted by the labels of the corresponding frequency bands.

DOI:10.15774/PPKE.ITK.2010.008

TABLE 3.V. CLUSTERING OF EEG CHANNELS INTO 4 CLUSTERS USING ALL MEASURES TOGETHER.

Cluster #	Sleep stage		
	NREM4	NREM2	REM
1	Fp1, Fp2, F3, F4, Fz	Fp1, Fp2, F7, F8	Fp1, Fp2, F7, F8
2	C3, C4, Cz	F3, F4, Fz, C3, C4, Cz	F3, F4, Fz, C3, C4, Cz
3	F7, F8, T3, T4	P3, P4	T3, T4, T5, T6
4	T5, T6, P3, P4, O1, O2	T3, T4, T5, T6, O1, O2	P3, P4, O1, O2

Hierarchical cluster trees were generated using the cosine similarity metric and the unweighted average linkage method. The cophenet correlation coefficient values were as follows: 0.75 (NREM4), 0.843 (NREM2) and 0.826 (REM).

When combining the fractal measures (Table 3.VI) only or the relative band powers only (Table 3.VII) less symmetrical and slightly different topographic grouping of channels was obtained. E.g. the separate cluster that was formed for the parietal channels during NREM2 using all measures together (Table 3.V) was not found using the fractal measures only.

TABLE 3.VI. CLUSTERING OF EEG CHANNELS INTO 4 CLUSTERS USING THE FRACTAL MEASURES ONLY.

Cluster #	Sleep stage		
	NREM4	NREM2	REM
1	Fp1, Fp2, F3, F4, Fz	Fp1, Fp2, F7, F8	Fp1, Fp2, F7, F8
2	C3, C4, Cz, P3	F3, F4, Fz,	F3, F4, Fz
3	F7, F8, T3, T4, P4	C3, C4, Cz, P3, P4	C3, C4, Cz, P3, P4
4	T5, T6, O1, O2	T3, T4, T5, T6, O1, O2	T3, T4, T5, T6, O1, O2

Hierarchical cluster trees were generated using the cosine similarity metric and the unweighted average linkage method. The cophenet correlation coefficient values were as follows: 0.739 (NREM4), 0.776 (NREM2) and 0.926 (REM).

In the next step we hierarchically clustered the computed EEG measures based on the 18 EEG channels (Figure 3.10). In all sleep stages H was closest to relative band powers of slow activities (SO and δ bands). Measure ΔD was clustered with $P_{\beta r}$ and $P_{\gamma r}$ during NREM4 and NREM2, while it formed a common cluster with $P_{\alpha r}$ and $P_{\sigma r}$ during REM. As expected from Eq. (2.14), with sleep deepening f_{se} was clustered with decreasing frequency bands, i.e. during REM f_{se} was clustered with $P_{\gamma r}$, during NREM2 with $P_{\alpha r}$ and during NREM4 with $P_{\theta r}$.

DOI:10.15774/PPKE.ITK.2010.008

TABLE 3.VII. CLUSTERING OF EEG CHANNELS INTO 4 CLUSTERS USING THE RELATIVE BAND POWER MEASURES ONLY.

Cluster #	Sleep stage		
	NREM4	NREM2	REM
1	Fp1, Fp2, F7, F8	Fp1, Fp2, F7, F8 F3, F4, Fz	Fp1, Fp2, F7, F8
2	F3, F4, Fz, C3, C4, Cz	C3, C4, Cz	F3, F4, Fz, C3, C4, Cz
3	T3, T4, P4	P3, P4	T3, T4, T6
4	T5, T6, P3, O1, O2	T3, T4, T5, T6, O1, O2	T5, P3, P4, O1, O2

Hierarchical cluster trees were generated using the cosine similarity metric and the unweighted average linkage method. The cophenet correlation coefficient values were as follows: 0.733 (NREM4), 0.876 (NREM2) and 0.842 (REM).

3.3.4. Gender-related differences

Topographic distributions of group-level medians (medians of individual medians) during all three sleep stages for males and females are shown in Figure 3.11. The distribution of the measures across sleep stages and different locations was in general agreement with results shown in Figure 3.5. Detailed results on gender-related differences (for all measures, channels and sleep stages) can be found in (Table 3.VIII). Across all sleep stages group-level median of H was higher in females than males in most of the channels (see Figure 3.12). Out of the 18 channels this was true for 17, 13 and 10 channels for NREM4, NREM2 and REM, respectively. Nevertheless, statistical comparisons reached significancy ($p = 0.0464$) in T4 during NREM4 only. At the same time ΔD was higher in males than females in all channels during all sleep stages. Statistical comparisons revealed significant differences in several channels during NREM4 (F7, F3, T3, T4, T6, C3, C4, Cz, P4) and in one channel (P4) during REM. Out of these results highest significance ($p = 0.0025$) was reached for the F7 channel. For other channels the significance level was as follows: C4 ($p = 0.0206$); Cz ($p = 0.0274$); T3 and T4 ($p = 0.0359$); F3, T6, C3 and P4 ($p = 0.0464$). Compared to ΔD less significant differences emerged for relative band powers. Nevertheless, we revealed some remarkable results. Group-level median of P_{SOr} during NREM4 was higher in females in all channels. Significant differences emerged for F8 ($p = 0.0274$) and P3 ($p = 0.0464$) channels. By contrast during NREM2 and REM P_{SOr} was higher in males

DOI:10.15774/PPKE.ITK.2010.008

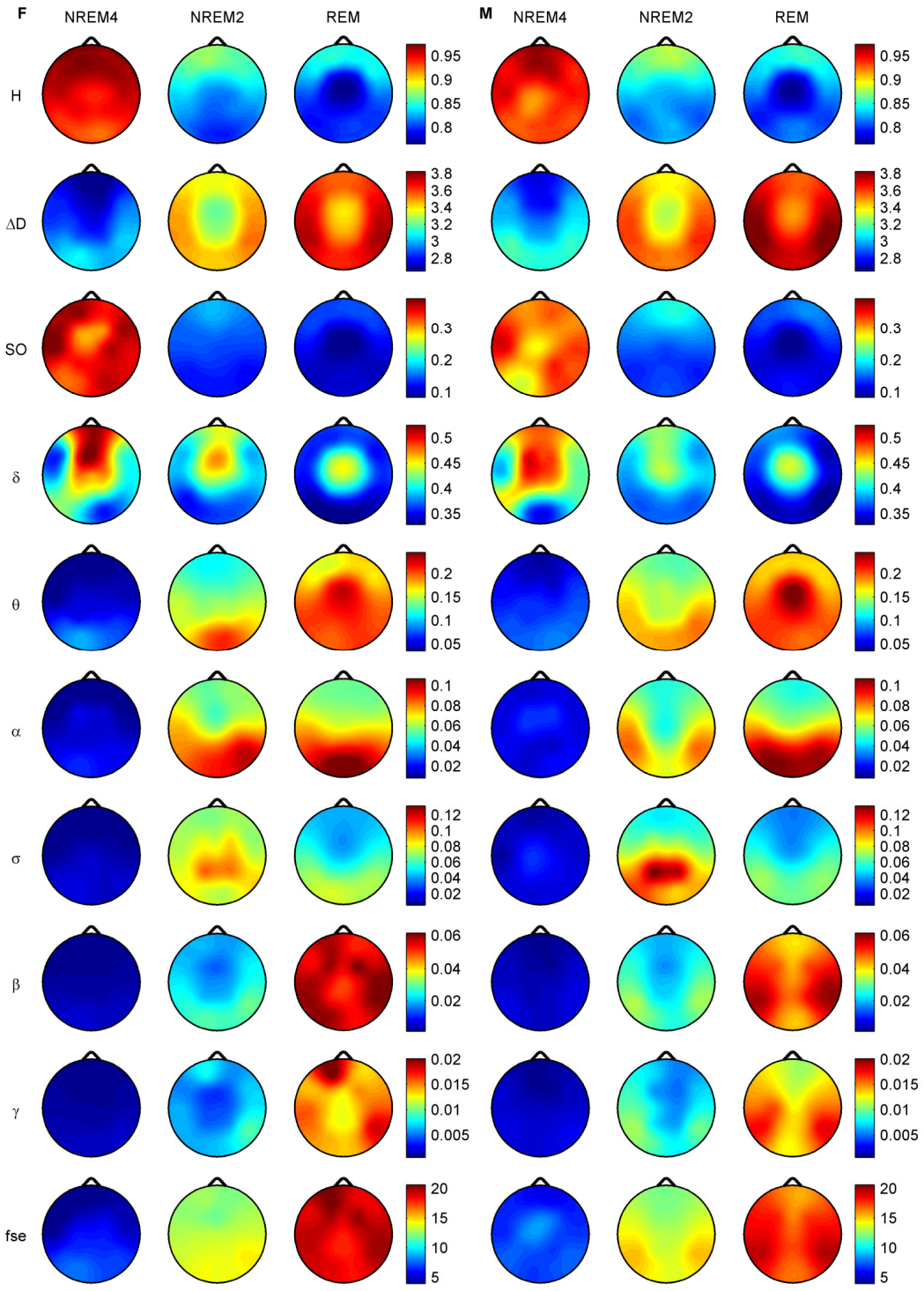

Figure 3.11. Topographic distribution of group-level medians (medians of individual medians) for the analyzed sleep stages presented for males (panel M) and females (panel F). Relative band powers are denoted by the labels of the corresponding frequency bands.

in most channels. Statistically significant differences emerged for Fp2 ($p = 0.0274$) and

DOI:10.15774/PPKE.ITK.2010.008

O1 ($p = 0.0055$) during REM. Compared to P_{SOr} the relative band power of delta activity showed an opposite trend. Namely, $P_{\delta r}$ was higher in males in more channels during NREM4, while it was higher in females in more channels during NREM2 and REM sleep stages. No significant differences were found for this measure between groups. Group-level median of $P_{\theta r}$ was higher in males in most channels in all three sleep stages. However, significant differences were present in channels F7 ($p = 0.0111$) and T4 ($p = 0.0206$) during NREM4 only. A common trend of activities above the theta band was that in most channels males exhibited higher band powers during NREM4

TABLE 3.VIII. RESULTS OF THE MANN-WHITNEY U TEST.

Measure	Stage	Channel																
		Fp2	F8	T4	T6	O2	Fp1	F7	T3	T5	O1	F4	C4	P4	F3	C3	P3	Fz	Cz
H	NREM4	>x	>x	>1	>x	<x	>x	>x	>x	>x	>x	>x	>x	>x	>x	>x	>x	>x	>x
	NREM2	<x	>x	>x	>x	<x	>x	>x	>x	>x	<x	>x	>x	>x	>x	>x	<x	>x	<x
	REM	<x	>x	<x	>x	<x	>x	>x	<x	>x	<x	<x	<x	>x	>x	>x	<x	>x	>x
ΔD	NREM4	<x	<x	<1	<1	<x	<x	<2	<1	<x	<x	<x	<1	<1	<1	<1	<x	<x	<1
	NREM2	<x	<x	<x	<x	<x	<x	<x	<x	<x	<x	<x	<x	<x	<x	<x	<x	<x	<x
	REM	<x	<x	<x	<x	<x	<x	<x	<x	<x	<x	<x	<x	<1	<x	<x	<x	<x	<x
SO	NREM4	>x	>1	>x	>x	>x	>x	>x	>x	>x	>x	>x	>x	>x	>x	>x	>1	>x	>x
	NREM2	<x	<x	<x	<x	<x	<x	<x	>x	>x	<x	<x	<x	<x	<x	>x	>x	<x	>x
	REM	<1	<x	<x	<x	<x	<x	>x	>x	<x	<2	<x	<x	<x	<x	<x	<x	<x	>x
δ	NREM4	>x	<x	<x	<x	>x	>x	<x	<x	<x	>x	>x	<x	<x	>x	<x	>x	>x	<x
	NREM2	>x	>x	>x	>x	>x	>x	>x	>x	<x	<x	>x	>x	>x	>x	>x	>x	>x	>x
	REM	>x	>x	>x	>x	<x	<x	<x	>x	<x	<x	>x	>x	>x	<x	>x	>x	>x	>x
θ	NREM4	<x	<x	<1	<x	<x	<x	<1	<x	<x	>x	<x	<x	<x	<x	<x	<x	<x	<x
	NREM2	<x	<x	<x	<x	>x	<x	<x	<x	<x	>x	<x	<x	>x	<x	<x	<x	<x	<x
	REM	<x	<x	>x	<x	>x	<x	<x	<x	<x	<x	<x	<x	<x	<x	<x	<x	<x	<x
α	NREM4	<x	<x	<x	<x	<x	<x	<1	<x	<x	>x	<x	<x	>x	<x	<x	>x	<x	<x
	NREM2	>x	<x	<x	>x	>x	>x	<x	<x	<x	>x	<x	>x	>x	<x	>x	>x	<x	>x
	REM	>x	>x	<x	<x	>x	>x	<x	<x	<x	>x	>x	<x	<x	>x	>x	<x	>x	>x
σ	NREM4	<x	<x	<x	<x	<x	<x	<x	<x	<x	<x	<x	<x	<x	<x	<x	<x	<x	<x
	NREM2	>x	>x	<x	<x	<x	>x	>x	<x	<x	<x	>x	<x	<x	<x	<x	<x	>x	<x
	REM	>x	>x	<x	>x	>x	>x	>x	>x	>x	>x	>x	>x	>x	>x	>x	>x	>x	>x
β	NREM4	<x	<x	<x	<x	<x	<x	<1	<x	<x	>x	<x	<x	<x	<x	<x	<x	<x	<x
	NREM2	<x	<x	<x	<x	>x	<x	<x	<x	<x	<x	<x	<x	<x	<x	<x	<x	<x	<x
	REM	>x	>x	>x	>x	>x	>1	>x	>x	>x	>1	>x	>x	>x	>x	>x	>x	>x	>x
γ	NREM4	<x	<x	<x	<x	<x	<x	<x	<x	<x	<x	<x	<x	<x	<x	<x	<x	<x	<x
	NREM2	>x	>x	<x	<x	<x	>x	<x	<x	<x	<x	<x	<x	<x	<x	<x	<x	<x	<x
	REM	>x	>x	>x	>x	>x	>1	>x	>x	<x	>x	>x	>x	<x	>x	<x	<x	>x	>x
fse	NREM4	<x	<x	<1	<x	<x	<x	<1	<1	<x	>x	<x	<x	<x	<x	<x	<x	<x	<x
	NREM2	<x	<x	<x	<x	>x	>x	<x	<x	<x	<x	<x	<x	<x	<x	<x	<x	<x	<x
	REM	>1	>x	>x	>x	>x	>1	>x	>x	<x	>1	>x	>x	>x	>x	>x	>x	>x	>x

Detailed statistical results are presented for all measures, sleep stages and channels separately. The > (<) sign denotes that the group-level median was higher in females (males). The level of significance is denoted as follows: x (not significant), 1 (p<0.05), 2 (p<0.01).

DOI:10.15774/PPKE.ITK.2010.008

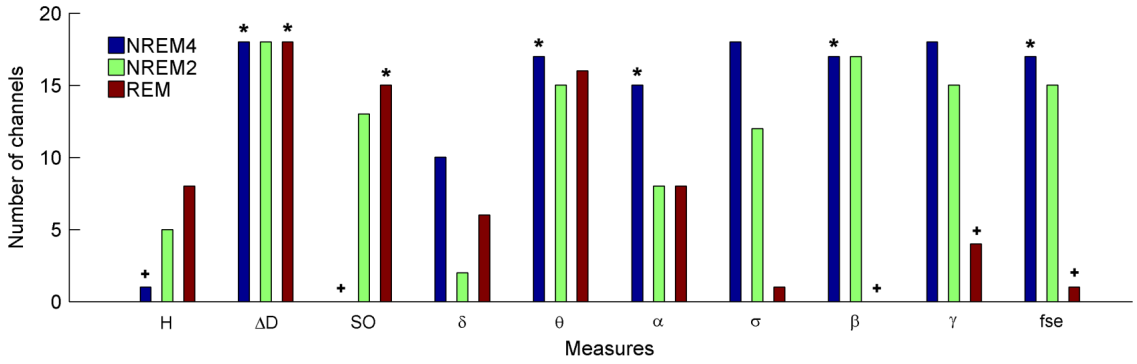

*Figure 3.12. Number of channels in which group-level medians were higher in males (case M>F) are presented for all measures and sleep stages separately. Number of channels in which group-level measure medians are higher in females (case F>M) can be obtained by subtracting these values from 18 (total number of channels). The * (+) sign denotes measure and sleep stage combinations exhibiting significant differences for the case M>F (F>M). Relative band powers are denoted by the labels of the corresponding frequency bands. For detailed statistical results see the text and Table 1 in the supplementary material.*

while females showed higher values in REM. Significant differences were found for $P_{\alpha r}$ ($p = 0.0359$) and $P_{\beta r}$ ($p = 0.0274$) in channel F7 during NREM4. During REM comparisons reached significancy for $P_{\beta r}$ in channels Fp1 ($p = 0.0206$) and O1 ($p = 0.0464$) and for $P_{\gamma r}$ in channel Fp1 ($p = 0.0464$). Spectral edge frequency followed the trend exhibited by activities above the theta band that is group-level median of f_{se} in males was higher during NREM4 and NREM2 while lower during REM in most channels. For this measure statistically significant gender differences were found in channels F7 ($p = 0.0111$), T3 and T4 ($p = 0.0464$) during NREM4 and in channels Fp1 ($p = 0.0206$), Fp2 ($p = 0.0464$) and O1 ($p = 0.0359$) during REM sleep.

3.4. Discussion

3.4.1. Topographic and sleep stage-wise distribution of measures

To our knowledge this is the first study providing a detailed comparison of fractal and power spectral features of the human EEG considering the effects of topography, sleep stages and gender. Fractality of EEG signals was assessed using both monofractal and multifractal measures. Power spectral properties were described by relative band powers and in a more compact way by estimating the spectral edge frequency. Sleep was analyzed considering sleep stages NREM4, NREM2 and REM separately as well as

DOI:10.15774/PPKE.ITK.2010.008

together. Topography was assessed with regard to functional connectivity by analyzing interhemispheric differences and regional clustering of EEG derivations.

Higher H values occurred for deeper sleep stages, while ΔD showed an opposite trend indicating that brain electrical activities tend to be less multifractal and to be more persistent during deeper sleep stages. The decrease of ΔD with the deepening of sleep was opposite to the behavior of another multifractal measure, the range of singularity strength in a previous study [75] where the multifractality of EEG signals was assessed analyzing the distribution of zero-crossings. However, our results fit more into the general theory assuming lower complexity of EEG signals during deeper sleep stages. The $H_{\mathrm{NREM4}} > H_{\mathrm{NREM2}} > H_{\mathrm{REM}}$ trend was in agreement with results of previous studies that assessed the DFA λ exponent [60, 72-74], the fractal exponent κ [76] or the fractal dimension D_f [78]. Namely, DFA exponent λ and κ increased with the deepening of sleep, while D_f exhibited the opposite trend. This suggests that the Hurst exponent estimated based on R/S statistics might be able to reflect the self-similarity properties of the sleep EEG, although the aforementioned trend could not be observed for H in [46]. Nevertheless, searching for the direct relationship between exact values of fractal measures and physiological processes has less sense, because of the already mentioned doubts related to estimation of fractal measures from time series of finite length. Even classification of actual brain dynamics into one of two types of fractional time series (fGn and fBm) is questionable. According to one part of the studies, fGn behavior of the sleep EEG could be conjectured based on DFA λ exponent values below 1 [73, 74] or estimated Hurst exponents below 1 using the R/S statistics approach such as in the present study and in[46]. Other studies, on the contrary, indicated fBm nature of the human sleep EEG by revealing DFA λ exponent values above 1 [60, 72] or fractal exponent values in the range $1 < \kappa < 3$ [76]. These discrepancies might be due to different estimation settings and indicate a need for a comprehensive comparison of different approaches used for the assessment of fractal properties, including classification of EEG signals into one of two classes of fractional time series (fGn or fBm) as it was proposed in [50, 52, 53]. Moreover, we should keep in mind that sleep EEG signals exhibit multifractal properties and thus monofractal analysis can only give a measure of the largest of their fractal dimensions. The 1/f noise-like power spectrum of EEG signals can be distorted during different conditions by characteristic peak frequencies (e.g. due to the α rhythm or intensive sleep spindles) that could destroy the self-similar nature of EEG. Possible analyses for such cases were proposed in [79, 80].

DOI:10.15774/PPKE.ITK.2010.008

Our data on the topography of relative band powers only partially agreed with those published earlier. Slow activities characterizing NREM4 occurred in anterior channels, while faster activities during REM dominated posteriorly. This antero-posterior tendency is in general agreement with previous studies [81-85]. During NREM sleep stages, the fronto-central maximum of slow activities as well as the posterior maximum of theta activity and the parietal maximum of the sigma band are also in agreement with results presented in [86, 87]. Nevertheless, the frontal maximum of alpha and beta band activities [86, 87] was not supported by our results. Also, instead of the frontal σ and β peaks during REM in the study of [87] we found posterior and temporal peaks in these activities. We could neither confirm the frontal peak of NREM4 slow oscillation activity described by [88]. We assume that discrepancies might be due to methodological differences. Firstly, previous studies mostly used absolute power values while we used relative band powers. Secondly, several previous studies [81, 83, 84, 86, 87] evaluated NREM sleep stages together, while we examined NREM4 and NREM2 stages separately. Nevertheless, we were able to confirm the known topographic spectral features of characteristic sleep EEG patterns. The revealed fronto-central peak in delta activity during NREM4 and NREM2 likely reflects delta waves and K-complexes [88, 89]. The parietal peak of sigma activity during NREM2 may stand for fast sleep spindles [90-92]. At the same time no salient topographic feature could be related to frontal slow spindle activity. Vertex peaks in delta and theta bands during REM sleep likely reflects saw tooth waves, characteristic EEG patterns during REM with a know central maximum [93].

3.4.2. Cross-correlations between measures

Combining all sleep stages we found a strong negative correlation between H and ΔD with a nadir in the posterior channels (Figure 3.7). As revealed by the sleep stage-wise analysis NREM2 and NREM4 contributed most to this occipital nadir. As compared to NREM4 weaker and less significant correlations emerged during NREM2. During REM there was a further weakening of correlations with a non-significant positive peak in the F3, Fz, F4 channels.

To reveal how spectral properties are reflected in fractal measures, we performed cross-correlation analysis between these measures (Figure 3.8). Measure H exhibited positive correlation with relative powers of slow activities (especially P_{SOr}), while it mostly showed negative correlation with faster activities. More significant values tended to

DOI:10.15774/PPKE.ITK.2010.008

occur for slower activities (except $P_{\delta r}$) and for deeper sleep stages. All these findings support the theory that H is linearly related to the spectral exponent κ (see section 2.2.2.1). Parameter κ is estimated by plotting the power spectrum on the log-log scale and by fitting a straight line to this plot. The slope of this line is equal to $-\kappa$. This indicates that higher amount of slow activities and lower amount of faster activities result in higher κ and H values and vice versa. The log-log plot of the power spectrum produces several points at higher frequencies and only few points at lower frequencies. Hence, the fitting of a straight line is much more affected by lower frequencies which might be the cause of more significant correlations of H with slower brain activities. Thus the correlation with H depends not only on the position, width and power amount of a given frequency band but it is also affected by properties of other bands. This provides an explanation why $P_{\delta r}$ exhibited weaker and less significant correlations with H as it could have been expected. As it could be conjectured from the overall negative cross-correlation between the fractal measures, ΔD generally revealed opposite correlations with power spectral measures compared to those of H. That is, ΔD was negatively correlated with slow activities and positively correlated with RBPs of higher frequency bands. Additionally, faster activities (> 4 Hz) showed more significant correlations with ΔD as compared to slower activities and for deeper sleep stages. All this suggests that slower EEG patterns tend to make the amplitude distribution more even, while the opposite is true for faster EEG patterns. Characteristic topography of cross-correlations between H and ΔD were also reflected in cross-correlations between the fractal measures and RBPs. E.g. one of the most striking topographic features of cross-correlations between fractal measures and relative band powers could be observed for REM sleep in the fronto-central region where weakest correlations occurred. This might explain weak and non-significant positive cross-correlation between the two fractal measures during REM. Multiple linear regressions supported results of cross-correlation analysis between fractal and RBP measures by revealing contribution of individual RBPs to the compact EEG measures. We found a positive contribution of slow (SO and δ bands) activities to H. Out of the faster activities $P_{\alpha r}$ and $P_{\gamma r}$ contributed positively while $P_{\theta r}$, $P_{\sigma r}$ and $P_{\beta r}$ contributed negatively to the same measure. The positive contribution of $P_{\alpha r}$ and $P_{\gamma r}$ might be explained by the observed weak positive cross-correlation between these measures and H during REM sleep in the central zone (see Figure 3.8). Highest coefficients were revealed for P_{SOr} and $P_{\theta r}$. Considering ΔD, negative and non-

DOI:10.15774/PPKE.ITK.2010.008

significant contribution of slow activities was obtained. Positive coefficients were found for faster activities (above 4 Hz) reaching the significance level only for $P_{\theta r}$. In addition, expected results were also found considering f_{se} as a predicted variable. Highest positive and significant coefficients were found for two fastest activities ($P_{\beta r}$ and $P_{\gamma r}$). Fraction of variation that could be explained by the relative band powers was highest in case of f_{se} ($Adjusted\ R^2 = 0.97$), while the worst regression result was found for ΔD ($Adjusted\ R^2 = 0.89$). This finding could have been anticipated since f_{se} is directly computed from power spectra and H may be related to the power spectrum, while ΔD reflects the amplitude distribution of time series. Distance of compact EEG features and RBPs was also analyzed by hierarchical clustering of the measures using group-level medians in all channels (Figure 3.10). These results were in agreement with those obtained by cross-correlation analyses and MLR. Namely, H was clustered with relative powers of slow brain activities (SO and δ frequency bands) in all sleep stages, while ΔD tended to clustered with faster activities (β and γ bands during NREM4 and NREM2; α and σ bands during REM sleep).

A direct comparison of our correlation results (between H and spectral measures) with those of previous investigators is not possible since previous investigators used different measures and only few EEG channels. Nevertheless, our results regarding the correlation between H and power spectral measures could be related to those results by [78] who revealed a similar trend of measures D_2 and D_f across sleep stages and a negative cross-correlation between D_2 and powers of slower frequency bands [76]. Another study revealing negative cross-correlation between D_2 and DFA exponent λ and negative cross-correlation between D_2 and slower activities [60] also seem to be in accordance with our data. On the contrary, the weak positive cross-correlation between D_2 and κ during NREM4 and NREM3 found by [76] would suggest negative correlation between H and slow activities. As far as we know there are no studies in the literature examining the relationship between multifractality and spectral measures of sleep EEG.

3.4.3. Interhemispheric differences and inter-site correlations

In the present study we also compared inter-site correlations (Figure 3.6) and interhemispheric differences of fractal and power spectral measures (Table 3.II). Surprisingly interhemispheric differences of specific measures varied with sleep stages and locations more than expected. In addition, it is difficult to relate these results to

DOI:10.15774/PPKE.ITK.2010.008

previous data where sleep stages were combined and/or EEG recording was limited to a few channels. Nevertheless, we were able to reveal some coherent tendencies regarding the interhemispheric differences of spectral powers. E.g. we observed a right-hemisphere predominance of SO during NREM4 which might be related to those results by [94] finding predominance of 0.5-2 Hz activity over the right hemisphere during all night sleep. At the same time delta activity on the left side tended to predominate in each sleep stage. During NREM4 and NREM2 we found higher theta activity on the right side, while during REM theta predominated on the left side corroborating the findings of [95]. The majority of interhemispheric comparisons of H and ΔD were not significant. Previous investigators revealed interhemispheric asymmetries for measures D_2, L_1 and D_f considering C3-C4 channels [78] and interhemishperic differences for D_2 in C3-C4, T3-T4 and O1-O2 locations [96]. Differences between earlier and the present data might be due to several methodological differences. Inter-site correlations of RBPs (Figure 3.6) partially agreed with those results of coherence analyses revealed in [97-99]. Specifically, we found stronger interhemispheric $P_{\gamma r}$ correlations during REM compared to NREM4 and NREM2, a finding similar to obtained by [97]. However, this result should be regarded with caution since disconnection of the hemispheres during NREM4 and NREM2 sleep regarding $P_{\gamma r}$ might also occur due to the application of two separate references [58, 100, 101].

As expected, less significant differences were found for the symmetrical channel pairs as compared with the non-symmetrical channel pair Fz-Cz. These results indicate stronger functional connectivity between the homologous hemispheric regions that could be mediated to a large part by the corpus callosum and other commissural pathways [102, 103]. During NREM4 most significant interhemispheric differences were found for occipital and parietal symmetrical channel pairs (Table 3.II). Results in the interhemispheric analysis were confirmed by the inter-site correlation analysis (Figure 3.6) revealing strongest correlations between the anterior channels during NREM4. During NREM2 and REM strongest correlations were located more posteriorly. The 9-cluster analysis (Table 3.III and Table 3.IV) also confirmed this trend by revealing a tendency of clustering together the frontal symmetrical channels during NREM4 and the posterior homologous channels during REM sleep. These findings suggest stronger interhemispheric functional connectivity anteriorly during NREM4 and posteriorly during REM sleep. Topography of inter-site correlations of compact EEG features

DOI:10.15774/PPKE.ITK.2010.008

(including fractal measures and f_{se}) reflect those of RBPs to some extent but due to the compression of information several properties are lost. E.g. the disconnection of the hemispheres during NREM4 and NREM2 regarding the gamma band activity cannot be revealed from compact features. The 4-cluster analysis revealed similar channel clusters (anterior, posterior, central and temporal) for the combined fractal measures (Table 3.VI) and for the combined RBPs (Table 3.VII). Nevertheless, there were some differences between these two latter clusterings which could be related to the aforementioned information loss. For example, the separate cluster that was formed for the parietal channels using the RBP measures was modified by clustering the parietal channels together with central derivations based on combination of fractal measures. Combination of fractal features and PSMs (Figure 3.10 and Table 3.V) provided more symmetrical topographic clusters than those obtained for the combined fractal measures or the combined RBP measures (as well as combined PSMs: data not presented) separately. Nevertheless, all these results indicate a re-organization of functional connectivity between brain regions across sleep stages.

3.4.4. Gender differences

In the present study we also compared fractal and power spectral measures between males and females during the analyzed sleep stages and according to 18 scalp locations. We were able to identify an EEG parameter, a recording site and a sleep stage differentiating genders most efficiently. As an EEG parameter we disclosed the multifractal measure ΔD which tended to be higher in all channels and during all sleep stages in males. Gender difference for ΔD also reached statistical significance for many channels. Regarding the number of significant differences ΔD was followed by the relative theta power which also tended to be higher in the vast majority of the EEG channels during all three sleep stages in males. Similar distribution of ΔD and relative theta activity between genders and across locations and sleep stages is likely due to the high correlation between the two measures. In contrast to the latter measures relative SO power during NREM4 was higher in females, a result in agreement with previous data on female excess in slow wave activity during NREM4 [104, 105]. Monofractal measure H also exhibited elevated values in females during NREM4, and distribution similar to that of the relative SO as could be presumed based on the high correlation between these measures. Activities above the theta band showed contrasting gender tendencies across sleep stages: in males higher activity was present in the α, σ, β and γ bands during

DOI:10.15774/PPKE.ITK.2010.008

NREM4 while females exhibited excess in the same frequency bands during REM sleep. The spectral edge frequency also followed this latter trend. These results are not entirely consistent with earlier data where higher spectral power in faster frequencies was found in females both during NREM [105] and REM sleep [104]. Yet a direct comparison is not possible since Carrier et al. [105] used a single while Dijk et al. [104] used two EEG channels only. Furthermore Dijk et al. [104] did not subdivide NREM sleep while Carrier at al. [105] studied NREM sleep only. Another important difference is that previous studies [104-106] used absolute power spectral measures while we used relative band powers. Since females usually have thinner skull than males this anatomical difference might have obscured neuronal gender differences and might have contributed to higher band powers over a wide frequency range in females as originally proposed by Dijk et al. [104].

A rather unexpected result from the present study is that among locations the highest number of significant gender differences (5 significant comparisons) was found for the F7 channel. Given that the F7 recording site lies over or near the Broca's area it is tempting to hypothesize that differences at this specific region reflect gender differences in verbal functions [107, 108]. Out of the 5 significant comparisons highest significance was found for the multifractal measure ΔD during NREM4.

Comparing sleep stages regarding the number of significant differences revealed that NREM4 exhibited most significant differences. At the same time no significant differences emerged during NREM2 and thus we could not replicate the result of Huupponen et al. [109] on female excess in spindle activity the left frontopolar channel.

The major finding from the present study is that the multifractal measure ΔD proved to exhibit larger gender differences overall compared to the monofractal measures H and the power spectral measures. In a previous study the DFA λ exponent did neither exhibit significant gender differences at specific locations during eyes-closed condition [28].

Superiority of the multifractal measure over the relative band powers might be due to the fact that ΔD reflects activities of several frequency bands that might not be enough to produce significant gender differences alone. Alternatively, it might be ascribed to the fact that ΔD also reflects signal characteristics independent of actual band powers as it was revealed by MLR. Since spectral edge frequency is a measure also reflecting spectral power values but here produced less significant comparisons we suggest that superior performance of ΔD is likely due to the non-linear information content of this compact measure.

DOI:10.15774/PPKE.ITK.2010.008

Finally, we should also note that recent investigations revealed effects of age [28] as well as genetic contributions to long-range temporal correlations [110] in wake EEG signals. Therefore, effects of these factors should be investigated during different sleep stages as well. Our preliminary analyses indicated that H tends to decrease, while ΔD tends to increase with age (Appendix A, Figure 7.1). However, our results cannot be considered representative due to the uneven age distribution.

DOI:10.15774/PPKE.ITK.2010.008

Chapter Four

CLASSIFICATION OF SLEEP STAGES BY COMBINING FRACTAL AND POWER SPECTRAL EEG FEATURES

4.1. Introduction

Motivated by different possible applications the automatic classification of the vigilance state has become a distinguished research topic. E.g. automatic classification of the sleep stages would be beneficial for clinicians when assessing long-term recordings. Other applications might be the real-time monitoring of the depth of anesthesia [111] during surgery or drowsiness detection [112] for people working under monotonic and at the same time dangerous circumstances. Furthermore, in more sophisticated applications such as the brain computer interfaces detection of vigilance state might enhance the system performance via optimizing the parameters of event detection/prediction algorithms.

Accordingly, numerous attempts have been made to automate the sleep stage discrimination [113, 114]. These methods are mostly based on extraction of certain features from EEG, EOG, and EMG signals after which the actual state is determined by a classifier. Classifiers are usually optimized using a supervised learning algorithm based on scoring results of human experts. These approaches include extraction of specific power spectral and non-linear measures [62, 115, 116] and apply conventional linear and nonlinear classification, such as linear discriminant analysis [117] and artificial neural networks [118-120]. Detection of waveforms by various pattern recognition algorithms can be also used for sleep staging [121-128]. Furthermore, different groups applied rule-based reasoning methods using contextual information [113, 129]. For a more detailed review of this research field see [116, 129].

According to the summary of Park et al. [129] the agreement rate between automated scoring and manual scoring is generally 75-85 % in recordings of normal young adults and somewhat lower (65-75 %) for populations with sleep disorders.

Recent studies showed that application of novel measures including the fractal features [75, 116] may improve the discrimination of sleep stages. However, the studies related to fractal analyses were limited by a low number of EEG channels: Fp1, Fp2, C3, C4, O1, O2 in [116] and Fpz-Cz, Pz-Oz in [75].

DOI:10.15774/PPKE.ITK.2010.008

Despite of the extent literature on automatic sleep staging several shortcomings remained. Namely, most of the studies are still restricted to analyses of the central channels, a thorough overview of channel x measure combinations and a comprehensive comparison of different classification paradigms are still lacking. Moreover, most of the studies disclosed results related to group-level classifications only. We admit that individual-level classification is unachievable e.g. when sleep staging has to be applied for assessment of ambulatory whole-night data since usually no training recordings are available. Nevertheless, some more user-specific applications might require the individual-level classification of the vigilance state.

In this study we attempted to address the aforementioned shortcomings by combining monofractal, multifractal and power spectral measures estimated for 18 EEG channels and by comparing different classification paradigms both at individual and group levels.

4.2. Methods

4.2.1. Recordings and feature extraction

All analyses were carried out using the 3×90 20 s long EEG epochs selected for all 22 subjects introduced in Chapter 2. Thus, here we examined discrimination of NREM4, NREM2 and REM sleep stages. Waking and remaining sleep stages (NREM1 and NREM3) were not evaluated due to the lack of appropriate number of segments for statistical analyses. Here we remark that according to the new guidelines of the American Academy of Sleep Medicine (AASM) [130] NREM3 is not anymore considered as a separate stage, but as a state of slow wave sleep (SWS) along with NREM4.

Monofractal and multifractal properties were evaluated by estimation of the self-similarity parameter H and the range of fractal spectra ΔD, respectively. Power spectral properties of the human sleep EEG were assessed by calculating relative band powers and the spectral edge frequency. Detailed description of estimation settings can be found in Chapter 2.

4.2.2. Classification of sleep stages

Classification of sleep stages was performed both at individual and group levels according to the steps presented in Figure 4.1. At the individual level 3×90 estimated values were used for each subject, while $22\times3\times90$ values were considered at the group level. Selection of the features was carried out using a 10-fold cross-validation procedure

DOI:10.15774/PPKE.ITK.2010.008

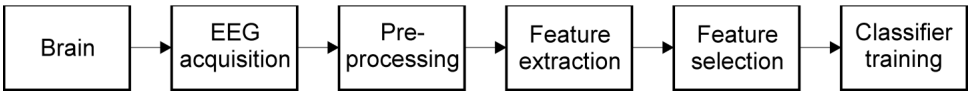

Figure 4.1. A process diagram of a sleep staging method development.

and applying Kappa analysis of confusion (also called error) matrices to obtain the accuracy of classifications.

4.2.2.1. Classification paradigms

Nine supervised classification methods were applied to differentiate the sleep stages at the individual level:

- Linear discriminant analysis (LD),
- Quadratic discriminant analysis (QD),
- Naïve Bayes classifier (NB),
- Feedforward neural network (FF),
- Radial basis function neural network (RB),
- Probabilistic neural network (PN),
- Adaptive neuro-fuzzy inference system (AN),
- Support vector machine with a linear kernel function (LS),
- Support vector machine with a radial basis kernel function (RS).

For all classifiers except of LS and RS we used the implementations available in different toolboxes of MATLAB. For support vector machine classifiers we applied the freely available LIBSVM library [131]. Based on individual-level classification accuracy performances and computational times RB and AN classification paradigms were excluded from group-level analysis. Namely, these two classifiers performed similarly or even worse, but their computational demand was higher several times (even more than 3 magnitudes in some cases) as compared to other classifiers. Thus, at the group level the remaining seven classification methods were applied only.

Here we provide a brief introduction of the applied classification paradigms, for more detailed description we refer to [132, 133]. LD and QD classifiers attempt to discriminate between different categories by separating them in the feature space using hyperplanes and hyperquadratic surfaces, respectively. In case of LD Matlab fits a multivariate normal density to each class, with a pooled estimate of covariance, while for QD it fits multivariate normal densities with covariance estimates stratified by class. These methods are attractive candidates for initial, trial classifiers [132]. The NB classifier

DOI:10.15774/PPKE.ITK.2010.008

applies the well-known Bayes classification rule and is designed for use when features are independent of one another within each class. However, it appears to work well in practice even when this independence assumption is not valid [132]. To model the distribution of features we used the *kernel* distribution since it does not require a strong assumption such as a normal distribution and can be used in cases where the distribution of a feature may be skewed or have multiple peaks or modes. For each feature a separate kernel density was estimated for each class based on the training data for that class. Usage of kernel distributions requires more computing time and more memory than the normal distribution. In demanding applications were the patterns are not linearly separable application of more sophisticated methods is advisable. A possible alternative approach may be multilayer neural networks. In this study we applied three different types of neural networks: FF, RB and PN. After optimizations of the parameters (see Appendix B) that have been carried out using the extracted features of the representative subject #16, we applied a FF classifier with a one hidden layer and five neurons. The spread of radial basis functions was equal to 1 and 0.1 for RB and PN classifiers, respectively. The AN classifier is a hybrid soft computational method that combines the advantages of fuzzy inference systems (FIS) and neural networks. A fuzzy inference system consists of three conceptual components: a fuzzy rule base, which contains a set of fuzzy if-then rules; a database, which defines the membership functions used in the fuzzy rules; and a reasoning mechanism, which performs the inference procedure upon the rules to derive a reasonable output or conclusion [134]. The extension of a FIS for optimization of its parameters and an example learning rule can be found in section 3.2 of [133]. After preliminary analyses we applied three Gaussian membership functions for all input features, a linear output membership function of the Sugeno-type inference system and the *genfis1* training method with default training parameters. Finally, we also assessed support vector machine (SVM) classifiers with linear and radial basis kernel functions. With an appropriate nonlinear function SVMs map the input features into sufficiently high dimension were the categories can be always separated by hyperplanes. The goal of SVMs is to find the separating hyperplanes with largest margins. The support vectors are transformed training patterns that are equally close to hyperplanes and denote the maximal margins. For a more detailed description of SVM classifiers see section 5.11 in [132]. After parameter optimization we used $C = 10$ cost parameter for LS and $C = 10000$, $\gamma = 0.01$ parameter combination for RS classifiers.

DOI:10.15774/PPKE.ITK.2010.008

4.2.2.2. Confusion matrix

A confusion matrix C is a $k \times k$ quadratic matrix, where k is the number of classes. Columns of C stand for the reference data (sleep staging performed by the human expert in this case) and rows denote the classified data. Hence, $C_{ij} = n_{ij}$ is a count of EEG segments scored by the human expert into the jth class but classified to the ith class using a specific classification paradigm. For an example see Table 4.I that presents the confusion matrix obtained by LD classification of sleep stages using ΔD measure in Cz channel of a representative subject #16.

TABLE 4.I. CONFUSION MATRIX OBTAINED FOR LD CLASSIFICATION OF SLEEP STAGES USING ESTIMATED ΔD VALUES IN CZ CHANNEL OF A REPRESENTATIVE SUBJECT #16.

		HEC (reference)			
		NREM 4	NREM 2	REM	n_{i+}
LDAC	NREM4	87	0	0	87
	NREM2	3	76	9	88
	REM	0	14	81	95
	n_{+j}	90	90	90	

The corresponding values are as follows: $\hat{K} = 0.85$, $\hat{\mathrm{var}}\left(\hat{K}\right) = 7.25\ 10^{-4}$ *and* $OA = 90.37$ *%. HEC: classification carried out by the human expert; LDAC: classification performed by linear discriminant analysis.*

The number of segments classified to the ith class using different classifiers is

$$n_{i+} = \sum_{j=1}^{k} n_{ij}, \tag{4.1}$$

while

$$n_{+j} = \sum_{i=1}^{k} n_{ij} \tag{4.2}$$

is the total number of segments scored to the jth sleep stage by the human expert. Let $p_{i,j}$ denote the proportion of samples in the i, jth cell of C, corresponding to $n_{i,j}$:

$$p_{ij} = \frac{n_{ij}}{n}, \tag{4.3}$$

where n is the total number of the analyzed EEG segments. Furthermore, marginals p_{i+} and p_{+j} can be defined by

DOI:10.15774/PPKE.ITK.2010.008

$$p_{i+} = \sum_{j=1}^{k} p_{ij} \tag{4.4}$$

and

$$p_{+j} = \sum_{i=1}^{k} p_{ij}. \tag{4.5}$$

4.2.2.3. Kappa analysis

The Kappa analysis is a technique used to statistically test whether two confusion matrices are significantly different. The result of Kappa analysis is a KHAT statistic ($\hat{K}$), an estimate of Kappa that is a measure of classification accuracy or agreement. It is based on the difference of the actual agreement (the major diagonal of the error matrix) and the chance agreement (indicated by the row and column totals, i.e. marginals). If the actual agreement is

$$p_o = \sum_{i=1}^{k} p_{ii} \tag{4.6}$$

and the chance agreement is defined as

$$p_c = \sum_{i=1}^{k} p_{i+} p_{+i}, \tag{4.7}$$

the estimate of Kappa is given by

$$\hat{K} = \frac{p_o - p_c}{1 - p_c} = \frac{n\sum_{i=1}^{k} n_{ii} - \sum_{i=1}^{k} n_{i+} n_{+i}}{n^2 - \sum_{i=1}^{k} n_{i+} n_{+i}}. \tag{4.8}$$

The variance of Kappa is as follows:

$$\hat{\mathrm{var}}\left(\hat{K}\right) = \frac{1}{n}\left[\frac{\theta_1(1-\theta_1)}{(1-\theta_2)^2} + \frac{2(1-\theta_2)(2\theta_1\theta_2 - \theta_3)}{(1-\theta_2)^3} + \frac{(1-\theta_2)^2(\theta_4 - 4\theta_2^2)}{(1-\theta_2)^4}\right], \tag{4.9}$$

where

$$\theta_1 = \frac{1}{n}\sum_{i=1}^{k} n_{ii}, \tag{4.10}$$

$$\theta_2 = \frac{1}{n^2}\sum_{i=1}^{k} n_{i+} n_{+i}, \tag{4.11}$$

DOI:10.15774/PPKE.ITK.2010.008

$$\theta_3 = \frac{1}{n^2}\sum_{i=1}^{k} n_{ii}\left(n_{i+} + n_{+i}\right), \tag{4.12}$$

and

$$\theta_4 = \frac{1}{n^3}\sum_{i=1}^{k}\sum_{j=1}^{k} n_{ij}\left(n_{j+} + n_{+i}\right)^2. \tag{4.13}$$

$\hat{K}$ can take values from the range $[-1,1]$. However, positive values are expected since there should be a positive correlation between classifications performed by human experts and machine classifiers. Landis and Koch characterized the possible ranges for KHAT into three groups [135]: a value greater than 0.80 (i.e., >80%) represents strong agreement; a value between 0.40 and 0.80 (i.e., 40–80%) represents moderate agreement; and a value below 0.40 (i.e., <40%) represents poor agreement. As it can be seen in Table 4.I, a strong agreement ($\hat{K} = 0.85$) between classifications performed by the human expert and LD was found using the ΔD measure in the central channel of subject #16.

It was shown that the Kappa analysis overestimates the proportion of randomness and thus underestimates the classification accuracy [136, 137]. Therefore, where applicable, we also provide the most widely used classification performance measure, the overall accuracy

$$OA = \frac{\sum_{i=1}^{k} n_{ii}}{n}. \tag{4.14}$$

For the particular confusion matrix presented in Table 4.I with $\hat{K} = 0.85$, the corresponding overall accuracy was 90.37 %.

The fact that the $\hat{K}$ statistic is asymptotically normally distributed provides a means for testing the significance of $\hat{K}$ for a single confusion matrix to determine if the agreement between the classifications performed by the human expert and a particular machine classifier is significantly grater than zero, i.e., the particular classification method performs better that than a random classifier. The test statistic is expressed by:

$$Z = \frac{\hat{K}}{\sqrt{\hat{\mathrm{var}}\left(\hat{K}\right)}}. \tag{4.15}$$

DOI:10.15774/PPKE.ITK.2010.008

Given the null hypothesis $H_0 : K = 0$, and the alternative $H_1 : K \neq 0$, H_0 is rejected if $Z \geq Z_{\alpha/2}$, where $\alpha/2$ is the confidence level of the two-tailed Z test.

Moreover, there is a test to compare if two confusion matrices are significantly different. This provides us the opportunity to compare classifications performed using different EEG measures, channels and classification paradigms. Let $\hat{K}_1$ and $\hat{K}_2$ ($\hat{\text{var}}\left(\hat{K}_1\right)$ and $\hat{\text{var}}\left(\hat{K}_2\right)$) denote the estimates of the Kappa statistic (estimates of variances) for confusion matrix #1 and #2, respectively. The test statistic in this case is defined as

$$Z = \frac{\left|\hat{K}_1 - \hat{K}_2\right|}{\sqrt{\hat{\text{var}}\left(\hat{K}_1\right) - \hat{\text{var}}\left(\hat{K}_2\right)}}. \tag{4.16}$$

Z is standardized and normally distributed. Given the null hypothesis $H_0 : K_1 - K_2 = 0$, and the alternative $H_1 : K_1 - K_2 \neq 0$, H_0 is rejected if $Z \geq Z_{\alpha/2}$.

Finally, in addition to computing statistics for an entire confusion matrix, it may be useful to look at the agreement of individual classes. Individual class accuracy can be tested using the conditional Kappa coefficient. The estimates of the conditional Kappa coefficient and its variance for the *i*th class are given by

$$\hat{K}_i = \frac{nn_{ii} - n_{i+}n_{+i}}{nn_{i+} - n_{i+}n_{+i}}, \tag{4.17}$$

and

$$\hat{\text{var}}\left(\hat{K}_i\right) = \frac{n\left(n_{i+} - n_{ii}\right)}{\left[n_{i+}\left(n - n_{+i}\right)\right]^3}\left[\left(n_{i+} - n_{ii}\right)\left(n_{i+}n_{+i} - nn_{ii}\right) + nn_{ii}\left(n - n_{i+} - n_{+i} + n_{ii}\right)\right], \tag{4.18}$$

respectively. The same comparison tests available for the Kappa coefficient also apply to this conditional Kappa for an individual class. For more details and comparison of Kappa analysis to other methods we refer to [136, 137].

4.2.2.4. Feature selection

Combination of the features was performed using the sequential forward feature selection (SFFS) method [138, 139]. A typical feature selection block diagram can be seen in Figure 4.2.

DOI:10.15774/PPKE.ITK.2010.008

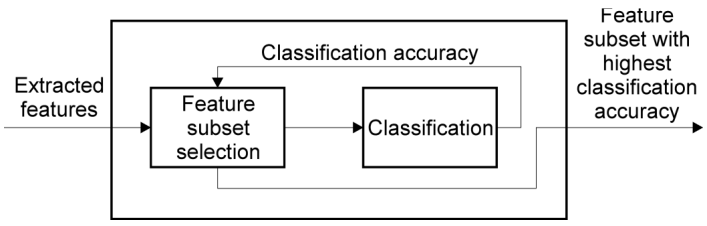

Figure 4.2. A process diagram of a feature selection.

A possible pseudo code of the SFFS algorithm is as follows:

```
already_selected_features = empty
#already_selected_features = 0
remaning_features = all_extracted_features
#remaning_features = #extracted_features
for i = 1 to #features_to_be_selected
    for j = 1 to #remaning_features
        actually_selected_features = already_selected_features + remaning_features(j)
        confusion_matrix = classification_with_nfold_cross_validation(actually_selected_features)
        classification_error(j) = 1 - abs(determine_KHAT(confusion_matrix))
    end
    jmin = index_of_the_minimal_value(classification_error)
    already_selected_fatures = already_selected_fatures + remaining_features(jmin)
    remaning_features = remaning_features - remaining_features(jmin)
    #already_selected_features = #already_selected_features + 1
    #remaning_features = #remaning_features - 1
end
```

In the first round the algorithm will select the best single feature that corresponds to the minimum value of the criterion function. In our case the criterion function is given by

$$\varepsilon(i) = 1 - \left|\hat{K}(i)\right|, \tag{4.19}$$

where $\hat{K}(i)$ stands for the classification accuracy of the *i*th feature and it is obtained from the confusion matrices after 10-fold cross-validation. In the next round the algorithm will select the second best feature from the remaining subset by combining all remaining features with the best one and by finding again the minimum of $\varepsilon(i)$. This procedure is continued until the desired number of features is achieved.

We applied the SFFS method in order to reveal the best single features and to find witch are the subsequent ones that provide most additional information. To assess the sleep

DOI:10.15774/PPKE.ITK.2010.008

stage discrimination capability of all measures and topographic locations we performed the feature selection using three different approaches:

- by combining the measures of single channels (*measure selection* - MS),
- by combining the channels for single measures (*channel selection* - CS),
- and by allowing the combination of all channel x measure pairs (*channel x measure selection* - CMS).

4.3. Results

4.3.1. Cross-validation and feature selection times

Cross-validation (CVT) and feature selection (FST) times obtained at the individual level can be seen in Figure 4.3. Considering CVT highest values were obtained for RB and AN classifiers. Cross-validations of the AN classifier were about 3000 times longer as compared to the LS paradigm that resulted in lowest values. The CVT increased systematically for higher feature numbers considering the NB and AN paradigms only. For other classifiers no systematic changes were found. However, FST increased for higher feature numbers for all feature selection approaches as well as for all classifiers.

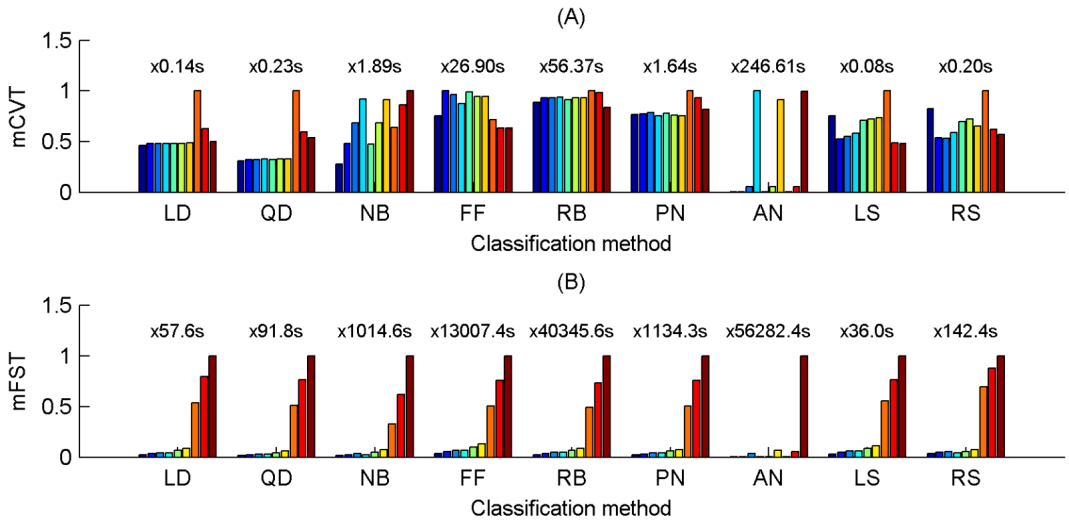

Figure 4.3. Individual-level overall median cross-validation (mCVT) and feature selection (mFST) times for all classification methods. Bars represent normalized values, real computation times in seconds can be obtained using multiplication factors presented above the bar diagrams. (A) First bars stand for cross-validations with a single input feature, 2^{nd}-4^{th} bars denote classifications with 2-4 measures of single channels, 5^{th}-7^{th} bars present results for classifications with 2-4 channels of single measures, 8^{th}-10^{th} bars stand for classifications using 2-4 measure x channel combinations as features. (B) Meaning of the bars is equal to those of 2^{nd}-10^{th} bars in (A) part of the Figure. To resolve the abbreviation of the classification methods see section 4.2.2.1.

DOI:10.15774/PPKE.ITK.2010.008

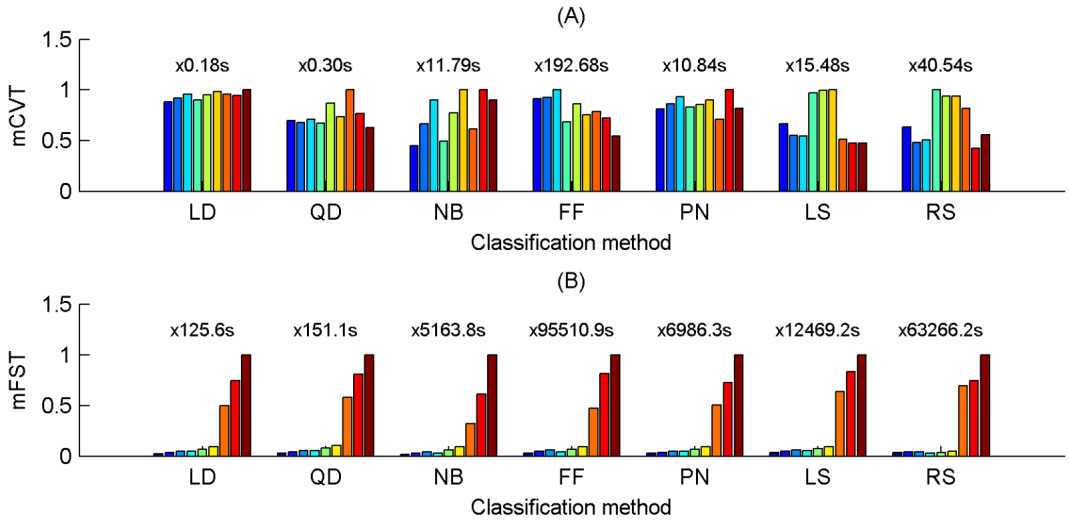

Figure 4.4. Group-level overall median cross-validation (mCVT) and feature selection (mFST) times for all classification methods. Bars represent normalized values, real computation times in seconds can be obtained using multiplication factors presented above the bar diagrams. (A) First bars stand for cross-validations with a single input feature, 2^{nd}-4^{th} bars denote classifications with 2-4 measures of single channels, 5^{th}-7^{th} bars present results for classifications with 2-4 channels of single measures, 8^{th}-10^{th} bars stand for classifications using 2-4 measure x channel combinations as features. (B) Meaning of the bars is equal to those of 2^{nd}-10^{th} bars in (A) part of the Figure. To resolve the abbreviation of the classification methods see section 4.2.2.1.

Similarly to CVT highest FST values occurred for RB and AN methods, while lowest values were found for the LS method. Based on these results we extrapolated the CVT and FST times for group-level analyses. Due to the high computation demand (and similar classification accuracy results as for other methods - see later) of RB and AN approaches we excluded these from further analyses.

At the group level (Figure 4.4) similar trends appeared for CVT and FST as compared to the individual-level. However, the computational time increased for specific paradigms by different factors. Highest increments were found for the SVM classifiers (350-450 times longer FSTs were obtained at the group level). LD and QD were found to be the fastest classifiers, while FF and RS methods were definitively the most computation demanding ones.

4.3.2. Discrimination of sleep stages using single EEG measures in single channels

Sleep stage classification results obtained by the LD classifier for all measures in all channels can be found in Figure 4.5. Maximal $\hat{K}$ values across subjects (Figure 4.5A) yielded best classifications for ΔD, f_{se} and $P_{\beta r}$ features. There were 9 channels with

DOI:10.15774/PPKE.ITK.2010.008

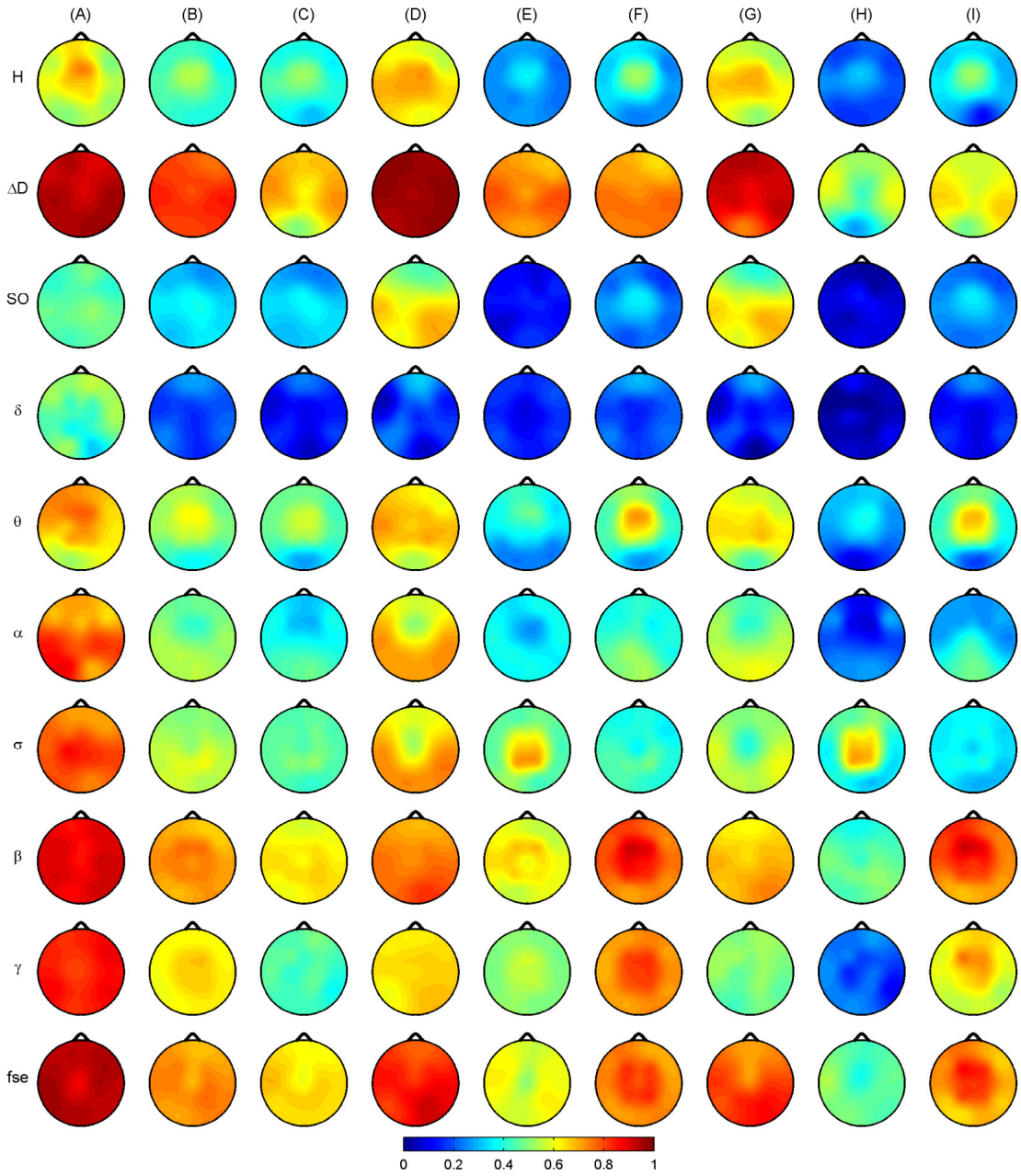

Figure 4.5. Sleep stage classification results obtained using linear discriminant analysis both at individual and group levels. (A) Maximal $\hat{K}$ values taken across subjects. (B) Averaged individual $\hat{K}$ values. (C) Group-level $\hat{K}$ values. (D) Individual conditional $\hat{K}$ values averaged across subjects for sleep stage NREM4. (E) Individual conditional $\hat{K}$ values averaged across subjects for sleep stage NREM2. (F) Individual conditional $\hat{K}$ values averaged across subjects for REM sleep. (G) Group-level conditional $\hat{K}$ for NREM4 sleep. (H) Group-level conditional $\hat{K}$ for sleep stage NREM2. (I) Group-level conditional $\hat{K}$ for REM sleep. Relative band powers are denoted by the labels of the corresponding frequency bands.

highest $\hat{K}$ values for ΔD and 8 channels for f_{se}. Kappa analysis did not reveal significant differences between the performances of these two measures at either channel

DOI:10.15774/PPKE.ITK.2010.008

TABLE 4.II. KAPPA ANALYSIS OF SLEEP STAGE CLASSIFICATIONS PERFORMED BY LINEAR DISCRIMINANT ANALYSIS.

Test	Measures	Channel																	
		Fp2	F8	T4	T6	O2	Fp1	F7	T3	T5	O1	F4	C4	P4	F3	C3	P3	Fz	Cz
imax (A)	ΔD vs. β	>	>	>	>	>*	>*	>	>	>	>*	>	>	>	>	>	>	>	>
	ΔD vs. fse	<	<	>	>	>	>	<	<	<	>	<	<	>	<	>	>	=	>
	fse vs. β	>	>*	>	>	>	>*	>	>*	>*	>*	>	>	>	>	>	>	>	>
g (C)	ΔD vs. β	>*	>*	>*	>*	<*	>*	>*	>*	>	<*	>	>	<	>*	>*	<	>	>
	ΔD vs. fse	>*	>*	>*	>*	<*	>*	>*	>*	<	<*	>	>	<	>	>*	<	>*	>
	fse vs. β	>*	>	>*	<	>	>*	>*	>*	>*	>*	<	>	>	>	>	>	<*	<
gcN4 (G)	ΔD vs. β	>*	>*	>*	>*	>*	>*	>*	>*	>*	>*	>*	>*	>*	>*	>*	>*	>*	>*
	ΔD vs. fse	>*	>*	>*	>*	<*	>*	>*	>*	>*	<*	>*	>*	>*	>*	>*	>*	>*	>*
	fse vs. β	>*	>*	>*	>*	>*	>*	>*	>*	>*	>*	>*	>*	>*	>*	>*	>*	>*	>*
gcN2 (H)	ΔD vs. β	>*	>*	>*	>	<*	>*	>*	>*	>	<*	>	>	<	>*	>*	<	>*	>
	ΔD vs. fse	>*	>*	>*	>*	<*	>*	>*	>*	<	<*	>*	>*	>	>*	>*	>	>*	>
	fse vs. β	>	>	>	<*	<	>*	>*	>*	>	>*	<	<	<*	>	<	<	<*	<
gcR (I)	ΔD vs. β	<*	<*	<*	<*	<*	<*	<*	<*	<*	<*	<*	<*	<*	<*	<*	<*	<*	<*
	ΔD vs. fse	<*	<*	<*	<	<*	<*	<*	<*	<*	<*	<*	<*	<*	<*	<*	<*	<*	<*
	fse vs. β	<*	<*	<*	<*	<	<*	<*	<*	<*	<	<*	<*	<	<*	<*	<	<*	<

imax: maximal $\hat{K}$ values taken across subjects; g: group-level $\hat{K}$ values; gcN4: group-level conditional $\hat{K}$ values for NREM4; gcN2: group-level conditional $\hat{K}$ values for NREM2; gcR: group-level conditional $\hat{K}$ values for REM. Letters in brackets indicate the appropriate columns in Figure 4.5. The > (<) sign denotes grater (smaller) $\hat{K}$ values of front measures. Significance of differences was determined using a 95% confidence level (Zc = 1.96) and marked by an asterisk. β denotes the relative power of the beta frequency band.

(Table 4.II, *imax* test). Taking the average of $\hat{K}$ values across subjects, ΔD provided the best performance in all channels (Figure 4.5B). At the group level (Figure 4.5C) highest $\hat{K}$ values were also found for ΔD in most of the channels (except for T5, P3, P4, O1 and O2 channels) followed by measures f_{se} and $P_{\beta r}$. Comparing these three measures there were 8 channels (with a predominance of circumferential electrodes) where ΔD achieved significantly better performance compared to measures f_{se} and $P_{\beta r}$ (Table 4.II, *g* test). Considering the individual-level conditional $\hat{K}$ values averaged across subjects ΔD showed best performance for NREM4 (Figure 4.5D) as well as for NREM2 (Figure 4.5E) in all channels while during REM ΔD, $P_{\beta r}$, $P_{\gamma r}$ and f_{se} revealed similar performance (Figure 4.5F). Group-level conditional $\hat{K}$ values were presented in the last three columns of Figure 4.5 (G, H, I). For NREM4 (Figure 4.5G), ΔD showed the best classification results in all channels except for the occipital electrodes (Table 4.II, *gcN4* test). During

DOI:10.15774/PPKE.ITK.2010.008

TABLE 4.III. MAXIMAL $\hat{K}$ VALUES, CORRESPONDING OVERALL ACCURACY VALUES AND EEG DERIVATIONS OF ΔD, $P_{\beta r}$ AND f_{se} MEASURES FOR ALL COLUMNS IN FIGURE 4.5.

	Measure		
	ΔD	**$P_{\beta r}$**	**fse**
(A)	0.9667, (97.78); T6, O2 (3)	0.9167, (94.44); T6 (3)	0.9611, (97.41); T3, T5 (3)
(B)	0.8432, (89.55); T4	0.7585, (83. 9); F3	0.7657, (84.38); P4
(C)	0.7210, (81.4); T4	0.6695, (77.97); P4	0.6877, (79.19); T3
(D)	0.9810; T4	0.8215; O2	0.9193; O2
(E)	0.7927; T3	0.6753; F4	0.6327; T6
(F)	0.7652; T6	0.9047; Fz	0.8270; F3
(G)	0.9440; Fp1	0.7361; O2	0.8649; O2
(H)	0.6053; T4	0.5153; P4	0.5305; T3
(I)	0.6616; T6	0.9083; F3	0.8599; F3

First column denote column labels in Figure 4.5. (A) Maximal $\hat{K}$ values taken across subjects. (B) Averaged individual $\hat{K}$ values. (C) Group-level $\hat{K}$ values. (D) Individual conditional $\hat{K}$ values averaged across subjects for sleep stage NREM4. (E) Individual conditional $\hat{K}$ values averaged across subjects for sleep stage NREM2. (F) Individual conditional $\hat{K}$ values averaged across subjects for REM sleep. (G) Group-level conditional $\hat{K}$ for NREM4 sleep. (H) Group-level conditional $\hat{K}$ for sleep stage NREM2. (I) Group-level conditional $\hat{K}$ for REM sleep. Overall accuracy is provided in brackets only where applicable (the first three rows only). In the first row the subject id is also provided in brackets after the channel labels to denote for which subject(s) were the maximal $\hat{K}$ values found.

NREM2 best performance was also achieved for ΔD in most channels (13 out of 18 channels) (Figure 4.5H). Performance of ΔD significantly exceeded those of f_{se} and $P_{\beta r}$ in 9 channels (Table 4.II, *gcN2* test). By contrast, during REM f_{se} and $P_{\beta r}$ significantly outperformed ΔD in all channels (Table 4.II, *gcR* test). Best classifications were obtained for measure $P_{\beta r}$ in all channels. For all columns presented in Figure 4.5 maximal $\hat{K}$ values of ΔD were found in the circumferential channels (Table 4.III) with the best performance in T4 channel in 4 cases including mean $\hat{K}$ values for the individual level (row B), $\hat{K}$ values at the group level (row C) as well as conditional $\hat{K}$ values in rows D and H. As can be seen in Table 4.III, best classification performance across EEG measures was found for ΔD considering all rows with the exception of rows (F, I) that is the conditional values for REM. In (rows A-C) best classifications of ΔD exceeded 80 % overall accuracy (peaking in 97.78 % at individual level for subject #3). Compared with other measures, H generally performed below the average with central peaks in $\hat{K}$ values. In contrast to its general low level of performance it quite efficiently

DOI:10.15774/PPKE.ITK.2010.008

TABLE 4.IV. MEASURE X CHANNEL COMBINATIONS CORRESPONDING TO MAXIMAL $\hat{K}$ VALUES.

Condition	Classification method							Best classifiers
	LD	QD	NB	FF	PN	LS	RS	
(A)	ΔD; 0.9667, (97.78); T6, O2 (3)	β; 0.9722, (98.15); F8, T4, O1, F4 (14), F3 (3)	β; 0.9778, (98.52); T4 (14)	β; 0.9722, (98.15); O2 (14) / fse; T3 (3)	ΔD; 0.9667, (97.78); T6, O2 (3) / fse; F3 (3)	fse; 0.9778, (98.52); T3 (3)	fse; 0.9667, (97.78); T3 (3)	NB / LS
(B)	ΔD; 0.8432, (89.55); T4	ΔD; 0.8483, (89.89); T3	ΔD; 0.8501, (90.02); T4	ΔD; 0.8288, (88.6); T4	ΔD; 0.8468, (89.8); T4	ΔD; 0.8463, (89.76); T4	ΔD; 0.8463, (89.76); T4	NB
(C)	ΔD; 0.721, (81.4); T4	ΔD; 0.7258, (81.72); T4	ΔD; 0.728, (81.87); T4	β; 0.7268, (81.79); F3	ΔD; 0.7283, (81.89); T4	ΔD; 0.7288, (81.92); T4	ΔD; 0.7273, (81.82); T3	LS
(D)	ΔD; 0.982; T4	ΔD; 0.9824; F7	ΔD; 0.9825; T4	ΔD; 0.9723; Fp1	ΔD; 0.9807; T4	ΔD; 0.9805; T4	ΔD; 0.9838; T4	RS
(E)	ΔD; 0.7927; T3	ΔD; 0.7888; T3	ΔD; 0.7826; T3	ΔD; 0.7597; T3	σ; 0.8949; P3	σ; 0.8499; F4	ΔD; 0.7752; T3	PN
(F)	β; 0.9047; F3	β; 0.8839; F3	β; 0.8609; F3	β; 0.8388; F3	β; 0.9354; Fz	β; 0.9662; Fz	β; 0.891; Fz	LS
(G)	ΔD; 0.944; Fp1	ΔD; 0.9353; Fp1	ΔD; 0.9173; Fp1	ΔD; 0.912; Fp2	ΔD; 0.9325; Fp1	ΔD; 0.9226; Fp1	ΔD; 0.9227; Fp1	LD
(H)	σ; 0.6778; Cz	σ; 0.7531; F4	σ; 0.6536; P3	σ; 0.6454; P4	σ; 0.8673; F4	σ; 0.6977; F3	σ; 0.6817; P3	PN
(I)	β; 0.9083; F3	β; 0.8867; F3	fse; 0.8192; F3	fse; 0.808; F3	β; 0.9733; F3	fse; 0.8445; Fz	fse; 0.8399; Fz	PN

Measure x channel combinations corresponding to maximal $\hat{K}$ values for columns of Figure 4.5 and figures in Appendix C. Overall accuracy is provided after the $\hat{K}$ values in brackets only where applicable (first three rows). In the first row the subject id is also provided in brackets after the channel labels to denote for which subject(s) were the maximal $\hat{K}$ values found. Labels in the first column of the table correspond to column labels of Figure 4.5 and figures in Appendix C with the following meaning. (A) Maximal $\hat{K}$ values taken across subjects. (B) Averaged individual $\hat{K}$ values. (C) Group-level $\hat{K}$ values. (D) Individual conditional $\hat{K}$ values averaged across subjects for sleep stage NREM4. (E) Individual conditional $\hat{K}$ values averaged across subjects for sleep stage NREM2. (F) Individual conditional $\hat{K}$ values averaged across subjects for REM sleep. (G) Group-level conditional $\hat{K}$ for NREM4 sleep. (H) Group-level conditional $\hat{K}$ for sleep stage NREM2. (I) Group-level conditional $\hat{K}$ for REM sleep. Relative band powers are denoted by the labels of the corresponding frequency bands. To resolve the abbreviation of the classification methods see section 4.2.2.1.

classified NREM4. When regarding results obtained for relative band powers (Figure 4.5), higher overall performance was found for faster brain activities. In general, better

DOI:10.15774/PPKE.ITK.2010.008

classification results were found for NREM4 as compared with NREM2 and REM. Worst and non-significant (comparing against a random classifier) classification results were obtained at group level for sleep stage NREM2 using measures P_{SOr} (channel Fp2) and $P_{\delta r}$ (channels F3, Fz, F4, F7, C4).

Classification results obtained by QD, NB, FF, PN, LS and RS paradigms can be found in Appendix C. Comparing the results obtained for all classifiers we found some differences considering specific channel x measure combinations. E.g. comparing to other classifiers lower group-level KHAT values appeared for PN and LS paradigms in all channels when the $P_{\gamma r}$ measure was applied. However, overall classification profiles were similar across the classification methods and this was also reflected in channel x measure combinations exhibiting best classifications (Table 4.IV). Considering both averaged individual and group-level results we obtained best sleep stage classification performance in most of the EEG channels and for most of the classifications methods by applying the multifractal measure ΔD.

Moreover, best classifications for ΔD were achieved in temporal channel T4 for most of the classifiers at both levels. Using the ΔD x T4 single feature at the group level highest overall accuracy (OA=81.92 %) was achieved by a support vector machine with a linear kernel function, while individual-level analysis revealed best average classification result (OA=90.02 %) for a naïve Bayes classifier. Overall maximal individual-level classifications were achieved by ΔD, f_{se} and $P_{\beta r}$ measures depending on the classification method. Best results were found for subjects #3 and #14 achieving even 98.52 % overall accuracy.

4.3.3. Combination of EEG measures and channels

Considering group-level results supplementation of the best single features by appropriate second ones significantly improved the overall sleep stage classification performance (Table 4.V, row *g*). Addition of a second measure for the same channel and addition of another channel x measure feature enhanced the performance of more classifiers as compared to addition of a second channel for the same measure. Conditional Kappa analysis (Table 4.V, rows *gcN4*, *gcN2* and *gcR*) revealed that the overall classification accuracy improved for many classifiers due to the higher classification accuracy of NREM2 and REM sleep stages. This can be also observed for the MS feature selection approach by comparing last three columns of Figure 4.6 and

DOI:10.15774/PPKE.ITK.2010.008

Figure 4.7. It can be seen that the addition of the second measures most significantly improves the classifications of NREM2 and REM stages and this is especially true for channels placed around the vertex. Going further by comparing Figure 4.7 and Figure 7.13 as well as by comparing Figure 7.13 and Figure 7.14 it can be seen that the addition of further measures improves the overall and conditional classification performance in several channels in most of the classifiers. However, significant improvements can be achieved by combining of up to three measures (Table 4.VI, first two rows). Comparing best classifications obtained by combining 2, 3 and 4 channels for single measures (Table 4.VI, rows 3-4) it becomes clear that addition of third and fourth channels does provide further significant improvements.

TABLE 4.V. A COMPARISON OF FEATURE SELECTION APPROACHES APPLYING ONLY ONE OR TWO FEATURES.

Level	Comparison	Classification method							SC
		LD	QD	NB	FF	PN	LS	RS	
g	2M/1CM	*	*	*	*	*	*	*	7
	2C/1CM	*	*	x	*	x	x	*	4
	2CM/1CM	*	*	*	*	*	*	*	7
gcN4	2M/1CM	x	x	x	x	x	x	x	0
	2C/1CM	x	x	x	*	x	x	x	1
	2CM/1CM	x	x	x	*	x	x	x	1
gcN2	2M/1CM	x	*	*	*	x	*	*	5
	2C/1CM	x	x	x	*	x	x	*	2
	2CM/1CM	*	x	*	*	*	*	*	6
gcR	2M/1CM	*	*	*	*	*	*	*	7
	2C/1CM	x	x	*	x	*	x	*	3
	2CM/1CM	*	*	*	x	*	*	*	6

Group-level overall (g) and conditional (gcN4-NREM4, gcN2-NREM2, gcR-REM) Kappa analyses were based on confusion matrices corresponding to maximal $\hat{K}$ values. 2M denotes selections of two best measures for single channels, 2C stands for selections of two best channels considering single measures and 1CM-2CM stand for selections of 1-2 best channel x measure combinations. Significant differences are denoted by an asterisk, while not significant differences are marked by x. Sums of classification methods that exhibited significant differences are presented in the last column (SC). A one-sided test was used with Zc = 2.45 value for the Bonferoni corrected $\alpha_B = 0.05/7$ since feature selection approaches before the slashes are supposed to provide better classifications by theory. To resolve the abbreviation of the classification methods see section 4.2.2.1.

DOI:10.15774/PPKE.ITK.2010.008

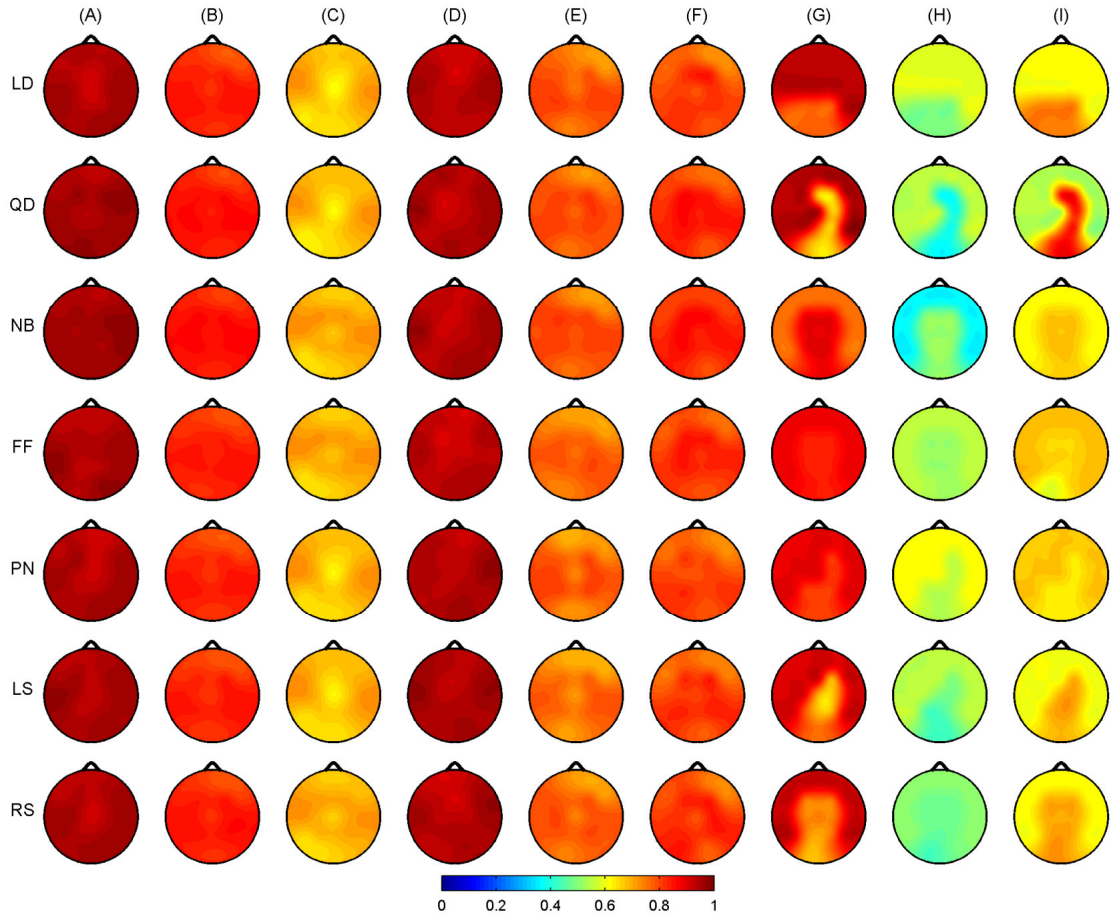

Figure 4.6. $\hat{K}$ *values achieved by first best measures in particular channels. Rows present results for different classifiers. Meaning of the column labels is as follows. (A) Maximal* $\hat{K}$ *values taken across subjects. (B) Averaged individual* $\hat{K}$ *values. (C) Group-level* $\hat{K}$ *values. (D) Individual conditional* $\hat{K}$ *values averaged across subjects for sleep stage NREM4. (E) Individual conditional* $\hat{K}$ *values averaged across subjects for sleep stage NREM2. (F) Individual conditional* $\hat{K}$ *values averaged across subjects for REM sleep. (G) Group-level conditional* $\hat{K}$ *for NREM4 sleep. (H) Group-level conditional* $\hat{K}$ *for sleep stage NREM2. (I) Group-level conditional* $\hat{K}$ *for REM sleep. To resolve the abbreviation of the classification methods see section 4.2.2.1.*

However, a combination of up to four channel x measure features may result in further significant improvements (Table 4.VI, rows 5-6). Table 4.VI also shows that combinations of measures in single channels provide significantly better classifications when compared to combinations of channels using single measures (rows 7-9). Furthermore, combinations of channel x measure features perform significantly better as compared to the other two feature selection approaches (CS and MS). Note that MS and CMS approaches may result in similar classification performances for combination of two features (Table 4.VI, row 13).

DOI:10.15774/PPKE.ITK.2010.008

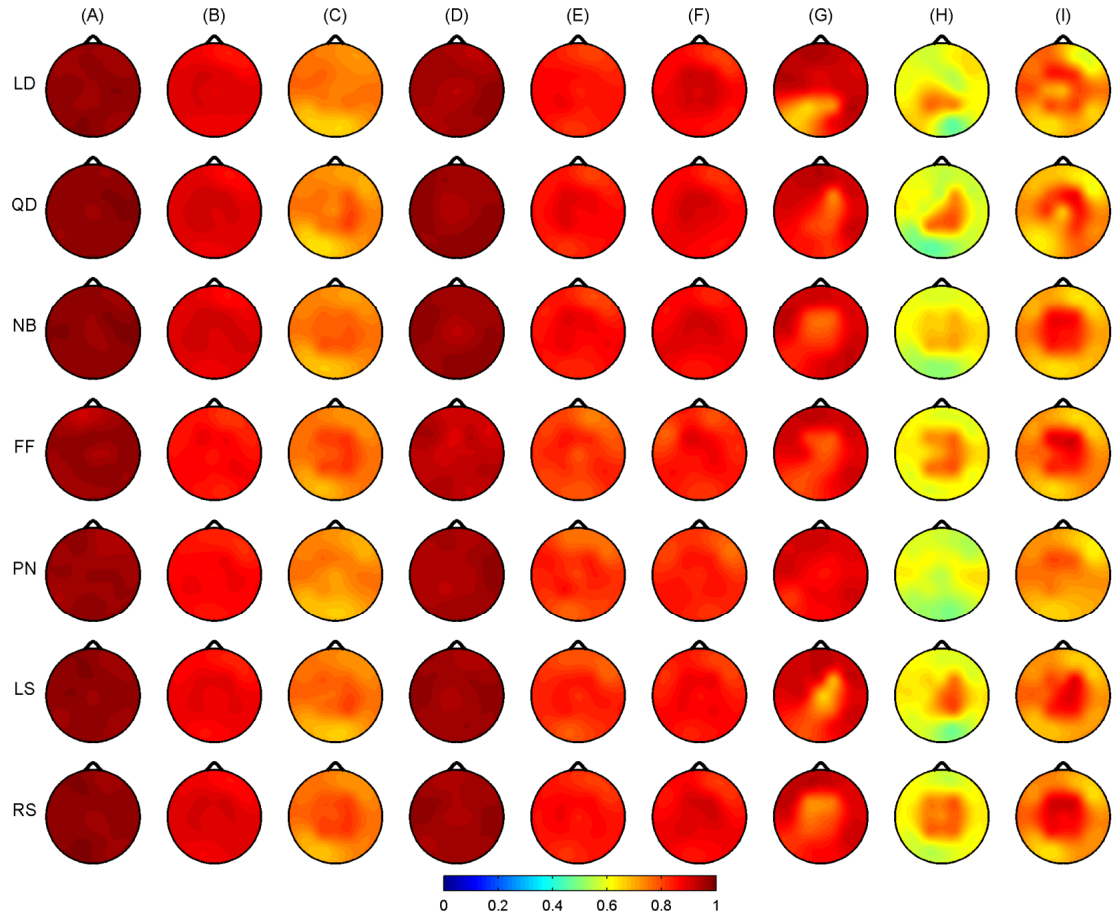

Figure 4.7. $\hat{K}$ *values achieved by combination of two best measures in particular channels. Rows present results for different classifiers. Meaning of the column labels is as follows. (A) Maximal* $\hat{K}$ *values taken across subjects. (B) Averaged individual* $\hat{K}$ *values. (C) Group-level* $\hat{K}$ *values. (D) Individual conditional* $\hat{K}$ *values averaged across subjects for sleep stage NREM4. (E) Individual conditional* $\hat{K}$ *values averaged across subjects for sleep stage NREM2. (F) Individual conditional* $\hat{K}$ *values averaged across subjects for REM sleep. (G) Group-level conditional* $\hat{K}$ *for NREM4 sleep. (H) Group-level conditional* $\hat{K}$ *for sleep stage NREM2. (I) Group-level conditional* $\hat{K}$ *for REM sleep. To resolve the abbreviation of the classification methods see section 4.2.2.1.*

Considering overall group-level classification results (Figure 4.8) better classification were obtained using FF and SVM classifiers as compared to the traditional methods such as LD, QD and NB. Nevertheless, this tendency was not true at the individual level, where the traditional methods performed even better, especially in cases where the number of features was higher (see Figure 1.0).

When comparing the maximal classification performances of individual and group levels it can be observed that as expected better discrimination of sleep stages can be obtained at the individual level achieving even 100 % overall accuracy for several subjects.

DOI:10.15774/PPKE.ITK.2010.008

TABLE 4.VI. A COMPARISON OF DIFFERENT FEATURE SELECTION APPROACHES BASED ON CONFUSION MATRICES CORRESPONDING TO MAXIMAL $\hat{K}$ VALUES OBTAINED AT THE GROUP LEVEL.

Comparison	Classification method							SC
	LD	QD	NB	FF	PN	LS	RS	
3M/2M	*	x	*	*	x	*	*	5
4M/3M	x	x	x	x	x	x	x	0
3C/2C	x	x	x	x	x	x	x	0
4C/3C	x	x	x	x	x	x	x	0
3CM/2CM	*	*	*	*	*	*	*	7
4CM/3CM	x	x	x	x	x	*	*	2
2M/2C[1]	>	>*	>*	>*	>	>*	>*	5
3M/3C[1]	>*	>*	>*	>*	>	>*	>*	6
4M/4C[1]	>*	>*	>*	>*	>	>*	>*	6
2CM/2C	*	*	*	*	*	*	*	7
3CM/3C	*	*	*	*	*	*	*	7
4CM/4C	*	*	*	*	*	*	*	7
2CM/2M	*	x	x	x	*	x	x	2
3CM/3M	*	*	*	*	*	*	*	7
4CM/4M	*	*	*	*	*	*	*	7

2M-4M denote selections of 2-4 best measures for single channels, 2C-4C stand for selections of 2-4 best channels considering single measures and 2CM-4CM stand for selections of 2-4 best channel x measure features. Significant differences are denoted by an asterisk, while not significant differences are marked by x. Sums of classification methods that exhibited significant differences are presented in the last column (SC). A one-sided test was used with Zc = 2.45 value for the Bonferoni corrected $\alpha_B = 0.05/7$ in those comparisons where feature selection approaches before the slashes provided better classifications by theory. For other comparisons[1] a two-sided test was used by applying a critical Zc = 2.69 value for the Bonferoni corrected $\alpha_B = (0.05/2)/7$. The > sign denotes that feature selection approaches before the slashes provided better classifications. To resolve the abbreviation of the classification methods see section

The superiority FF and SVM classifiers also appeared for the best group-level classification results obtained for different feature selection approaches and feature numbers (Table 4.VII). Specifically, the FF and RS methods were found to be the best classifiers significantly outperforming the traditional paradigms in most of the cases (see Table 4.VII, last column). Combining different measures in single channels (Table 4.VII, rows 2M, 3M and 4M) best classifications appeared for F3, C3, C4 and P4 channels by combining in most of the cases ΔD, $P_{\beta r}$, $P_{\sigma r}$, f_{se} and H measures. ΔD was selected usually as the best or third best (after $P_{\beta r}$, $P_{\sigma r}$) measure. H was selected only as the fourth measure. Best classifications for the CS feature selection approach (Table 4.VII, rows 2C, 3C and 4C) were achieved in most of the cases by ΔD and $P_{\beta r}$ measures. For measure ΔD best classifications were obtained usually by combining T3, T4, F8, O1, O2, Fp1 and Fp2 channels. For $P_{\beta r}$ the F3, F4, O2, F7, F8 and Fz channels were selected.

DOI:10.15774/PPKE.ITK.2010.008

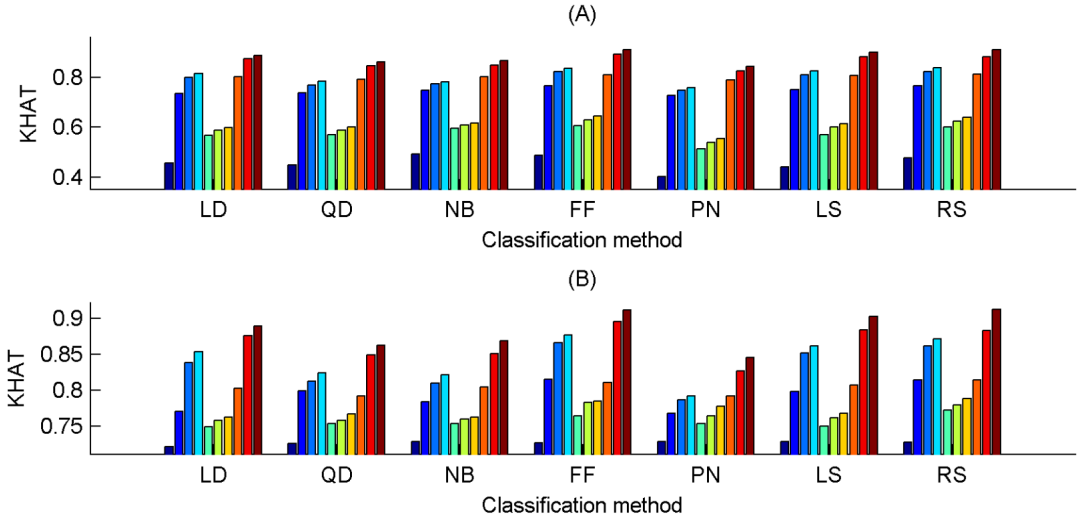

Figure 4.8. Overall averages of group-level $\hat{K}$ values (A) and maximal group-level $\hat{K}$ values (B) f for different feature selection approaches and classification methods. First bars stand for classifications based on a single feature, 2^{nd}-4^{th} bars denote classifications with 2-4 measures of single channels, 5^{th}-7^{th} bars present results for classifications obtained by combination of 2-4 channels for a same measure, 8^{th}-10^{th} bars stand for classifications using 2-4 channel x measure combinations as features. Note that the last three bars are equal in (A) and (B) cases. To resolve the abbreviation of the classification methods see section 4.2.2.1.

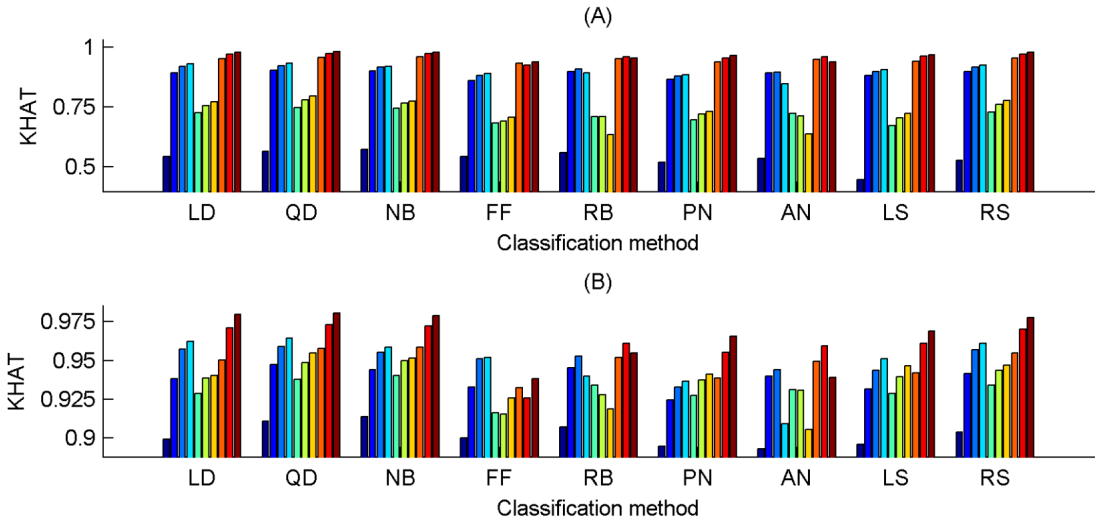

Figure 4.9. Overall averages of individual $\hat{K}$ values (A) and averages of individual-level maximal $\hat{K}$ values (B) for different feature selection approaches and classification methods. First bars stand for classifications based on a single input feature, 2^{nd}-4^{th} bars denote classifications with 2-4 measures of single channels, 5^{th}-7^{th} bars present results for classifications with 2-4 channels of single measures, 8^{th}-10^{th} bars stand for classifications using 2-4 measure x channel combinations as features. To resolve the abbreviation of the classification methods see section 4.2.2.1.

DOI:10.15774/PPKE.ITK.2010.008

TABLE 4.VII. FEATURE COMBINATIONS CORRESPONDING TO MAXIMAL $\hat{K}$ VALUES OBTAINED AT THE GROUP LEVEL.

FS	Classification method							DOC
	LD	QD	NB	FF	PN	LS	RS	
2M	ΔD, β; 0.7708, (84.72); F3	β, σ; 0.799, (86.6); P4	β, σ; 0.784, (85.6); P4	β, σ; 0.8149, (87.66); C4	ΔD, fse; 0.7673, (84.49); F3	β, σ; 0.7985, (86.56); C4	β, σ; 0.8139, (87.59); C4	FF, RS, QD, LS, NB*, LD*, PN*
3M	ΔD, σ, β; 0.8382, (89.21); C3	β, σ, ΔD; 0.8126, (87.51); C4	β, σ, ΔD; 0.8098, (87.32); C4	β, σ, ΔD; 0.8655, (91.04); F3	ΔD, fse, σ; 0.786, (85.74); F3	ΔD, β, σ; 0.8516, (90.11); F3	β, σ, ΔD; 0.8612, (90.75); F3	FF, RS, LS, LD*, QD*, NB*, PN*
4M	ΔD, σ, β, H; 0.8536, (90.24); C3	β, σ, ΔD, H; 0.8238, (88.25); C4	β, σ, ΔD, H; 0.821, (88.07); C3	β, σ, ΔD, γ; 0.8767, (91.78); F3	ΔD, fse, σ, θ; 0.7918, (86.12); F3	ΔD, β, σ, H; 0.8612, (90.75); C3	β, σ, ΔD, H; 0.8711, (91.41); F3	FF, RS, LS, LD*, QD*, NB*, PN*
2C	ΔD; 0.7488, (83.25); T4, T3	ΔD; 0.7537, (83.58); T4, T3	β; 0.7534, (83.56); F3, O2	β; 0.7643, (84.28); F4, O2	ΔD; 0.7536, (83.58); T4, T3	ΔD; 0.7501, (83.34); T4, T3	β; 0.7724, (84.82); F3, O2	RS, FF, QD, PN, NB, LS, LD
3C	ΔD; 0.7582, (83.88); T4, T3, F8	ΔD; 0.7577, (83.85); T4, T3, F8	β; 0.7594, (83.96); F3, O2, F8	β; 0.7825, (85.5); F3, O2, F8	ΔD; 0.7642, (84.28); T4, T3, O1	ΔD; 0.7612, (84.08); T4, T3, Fp1	β; 0.7792, (85.28); F3, O2, F8	FF, RS, PN, LS, NB, LD*, QD*
4C	ΔD; 0.7623, (84.15); T4, T3, F8, O2	ΔD; 0.7671, (84.47); T4, T3, F8 , O1	β; 0.762, (84.13); F3, O2, F8, Fz	β; 0.785, (85.67); F3, O2, F7, T4	ΔD; 0.7779, (85.2); T4, T3, O1, Fp2	ΔD; 0.7675, (84.5); T4, T3, Fp1, T5	fse; 0.7886, (85.9); T3, F3, O2, T4	RS, FF, PN, LS, QD, LD*, NB*
2CM	ΔDxT4, βxFz; 0.8025, (86.83)	ΔDxT4, βxFz; 0.7921, (86.14)	ΔDxT4, βxF3; 0.8043, (86.95)	ΔDxT4, βxF3; 0.8108, (87.39)	ΔDxT4, fsexF3; 0.7916, (86.11)	ΔDxT4, βxF3; 0.8073, (87.15)	ΔDxT3, βxF3; 0.8139, (87.59)	RS, FF, LS, NB, LD, QD, PN
3CM	ΔDxT4, βxFz, σxP3; 0.8759, (91.73)	ΔDxT4, βxFz, σxC4; 0.8486, (89.91)	ΔDxT4, βxF3, σxCz; 0.8509, (90.06)	βxF3, σxCz, ΔDxF8; 0.8952, (93.01)	ΔDxT4, fsexF3, σxP3; 0.8268, (88.45)	ΔDxT4, βxF3, σxCz; 0.8835, (92.23)	ΔDxT3, βxF3, σxCz; 0.8825, (92.17)	FF, LS, RS, LD*, NB*, QD*, PN*
4CM	ΔDxT4, βxFz, σxP3, αxP3; 0.8896, (92.64)	ΔDxT4, βxFz, σxC4, ΔDxFp2; 0.8628, (90.85)	ΔDxT4, βxF3, σxCz, αxO2; 0.8688, (91.26)	ΔDxT4, βxF3, σxCz, αxO2; 0.9116, (94.11)	ΔDxT4, fsexF3, σxP3, ΔDxFp1; 0.8455, (89.7)	ΔDxT4, βxF3, σxCz, αxO2 ; 0.9025, (93.5)	ΔDxT3, βxF3, σxCz, αxO2; 0.9126, (94.18)	RS, FF, LS, LD*, NB*, QD*, PN*

Best feature combinations, corresponding $\hat{K}$ and overall accuracy (in brackets) values are shown for different feature selection (FS) approaches and different classification paradigms. 2M-4M denote selections of 2-4 best measures for single channels, 2C-4C stand for selections of 2-4 best channels considering single measures and 2CM-4CM stand for selections of 2-4 best measure x channel combinations. Last column denotes decreasing orders of classifiers (DOC) according to the achieved $\hat{K}$ values. Best classifiers were statistically compared to other methods using a one-sided Z test with a critical Zc = 2.4 value for the Bonferoni corrected $\alpha_B = 0.05/6$. Methods with significantly lower performance are marked by an asterisk. Relative band powers are denoted by the labels of the corresponding frequency bands. For abbreviations of the classification methods see section 4.2.2.1.

Combining arbitrary channel x measure features best classifications were found in most of the cases by combining ΔD measure of temporal (T3, T4) channels, $P_{\beta r}$ in F3 and Fz channels, $P_{\sigma r}$ in centro-parietal (C4, Cz, P3) channels and $P_{\alpha r}$ in channel O2. ΔD was

DOI:10.15774/PPKE.ITK.2010.008

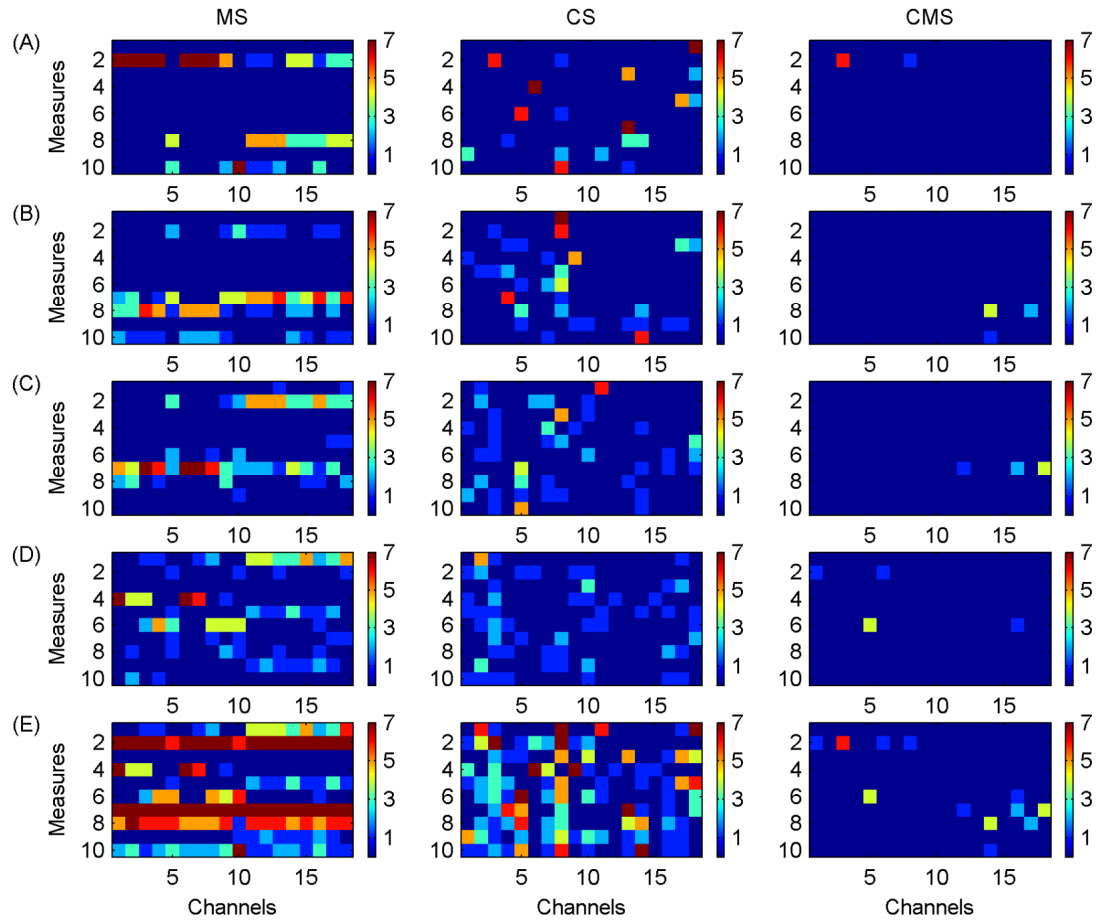

Figure 4.10. Group-level feature selection results. Number of cases (paradigms) when particular measures were selected as the best measures in single channels (MS), particular channels were selected as the best channels considering particular measures (CS) and when particular channel x measure combinations were selected as the best features according to the obtained $\hat{K}$ values. (A)-(D) denote cases when particular measures, channels and channel x measure combinations were found to be the 1st, 2nd, 3rd and 4th best features, respectively. Row (E) stands for sums of cases presented in rows (A)-(D). The order of the measures is H, ΔD, P_{SOr}, $P_{\delta r}$, $P_{\theta r}$, $P_{\alpha r}$, $P_{\sigma r}$, $P_{\beta r}$, $P_{\gamma r}$, f_{se}, while the order of the channels is as follows: Fp2, F8, T4, T6, O2, Fp1, F7, T3, T5, O1, F4, C4, P4, F3, C3, P3, Fz, Cz.

selected as the best feature in most of the cases and it was usually followed by $P_{\beta r}$, $P_{\sigma r}$ and $P_{\alpha r}$. This order was also true for the best overall classification (OA=94.18 %) that was obtained by combining the ΔD x T3, $P_{\beta r}$ x F3, $P_{\sigma r}$ x Cz and $P_{\alpha r}$ x O2 features and applying a support vector machine classifier with a radial basis kernel function.

The previously described trends in selection of specific measures and channels are presented in a more detailed way in Figure 4.10 and summarized in Figure 4.11 and Figure 4.12 to emphasize the importance of particular features.

As it can be seen from these figures the selection of measures and channels was very similar across the classification paradigms when feature selection was carried out on

DOI:10.15774/PPKE.ITK.2010.008

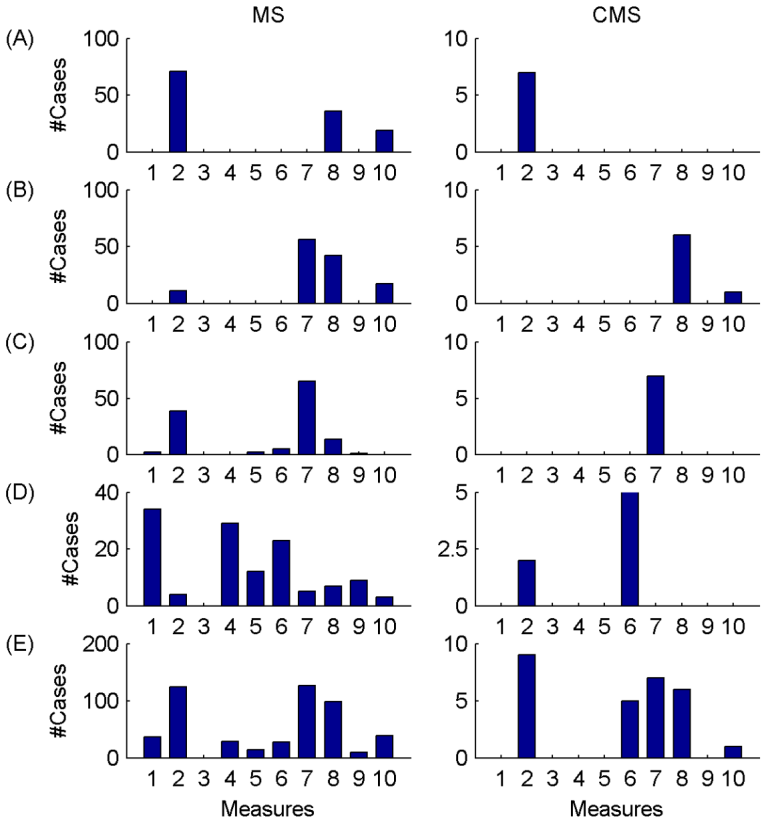

Figure 4.11. Group-level results. Number of cases (paradigms x channels) when particular measures were selected within the best four features. MS denotes the selection of measures in single channels, while CMS stands for the selection of channel x measure features. (A)-(D) denote cases when particular measures were found to be within the 1st, 2nd, 3rd and 4th best features, respectively. Row (E) stands for sums of cases presented in rows (A)-(D). The order of the measures is as follows: H, ΔD, P_{SOr}, $P_{\delta r}$, $P_{\theta r}$, $P_{\alpha r}$, $P_{\sigma r}$, $P_{\beta r}$, $P_{\gamma r}$, f_{se}. Bars can be considered as sums across the columns of corresponding subplots in Figure 4.10.

channel x measure pairs (CMS). Selections of the best measures in single channels (MS) and selections of channels for specific measures (CS) resulted in slightly different distributions of selected features as compared to the CMS approach. Generally, individual-level feature selection results (Appendix E) were very similar to those obtain at the group level. However, some differences also emerged. As it could be expected selections of channel and measures were more uneven. In addition, measure *H* was selected in more cases (especially as the third or fourth best feature) as compared to the group-level results.

DOI:10.15774/PPKE.ITK.2010.008

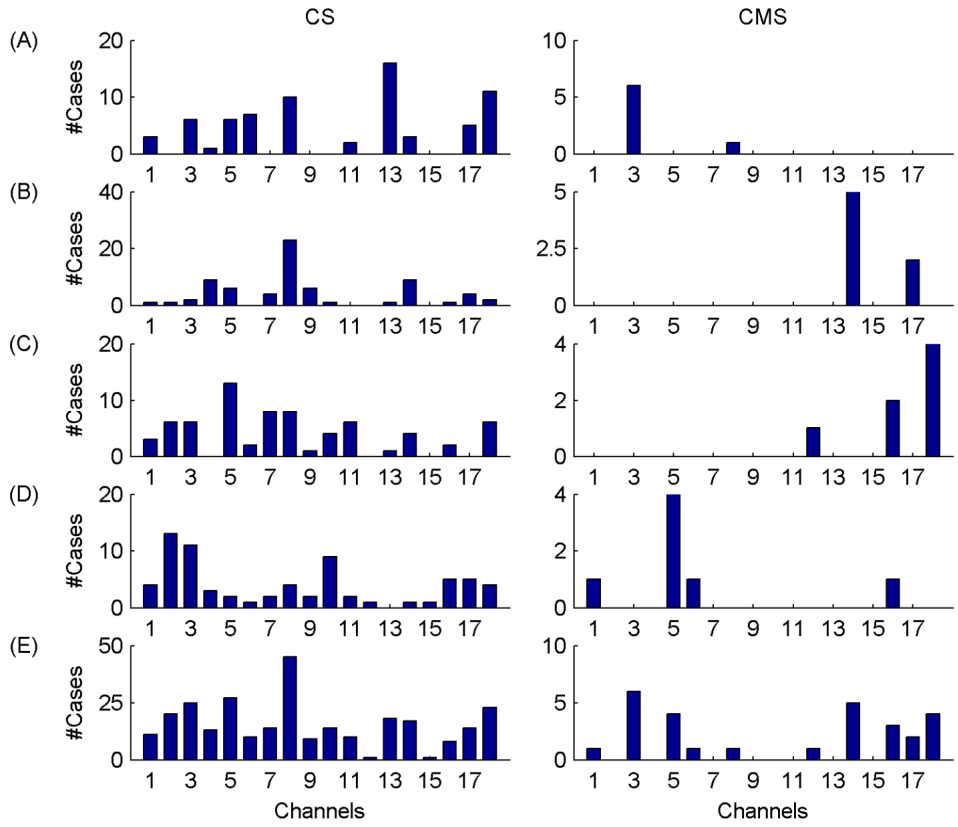

Figure 4.12. Group-level results. Number of cases (paradigms x measures) when particular channels were selected within the best four features. CS denotes the selection of channels considering single measures, while CMS stands for the selection of channel x measure features. (A)-(D) denote cases when particular channels were found to be within the 1st, 2nd, 3rd and 4th best features, respectively. Row (E) stands for sums of cases presented in rows (A)-(D). The order of the channels is as follows: Fp2, F8, T4, T6, O2, Fp1, F7, T3, T5, O1, F4, C4, P4, F3, C3, P3, Fz, Cz. Bars can be considered as sums across the rows of corresponding subplots in Figure 4.10.

4.4. Discussion

To our best knowledge this is the first study that assessed sleep stage discrimination capabilities of fractal and power spectral measures of EEG signals recorded at different topographic locations by applying different classification paradigms at both individual and group levels.

Our results revealed that considering both averaged individual- and group-level classification results best performance was achieved by the multifractal measure ΔD in most of the channels. Subsequent best measures were f_{se} and $P_{\beta r}$. This tendency was true for most of the applied classification paradigms. Furthermore, best classifications for ΔD were found in temporal channel T4.

DOI:10.15774/PPKE.ITK.2010.008

Examination of conditional $\hat{K}$ values revealed that high overall performance of ΔD was achieved due to significantly better classification of the NREM4 sleep stage. Comparatively, measure ΔD was found to be less efficient in classifying NREM2 and REM. Nevertheless, topographic maps in Figure 4.5 (and figures in Appendix C) indicated that these latter stages could be classified better based on other specific EEG measures at specific locations. E.g. best classification of NREM2 was revealed using $P_{\sigma r}$ centrally (Figure 4.5H) and best classification of REM was achieved using $P_{\beta r}$ in frontal channels (Figure 4.5I). Thus, we assumed that overall sleep stage classification performance could be improved by combining different measures at different locations. And indeed, combinations of up to two channels for same measures and combinations of up to three measures in single channels resulted in significant classification improvements. Our results also revealed that combinations of measures in single channels provide significantly better classifications as compared to combinations of different channels for single measures. This might be considered as a promising result since usage of single channels can enable the development of cheaper and more ergonomic vigilance state detector devices. Best classifications were found in F3, C3, C4 and P4 channels by combining in most of the cases ΔD, $P_{\beta r,}$ $P_{\sigma r}$ and f_{se} measures. H was found to be the fourth best measure for most of the classifiers, but its addition did not resulted in a significant improvement. Topography of the best channels is in a general agreement with previous studies that revealed supremacy of central derivations. However, further significant improvement of the classification performance can be achieved by combining up to four appropriate channel x measure features. For this feature selection approach ΔD of temporal (T3 or T4) channels was found to be the best feature followed by the $P_{\beta r}$ x F3, $P_{\sigma r}$ x Cz and $P_{\alpha r}$ x O2. Using the combination of these features even 94.18 % overall accuracy could be achieved at the group level.

As expected, better classifications were achieved at the individual level as compared to the group level. This finding could be related to the considerable individual variability of sleep EEG features [140, 141]. In line with this in Chapter 2 we revealed significant gender-related differences of the multifractal measure ΔD suggesting separate gender groups for training of sleep stage classifiers.

Superior performance of ΔD and f_{se} is in agreement with results obtained previously for the entropy of amplitudes and spectral edge frequency measures [62]. Measure H performed below the average considering all measures. This result is in contrast with a

DOI:10.15774/PPKE.ITK.2010.008

previous study [116] finding a superior performance of two other monofractal measures (the fractal exponent and the fractal dimension) when compared to spectral measures. To our surprise, worst classification performance was obtained for the relative band power of slow activities. This might be explained by confining the δ band to the 1-4 Hz range and considering slow oscillations (0.5-1 Hz) separately. Furthermore, the outstanding performance of $\Delta D, f_{se}$ and $P_{\beta r}$ indicate that it is the faster rather than the slow activities that might be of superior performance in the classification of the analyzed sleep stages.

Comparing different classification paradigms we found that at the group level feedforward neural networks and support vector machine classifiers with radial basis kernel function significantly outperform the traditional approaches such as linear discriminant analysis, quadratic discriminant analysis and naïve Bayes classifiers. This result is not in agreement with the finding that non-linear classifiers produce only slightly better classification results as compared to LD [142]. However, classification results in [142] were obtained for discrimination of five mental tasks. FF and RS methods are highly computation demanding as compared to other classifiers. An optimal selection could be the LS method that performed similarly to the best ones, but exhibited about 5-8 times lower feature selection times. In contrast to the group-level results traditional methods outperformed the more sophisticated approaches at the individual level. This was especially true for higher number of input features. The reason could be the relatively low number of training samples at the individual level causing insufficient parameter optimizations for the sophisticated methods. Thus, at the individual level we suggest the usage of traditional classification methods that exhibit also lower computational times. We also note that preliminary parameter optimizations (Appendix B) were carried out for a single subject and measure. By optimizing the parameters always for the subjects (individual or group) and features of particular interest further improvements could be achieved.

In this study we used the SFFS method to reveal the best channel x measure features and the following supplementing ones. We admit that application of exhaustive feature selection algorithms could reveal even better classifications using combination of features not revealed here.

Polygraphic information (EMG, EOG, ECG) might obviously improve the sleep stage classification performance [116]. Nevertheless, developing sleep stage classifications not

DOI:10.15774/PPKE.ITK.2010.008

relying on polygraphic information might be useful for invasive intracranial EEG recordings where polygraphy is typically not available.

In this study we assessed the relatively well-distinguishable sleep stages NREM4, NREM2 and REM. It remains to be tested whether other sleep stages (NREM1 and NREM3), waking states or the wake-sleep transition can be classified and detected with a same performance using fractal measures alone or combined with other features. However, we must also keep in mind that although the Rechtschaffen and Kale's standard was the only widely accepted standard for approximately 40 years, its rules were criticized for leaving plenty of room for subjective interpretation and different amendments were suggested [143-145]. As a results a modified standard was proposed by the AASM in 2007 [130]. It remains to be tested how this new standard affects the already developed automatic sleep staging methods. Finally, it also remains to be more deeply investigated whether sleep scoring of human experts (mostly based on visual inspection of recordings) appropriately reflects sleep dynamics or unsupervised classification algorithms could reveal additional information.

DOI:10.15774/PPKE.ITK.2010.008

Chapter Five

CONCLUSIONS

The aim of this dissertation was to reveal spatio-temporal fractal properties of the human sleep and to assess sleep stage discrimination capability of monofractal and multifractal EEG features.

It was found that the topography of both monofractal and multifractal EEG properties exhibit sleep stage-specific distributions. Moreover, the monofractal measure H tended to increase ($H_{\mathrm{NREM4}} > H_{\mathrm{NREM2}} > H_{\mathrm{REM}}$), while the multifractal measure ΔD tended to decrease ($\Delta D_{\mathrm{NREM4}} < \Delta D_{\mathrm{NREM2}} < \Delta D_{\mathrm{REM}}$) with the deepening of sleep. Thus, one can conclude that EEG signals tend to be more persistent and less multifractal with the deepening of sleep.

Based on the observed spatio-temporal trends we speculate that the brain modulates its information processing capability and susceptibility to outer and inner stimuli via re-organization of spatio-temporal correlations. By building up longer spatio-temporal correlations and by shrinking the fractal spectrum the localized processing elements of the brain (e.g. columns of the neocortex) become less reactive to stimuli and their selective information processing capability decreases as the sleep deepens because of the activities that spread over longer distances.

Furthermore, sleep stage-specific topographies were also revealed for inter-site correlations of the fractal measures as well as for cross-correlations between them. These results suggest that despite of the general opposite tendency of the two fractal properties there might be different mechanisms in the brain that control multifractality and monofractality of the spatio-temporal dynamics in a more complex way.

Despite of the strong cross-correlations that appeared between the fractal and specific power spectral features it was found that fractal properties (especially ΔD) carry additional information about brain dynamics as compared to the traditional spectral measures. This finding might indicate that brain electrical activities are more complex than they could be fully described by spectral measures or by a single monofractal exponent and therefore the multifractal approach may be more appropriate for modeling the SOC properties of brain dynamics. Nevertheless, we should note that several studies revealed power-law neural fluctuations that do not necessarily reflect self-organized

DOI:10.15774/PPKE.ITK.2010.008

critical states of brain [146-148]. All these findings indicate that combination of different approaches may be needed for overall modeling of brain dynamics.

Regarding the overall sleep stage discrimination capability of the analyzed EEG features the multifractal measure outperformed relative band powers, the compact power spectral measure f_{se} as well as the monofractal exponent H. Considering the averaged individual-level as well as the group-level classifications results obtained using single features best classifications were exhibited by ΔD in temporal channels T3 and T4. Classification performance exceeded 80 % overall accuracy at the group level, and achieved even 97.78 % at the individual level. Furthermore, by supplementing the best single features with up to three additional appropriate channel x measure combinations the classification performance could be significantly improved. By combining four features 94.18 % overall accuracy was achieved at the group level, while at the individual level even 100 % performance was obtained for several subjects. Although the selection of the appropriate channels and measures was slightly different at individual and group levels we conclude that when combining fractal and power spectral measures the most appropriate features generally are: multifractality in temporal channels T3 and T4, relative band powers of β and σ frequency bands over the fronto-centro-parietal region and relative band power of α activity in the occipital region.

DOI:10.15774/PPKE.ITK.2010.008

Chapter Six

SUMMARY

6.1. New scientific results

Thesis I: Fractal properties of the human sleep EEG and their relation to power spectral measures

(Related publications: [1-3], [5].)

I.1. I have revealed that EEG signals tend to be more persistent and less multifractal with the deepening of sleep. In addition, both monofractal and multifractal EEG measures exhibit topographic distributions that are sleep stage-specific.

Topographic distributions of the fractal measures for the analyzed sleep stages are shown in Figure 6.1. Highest values of the monofractal measure H emerged frontally during all sleep stages, while the overall minimum was found during REM in the central zone. A $H_{\mathrm{NREM4}} > H_{\mathrm{NREM2}} > H_{\mathrm{REM}}$ trend was present across the whole head surface. The multifractal measure ΔD showed an opposite trend: $\Delta D_{\mathrm{REM}} > \Delta D_{\mathrm{NREM2}} > \Delta D_{\mathrm{NREM4}}$. Minima of ΔD could be found in the fronto-central region during all sleep stages, while higher values were observed in the posterior circumferential channels. Based on the observed spatio-temporal trends I speculate that the brain modulates its information processing capability and susceptibility to outer and inner stimuli via re-organization of spatio-temporal correlations. By building up longer spatio-temporal correlations and by shrinking the fractal spectrum the localized processing elements of the brain (e.g. columns of the neocortex) become less reactive to stimuli and their selective information processing capability decreases as the sleep deepens because of

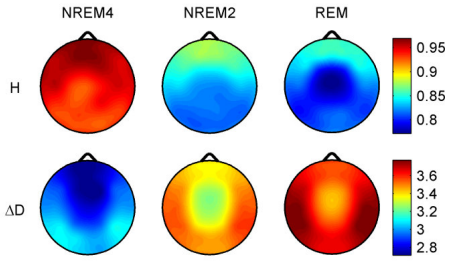

Figure 6.1. Topographic distributions of group-level medians of the fractal measures.

DOI:10.15774/PPKE.ITK.2010.008

the activities that spread over longer distances.

I.2. I have found that the topography of inter-site correlations of *H* is more variable than that of Δ*D* across sleep stages. Furthermore, I have shown that the cross-correlation between *H* and Δ*D* exhibits sleep stage-specific topography.

As it can be seen in Figure 6.2 (column ALL) both fractal measures exhibited strongest inter-site correlations in the central region when all sleep stages were considered together. However, *H* exhibited higher posterior inter-site correlations during NREM4 and higher anterior correlations during NREM2 and REM. At the same time Δ*D* did not reveal such differences between sleep stages. Measure Δ*D* showed higher inter-site correlations as compared to *H*.

By combining all sleep stages I found a strong negative correlation between *H* and Δ*D* with a nadir in the posterior channels (Figure 6.3). As revealed by the sleep stage-wise analysis NREM2 and NREM4 contributed most to this occipital nadir. As compared to NREM4 weaker and less significant correlations emerged during NREM2. During REM there was a further weakening of correlations with a non-significant positive peak in the F3, Fz, F4 channels.

These results suggest that despite of the general opposite tendency of the two fractal properties there might be different mechanisms in the brain that control multifractality and monofractality of the spatio-temporal dynamics in a more complex way.

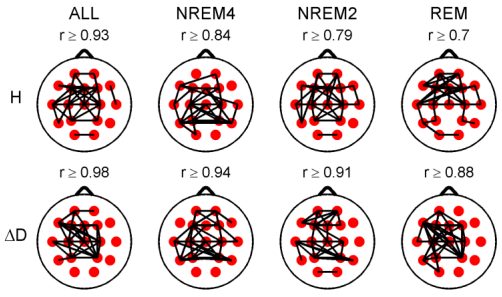

Figure 6.2. Highest 35 inter-site correlations of the fractal measures denoted by black lines drawn between the appropriate locations. Spearman's correlation coefficients were calculated considering all sleep stages together (column ALL) as well as separately. Only significant ($p < 0.05$) correlations are depicted. Lowest presented correlation values can be found above the topographic maps.

DOI:10.15774/PPKE.ITK.2010.008

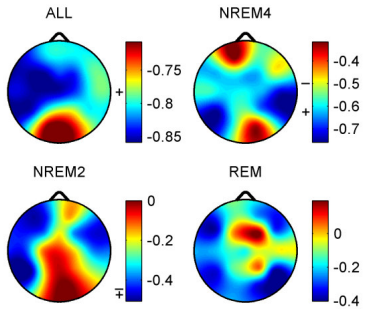

Figure 6.3. Spearman cross-correlations between H and ΔD considering all sleep stages together as well as separately. Significant values ($p < 0.05$) are denoted on the left side of the color bars using the following notations: no sign (none of the values are significant); only + (all values are significant); + with a dash (only values below the dashes are significant).

I.3. I have assessed the relationship between fractal and power spectral EEG measures as well as the contribution of individual frequency band activities to the fractal measures.

Overall, I found stronger correlations between the fractal and the power spectral measures during deeper sleep stages than in lighter stages. Additionally, I also revealed that the monofractal measure H is positively correlated with relative powers of slow activities (especially P_{SOr}) and negatively correlated with faster activities (above 4 Hz) exhibiting strongest negative correlations with $P_{\theta r}$. By contrast, ΔD is negatively correlated with slow activities and positively correlated with relative powers of higher frequency bands achieving strongest correlations with $P_{\theta r}$, $P_{\alpha r}$ and $P_{\sigma r}$ in temporal channels during NREM4. However, despite of the strong correlations revealed between the fractal and the power spectral measures, using a multiple linear regression analysis I found that fractal measures (especially ΔD) carry additional information about EEG signals compared to the power spectral features.

I.4. I have revealed gender-related differences of monofractal and multifractal EEG measures at specific topographic locations and during different sleep stages.

I found that sleep EEG signals are more multifractal during NREM4, NREM2 and REM sleep stages at all topographic locations in males than in females (Figure 6.4). Most significant differences occurred during sleep stage NREM4 exhibiting a minimal $p = 0.0025$ value in channel F7. By contrast, the monofractal measure H was higher in

DOI:10.15774/PPKE.ITK.2010.008

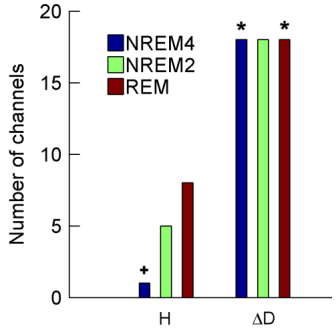

*Figure 6.4. Number of channels in which group-level medians were higher in males (case M>F) are presented for both fractal measures and sleep stages separately. Number of channels in which group-level measure medians are higher in females (case F>M) can be obtained by subtracting these values from 18 (total number of channels). The * (+) sign denotes measure and sleep stage combinations exhibiting significant differences for the case M>F (F>M).*

females in most of the channels, however, a significant difference ($p = 0.0464$) appeared during NREM4 in channel T4 only.

Given that the F7 recording site lies over or near the Broca's area I hypothesize that differences at this specific region reflect gender differences in verbal functions.

Thesis II: Classification of sleep stages by combining fractal and power spectral EEG features

(Related publications: [2], [4].)

II.1. I have assessed sleep stage discrimination capability of fractal and power spectral measures of EEG signals at specific topographic locations by applying different classification paradigms at both individual and group levels.

Considering both averaged individual- and group-level results, I obtained best sleep stage classification performance in most of the EEG channels and for most of the classification methods by applying the multifractal measure ΔD. Moreover, I found best classifications for ΔD in temporal channel T4 for most of the classifiers at both levels. Using conditional Kappa analysis I revealed that overall high performance of ΔD emerged due to the high classification accuracy of the NREM4 stage. Using the ΔD x T4 single feature at the group level highest overall accuracy (OA=81.92 %) was achieved by a support vector machine with a linear kernel function, while individual-level analysis revealed best average classification result (OA=90.02 %) for a naïve Bayes classifier.

DOI:10.15774/PPKE.ITK.2010.008

II.2. I have shown that a combination of fractal and power spectral measures of EEG signals recorded at different topographic locations significantly improves the discrimination of sleep stages.

I found that supplementation of the best single feature with an appropriate second one may significantly improve the sleep stage classification performance. Addition of a second measure for the same channel and addition of another channel x measure feature enhances the performance in more classifiers as compared to addition of a second channel for the same measure. Using conditional Kappa analysis I revealed that the overall classification accuracy improves due to the higher classification accuracy of NREM2 and REM sleep stages. Addition of a third channel considering the same measure does not improve significantly the classification. However, a combination of up to three measures of single channels and a combination of up to four channel x measure features may result in further significant improvements. Combinations of measures in single channels provide significantly better classifications when compared to combinations of channels using single measures. Furthermore, combinations of channel x measure features perform significantly better as compared to combinations of measures in single channels. Considering feature combinations at the group level I obtained the best classification results using feedforward neural network and support vector machine classifiers that performed in most of the cases significantly better that the traditional methods such as the linear discriminant analysis, the quadratic discriminant analysis and the naïve Bayes classifier. This tendency was not true at the individual level, where due to the lower number of training samples the traditional

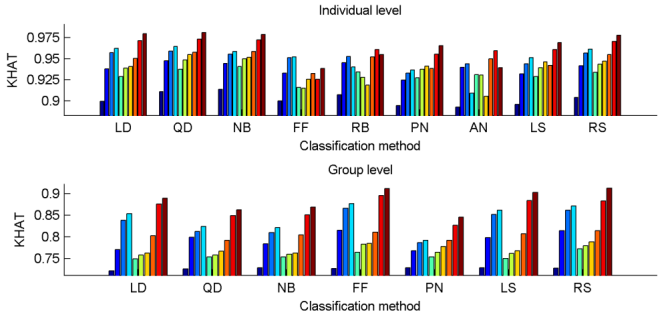

Figure 6.5. Averages of individual maximal $\hat{K}$ values and group-level maximal $\hat{K}$ values. First bars stand for classifications based on the best single input features, 2^{nd}-4^{th} bars denote classifications with 2-4 measures of single channels, 5^{th}-7^{th} bars present results for classifications with 2-4 channels of single measures, 8^{th}-10^{th} bars stand for classifications using 2-4 channel x measure feature combinations. RB and AN classifiers were excluded from group-level analyses due to their high computational demand.

DOI:10.15774/PPKE.ITK.2010.008

methods performed even better, especially in those cases where the number of features was higher (see Figure 6.5).

When comparing the maximal classification performances of individual and group levels it can be observed that as expected better discrimination of sleep stages can be obtained at the individual level achieving even 100 % overall accuracy for several subjects.

At the group level I achieved the best classification performance (OA=94.18 %) using the combination of ΔD x T3, $P_{\beta r}$ x F3, $P_{\sigma r}$ x Cz and $P_{\alpha r}$ x O2 features and by applying a support vector machine classifier with a radial basis kernel function. As it can be seen in Figure 6.6 and Figure 6.7, selection of these measures and channels was very similar across classification paradigms when feature selection was carried out on channel x measure pairs (CMS). Selections of the best measures in single channels (MS) and selections of channels for specific measures resulted in slightly different distributions of selected features as compared to the CMS approach. In addition, individual-level results were comparable to those found at the group level. Measures ΔD, $P_{\beta r}$, $P_{\sigma r}$ and channels T3-T4, O2, Cz proved to be the most appropriate features in all cases. Thus, I conclude that when combining fractal and power spectral measures

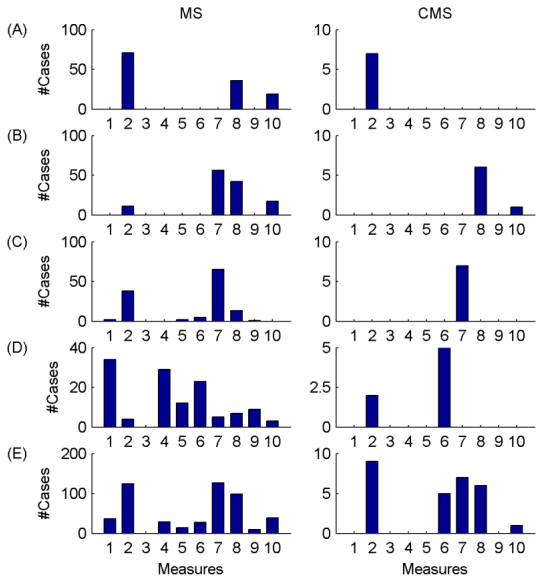

Figure 6.6. Group-level results. Number of cases (paradigms x channels) when particular measures were selected within the best four features. MS denotes the selection of measures in single channels, while CMS stands for the selection of channel x measure features. (A)-(D) denote cases when particular measures were found to be within the 1st, 2nd, 3rd and 4th best features, respectively. Row (E) stands for sums of cases presented in rows (A)-(D). The order of the measures is as follows: H, ΔD, P_{SOr}, $P_{\delta r}$, $P_{\theta r}$, $P_{\alpha r}$, $P_{\sigma r}$, $P_{\beta r}$, $P_{\gamma r}$, f_{se}.

DOI:10.15774/PPKE.ITK.2010.008

the most appropriate features generally are: multifractality in temporal T3 and T4 channels, relative band powers of β and σ frequency bands over the fronto-centro-parietal region and relative band power of α activity in the occipital region.

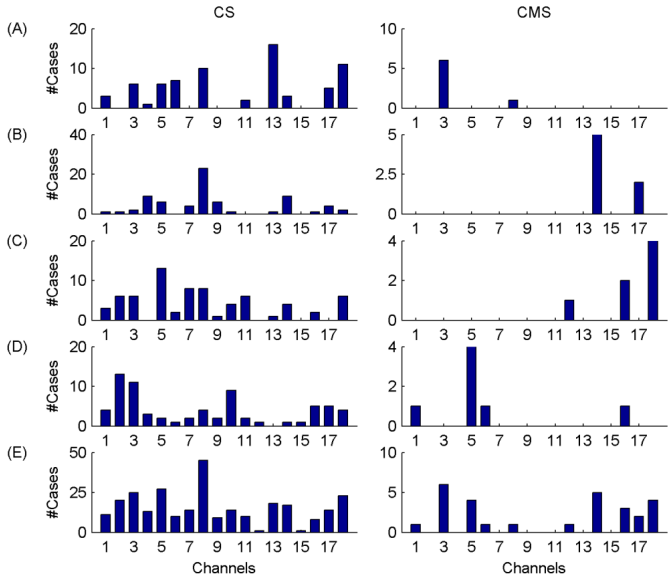

Figure 6.7. Group-level results. Number of cases (paradigms x measures) when particular channels were selected within the best four features. CS denotes the selection of channels considering single measures, while CMS stands for the selection of channel x measure features. (A)-(D) denote cases when particular channels were found to be within the 1st, 2nd, 3rd and 4th best features, respectively. Row (E) stands for sums of cases presented in rows (A)-(D). The order of the channels is as follows: Fp2, F8, T4, T6, O2, Fp1, F7, T3, T5, O1, F4, C4, P4, F3, C3, P3, Fz, Cz.

6.2. Possible applications

The more theoretical results presented in *Thesis I* might contribute to reveal how the brain re-organizes itself across different vigilance states to modulate its information processing and reactivity to stimuli. However, more refined analyses are needed to assess fractal properties of the sleep EEG during cyclic alternating pattern (CAP) and non-CAP sequences since CAP translates a condition of sustained arousal instability between greater and lesser arousal levels, while non-CAP denotes a condition of arousal stability [149-151]. In addition, to reveal the origin of self-similarity properties of macro EEG signals fractal analysis of brain activities at different scales is required. Application possibilities of the more practical results summarized in *Thesis II* are straightforward. E.g. automatic classification of the vigilance state would be beneficial for clinicians when assessing long-term recordings. Other applications might be the real-time monitoring of the depth of anesthesia during surgery [111] or drowsiness detection [112]

DOI:10.15774/PPKE.ITK.2010.008

for people working under monotonic and at the same time dangerous circumstances. Going even further, based on the current state of neural engineering it is evident that the widespread usage of brain computer interfaces for clinical and entertaining purposes will be among future trends. One of the clinical applications might be the real-time modulation of the brain activity for control of epileptic seizures by local drug delivery or electrical stimulation [152]. During recent years several seizure detection/prediction methods have been proposed based on different measures of brain activities [153]. However, background of false event recognitions, the reason of relatively low performance of algorithms remained unclear since generally not even the systematic assessment of possible effects of the vigilance state variation was carried out. My investigations (not presented in the dissertation) of fractal properties of epileptic brain activities [7-14] disclosed that both monofractal and multifractal measures exhibit sudden drops during the seizures and show slower trends during preictal and postictal states. Combining these findings with the results presented in the dissertation it becomes evident that the variation of the vigilance state might modulate epileptic events and hereby it might also affect their detections/predictions by applying these measures. Since probably all measures are affected by the vigilance state I suggest a novel approach for detection/prediction of seizures that is enhanced by the determination of the vigilance state (Figure 6.8).

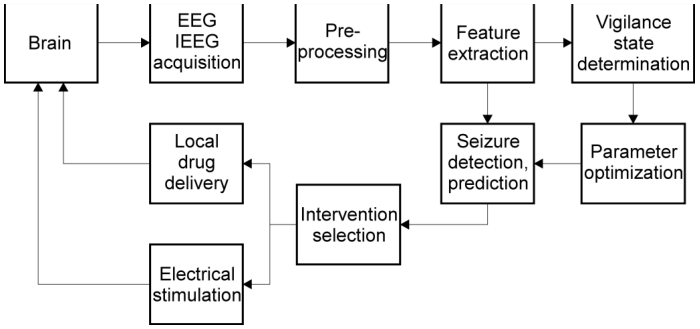

Figure 6.8. A possible enhancement of seizure detection/prediction capabilities by determination of the vigilance state for control of epileptic seizures.

DOI:10.15774/PPKE.ITK.2010.008

Chapter Seven

APPENDICES

A. Cross-correlations between EEG measures and age

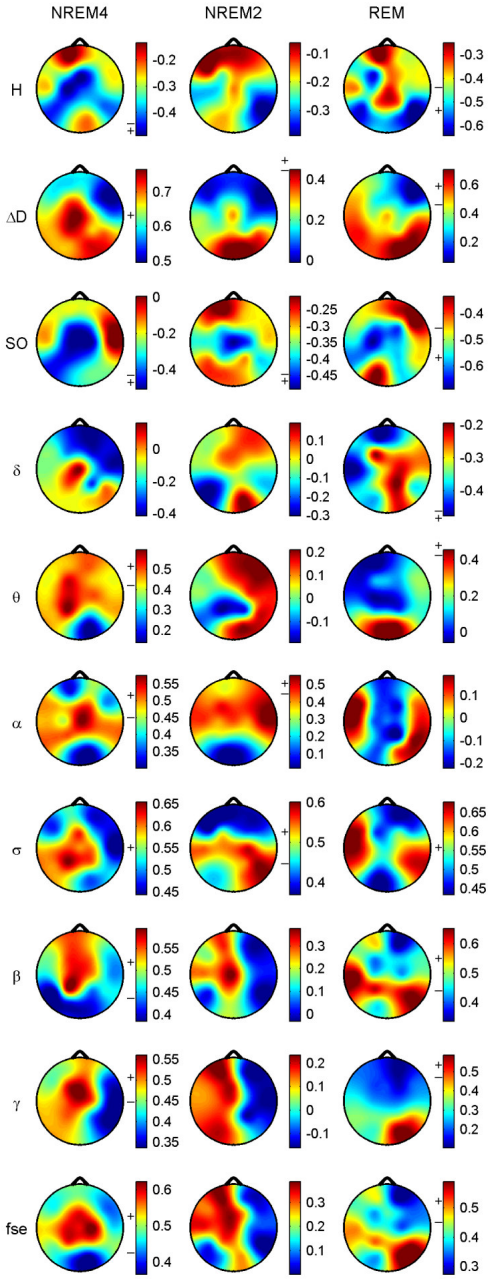

Figure 7.1. Spearman cross-correlations between EEG measures and age. Significant values ($p < 0.05$) are marked on the left side of the color bars using the following notations: no sign (none of the values are significant); only + (all values are significant); + with a dash (only values above/below the dash are significant). Relative band powers are denoted by the labels of the corresponding frequency bands.

DOI:10.15774/PPKE.ITK.2010.008

B. Optimization of classifier parameters

B.1. Feedforward neural network classifier

The number of hidden layers and neurons of feedforward neural network classifiers was optimized using the Levenberg-Marquardt training algorithm and settings indicated in Table 7.I. See Figure 7.7 for detailed information on optimization process and for the obtained classification results using different number of hidden layers and neurons.

TABLE 7.I. APPLIED PARAMETER SETTINGS

Parameters	Values
epochs	100
time	Inf
goal	0
max_fail	5
mem_reduc	1
min_grad	1.0e-10
mu	1.0e-03
mu_dec	0.1
mu_inc	1.1
mu_max	1.0e100

For the meaning of particular parameters see the Matlab help. The goal parameter was changed to 1e-06 at the group level to improve the generalization capability of the classifier.

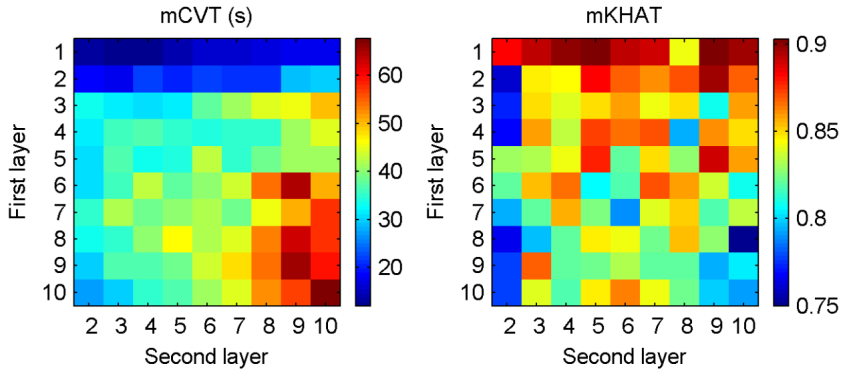

Figure 7.2. Parameter optimization results obtained for a feedforward neural network classifier by considering different numbers of hidden layers and different numbers of neurons in particular layers. Top rows indicate cases when only one hidden layer was used with 2-10 numbers of neurons. Median cross-validation times (mCVT) and mean $\hat{K}$ values ($m\hat{K}$) were obtained by classifications performed using the ΔD measure and considering all channels separately as well as by combining up to four channels for subject #16. As an optimal combination we selected an architecture consisting of a single hidden layer with five neurons based on the maximal $m\hat{K}$ values and low cross-validation time achieved by this configuration.

DOI:10.15774/PPKE.ITK.2010.008

B.2. Radial basis function neural network classifier

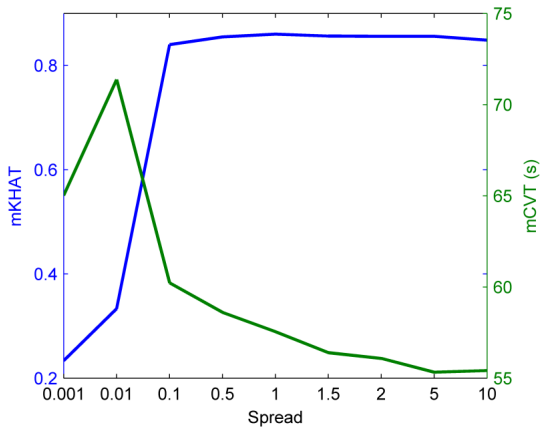

Figure 7.3. Parameter optimization results obtained for a radial basis function neural network classifier by considering different spread values. Median cross-validation times (mCVT) and mean $\hat{K}$ values ($m\hat{K}$) were obtained by classifications performed using the ΔD measure and considering all channels separately for subject #16. We selected the default spread value 1 as the optimum based on the maximal $m\hat{K}$ value and low cross-validation time achieved by this setting.

B.3. Probabilistic neural network classifier

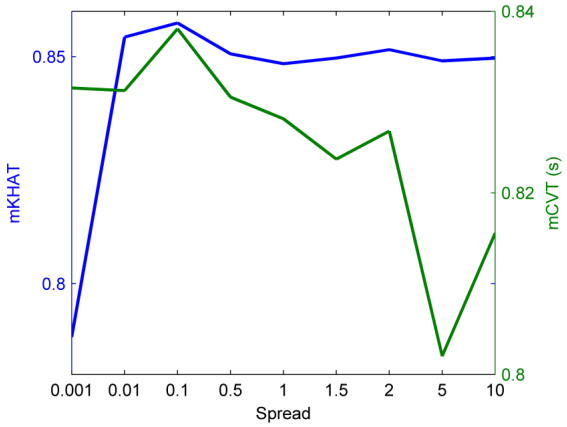

Figure 7.4. Parameter optimization results obtained for a probabilistic neural network classifier by considering different spread values. Median cross-validation times (mCVT) and mean $\hat{K}$ values ($m\hat{K}$) were obtained by classifications performed using the ΔD measure and considering all channels separately for subject #16. We selected the default spread value 0.1 as the optimum based on the maximal $m\hat{K}$ value achieved by this setting. Although the mCVT was highest for this particular spread setting, it was higher only with about 0.03 s from the minimum.

DOI:10.15774/PPKE.ITK.2010.008

B.4. Support vector machine with a linear kernel function

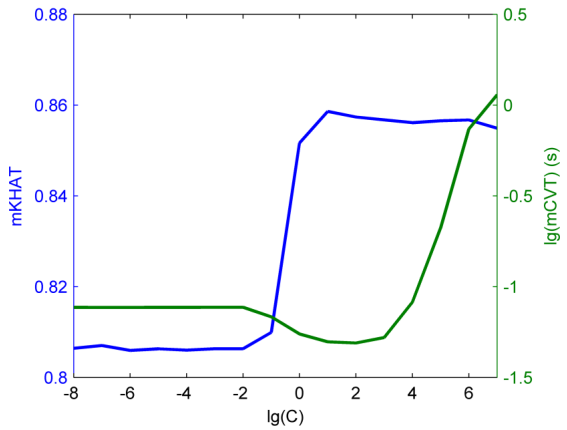

Figure 7.5. Parameter optimization results obtained for a support vector machine classifier with a linear kernel function by considering different C values. Median cross-validation times (mCVT) and mean $\hat{K}$ values ($m\hat{K}$) were obtained by classifications performed using the ΔD measure and considering all channels separately for subject #16. We selected the C=10 parameter value as the optimum based on the maximal $m\hat{K}$ value and low cross-validation time achieved by this setting.

B.5. Support vector machine with a radial basis kernel function

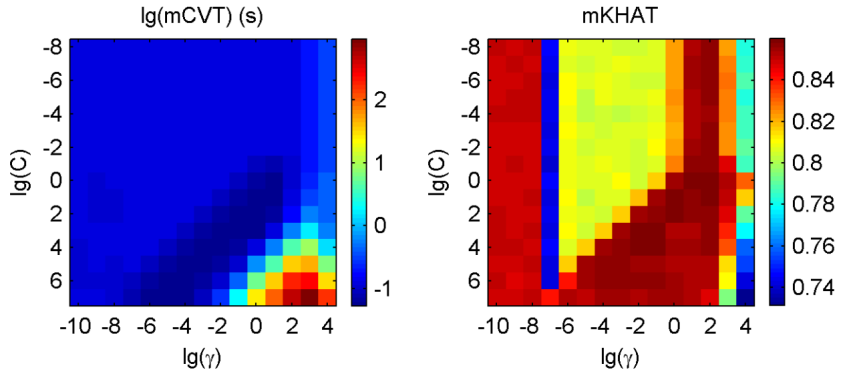

Figure 7.6. Parameter optimization results obtained for a support vector machine classifier with a radial basis kernel function by considering different C and γ parameter values. Median cross-validation times (mCVT) and mean $\hat{K}$ values ($m\hat{K}$) were obtained by classifications performed using the ΔD measure and considering all channels separately for subject #16. We selected the C=10000, γ=0.01 parameter combination as the optimum based on the maximal $\hat{K}$ and high $m\hat{K}$ values and low cross-validation time achieved by this setting.

DOI:10.15774/PPKE.ITK.2010.008

C. Classification of sleep stages using single features

C.1. Quadratic discriminant analysis

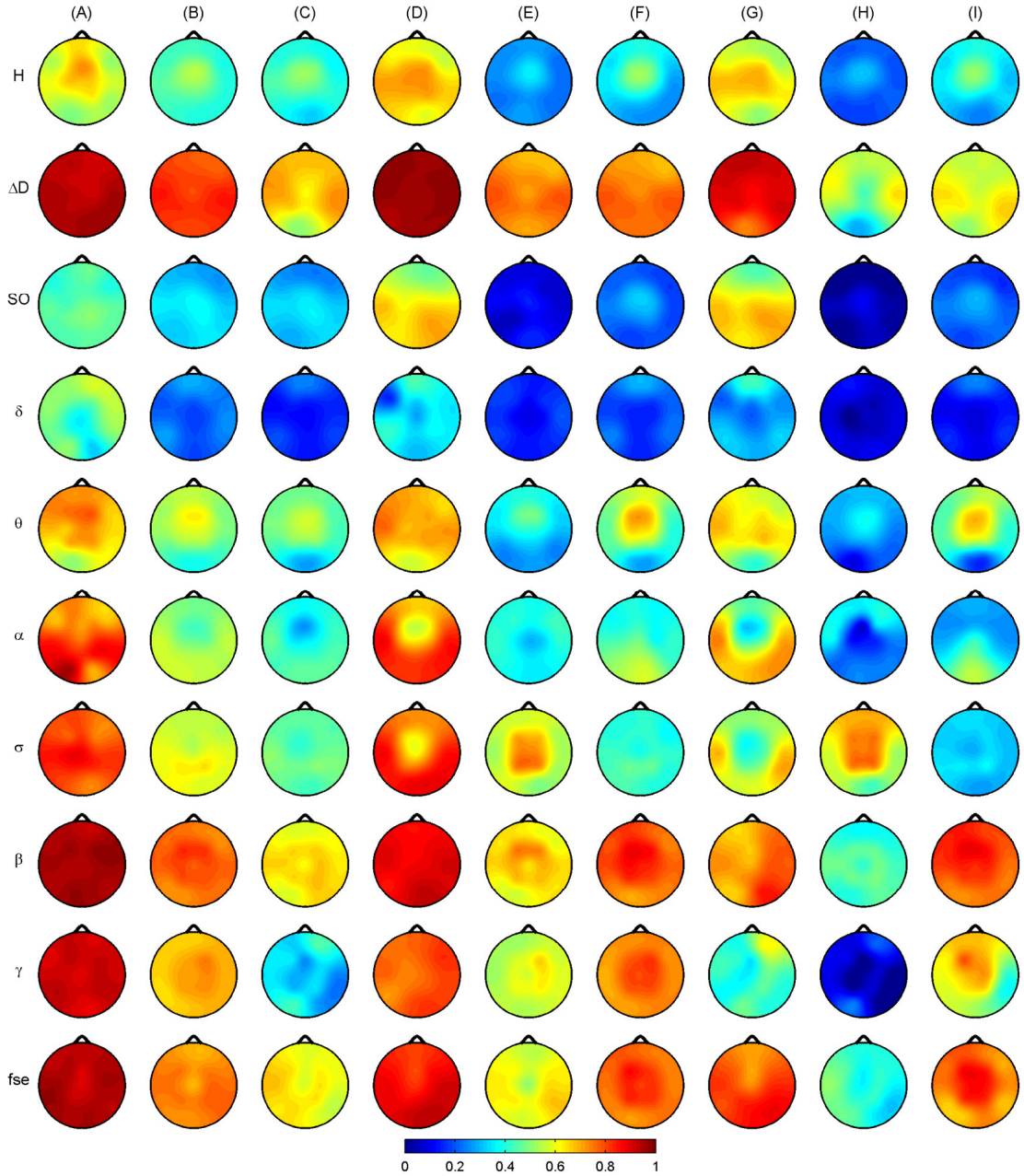

Figure 7.7. Sleep stage classification results obtained using quadratic discriminant analysis both at individual and group levels. (A) Maximal $\hat{K}$ values taken across subjects. (B) Averaged individual $\hat{K}$ values. (C) Group-level $\hat{K}$ values. (D) Individual conditional $\hat{K}$ values averaged across subjects for sleep stage NREM4. (E) Individual conditional $\hat{K}$ values averaged across subjects for sleep stage NREM2. (F) Individual conditional $\hat{K}$ values averaged across subjects for REM sleep. (G) Group-level conditional $\hat{K}$ for NREM4 sleep. (H) Group-level conditional $\hat{K}$ for sleep stage NREM2. (I) Group-level conditional $\hat{K}$ for REM sleep. Relative band powers are denoted by the labels of the corresponding frequency bands.

DOI:10.15774/PPKE.ITK.2010.008

C.2. Naïve Bayes classifier

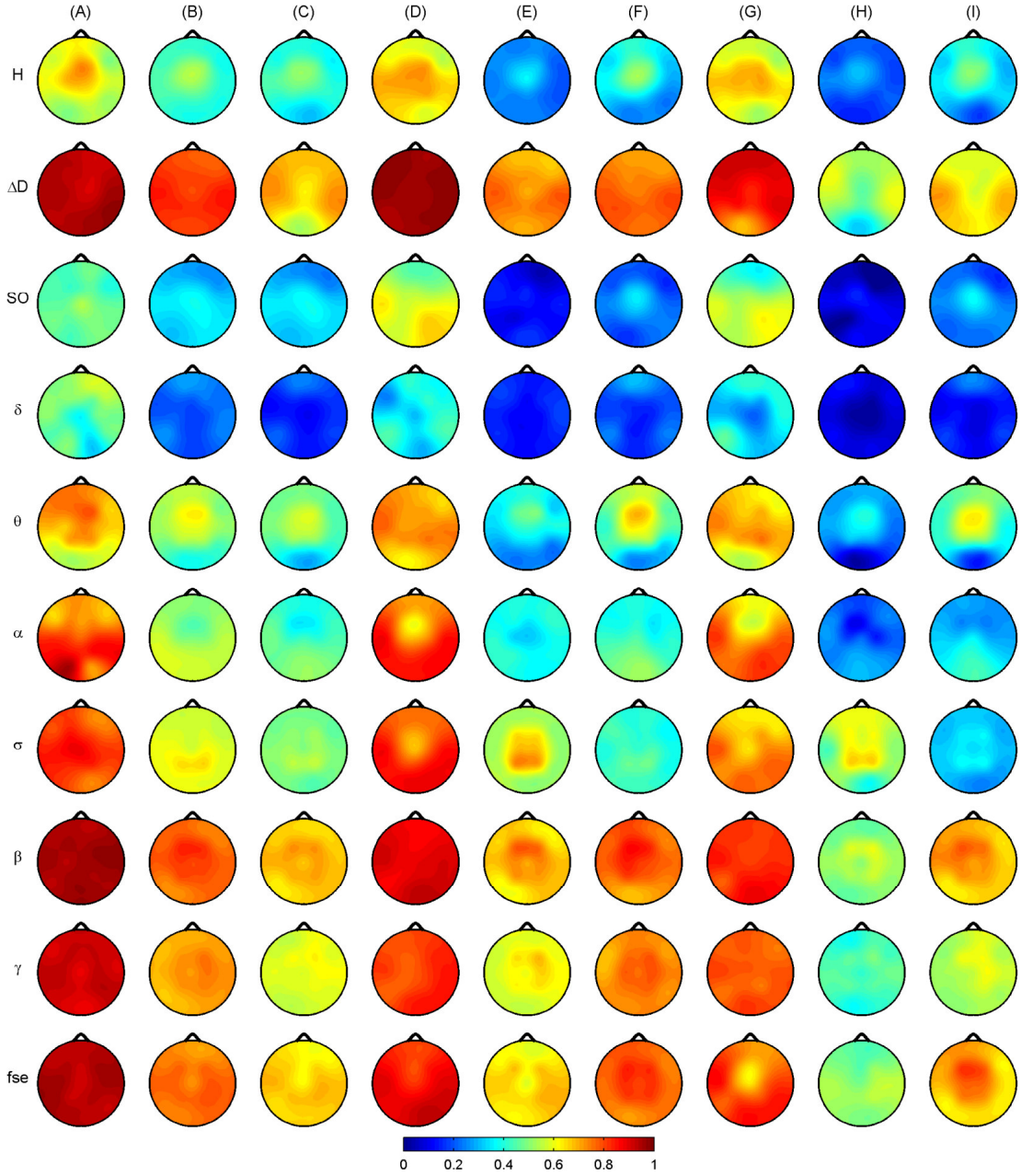

Figure 7.8. Sleep stage classification results obtained using a naïve Bayes classifier both at individual and group levels. (A) Maximal $\hat{K}$ values taken across subjects. (B) Averaged individual $\hat{K}$ values. (C) Group-level $\hat{K}$ values. (D) Individual conditional $\hat{K}$ values averaged across subjects for sleep stage NREM4. (E) Individual conditional $\hat{K}$ values averaged across subjects for sleep stage NREM2. (F) Individual conditional $\hat{K}$ values averaged across subjects for REM sleep. (G) Group-level conditional $\hat{K}$ for NREM4 sleep. (H) Group-level conditional $\hat{K}$ for sleep stage NREM2. (I) Group-level conditional $\hat{K}$ for REM sleep. Relative band powers are denoted by the labels of the corresponding frequency bands.

DOI:10.15774/PPKE.ITK.2010.008

C.3. Feedforward neural network

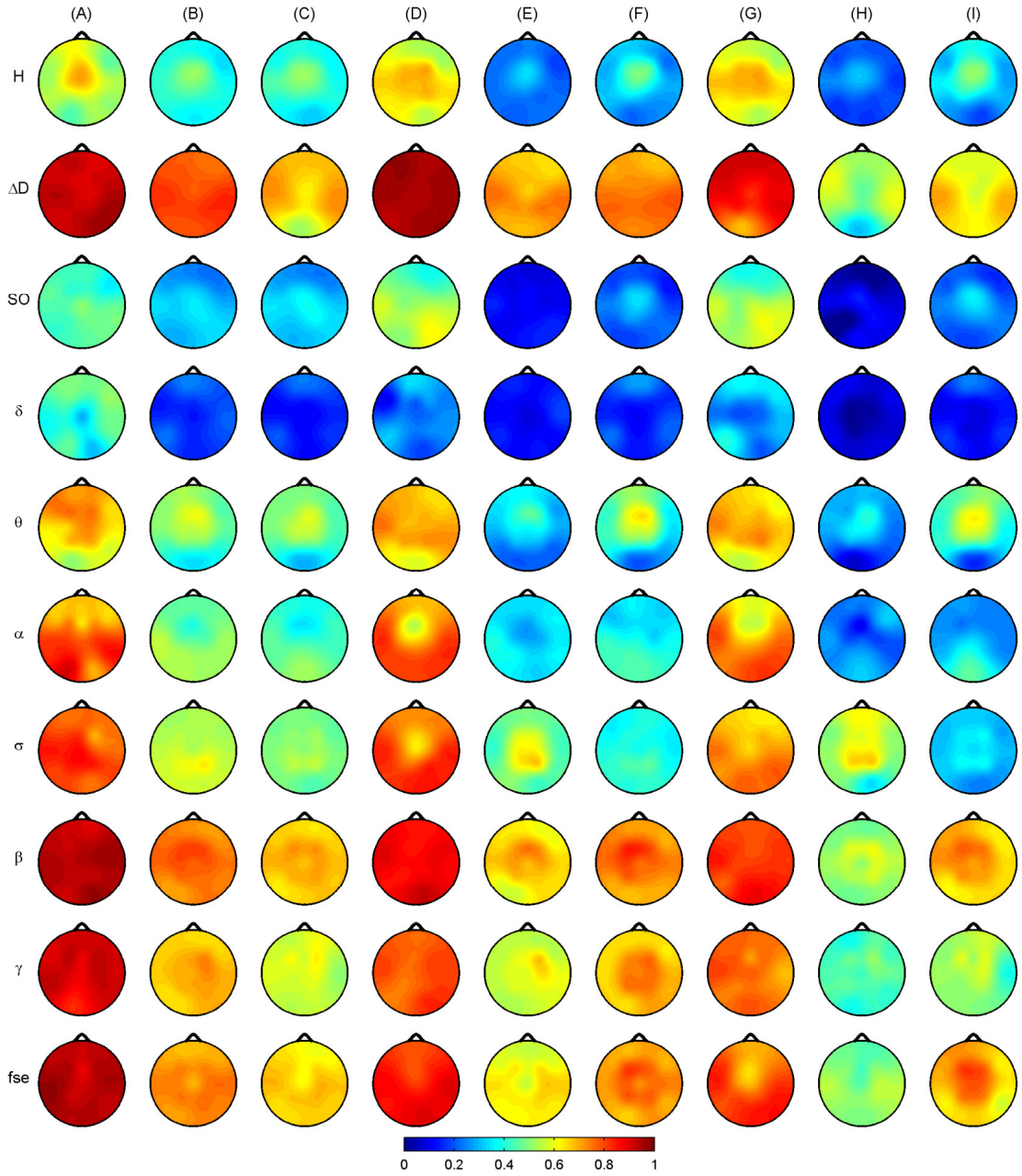

Figure 7.9. Sleep stage classification results obtained using a feedforward neural network classifier both at individual and group levels. (A) Maximal $\hat{K}$ values taken across subjects. (B) Averaged individual $\hat{K}$ values. (C) Group-level $\hat{K}$ values. (D) Individual conditional $\hat{K}$ values averaged across subjects for sleep stage NREM4. (E) Individual conditional $\hat{K}$ values averaged across subjects for sleep stage NREM2. (F) Individual conditional $\hat{K}$ values averaged across subjects for REM sleep. (G) Group-level conditional $\hat{K}$ for NREM4 sleep. (H) Group-level conditional $\hat{K}$ for sleep stage NREM2. (I) Group-level conditional $\hat{K}$ for REM sleep. Relative band powers are denoted by the labels of the corresponding frequency bands.

DOI:10.15774/PPKE.ITK.2010.008

C.4. Probabilistic neural network

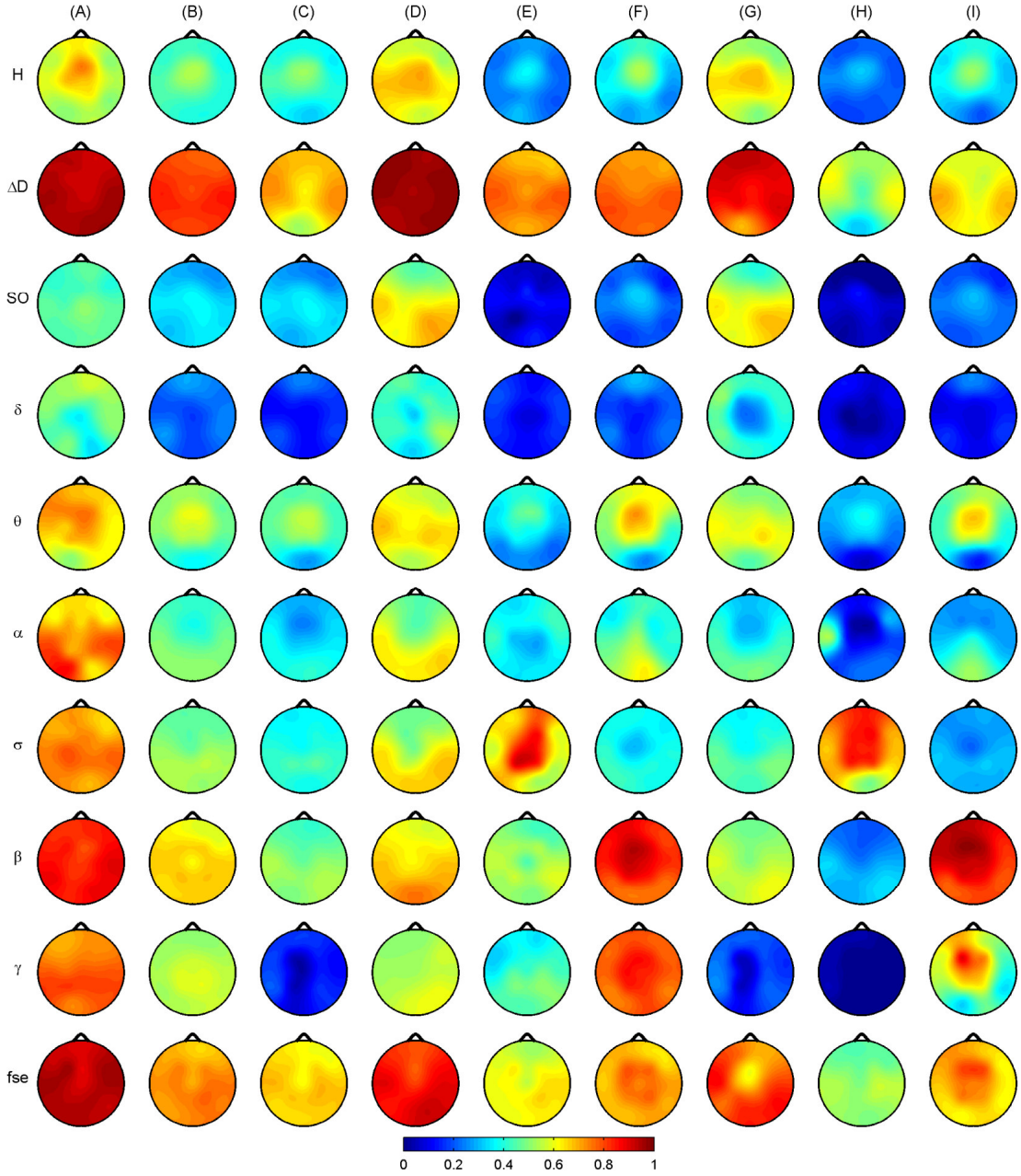

Figure 7.10. Sleep stage classification results obtained using a probabilistic neural network classifier both at individual and group levels. (A) Maximal $\hat{K}$ values taken across subjects. (B) Averaged individual $\hat{K}$ values. (C) Group-level $\hat{K}$ values. (D) Individual conditional $\hat{K}$ values averaged across subjects for sleep stage NREM4. (E) Individual conditional $\hat{K}$ values averaged across subjects for sleep stage NREM2. (F) Individual conditional $\hat{K}$ values averaged across subjects for REM sleep. (G) Group-level conditional $\hat{K}$ for NREM4 sleep. (H) Group-level conditional $\hat{K}$ for sleep stage NREM2. (I) Group-level conditional $\hat{K}$ for REM sleep. Relative band powers are denoted by the labels of the corresponding frequency bands.

DOI:10.15774/PPKE.ITK.2010.008

C.5. Support vector machine with a linear kernel function

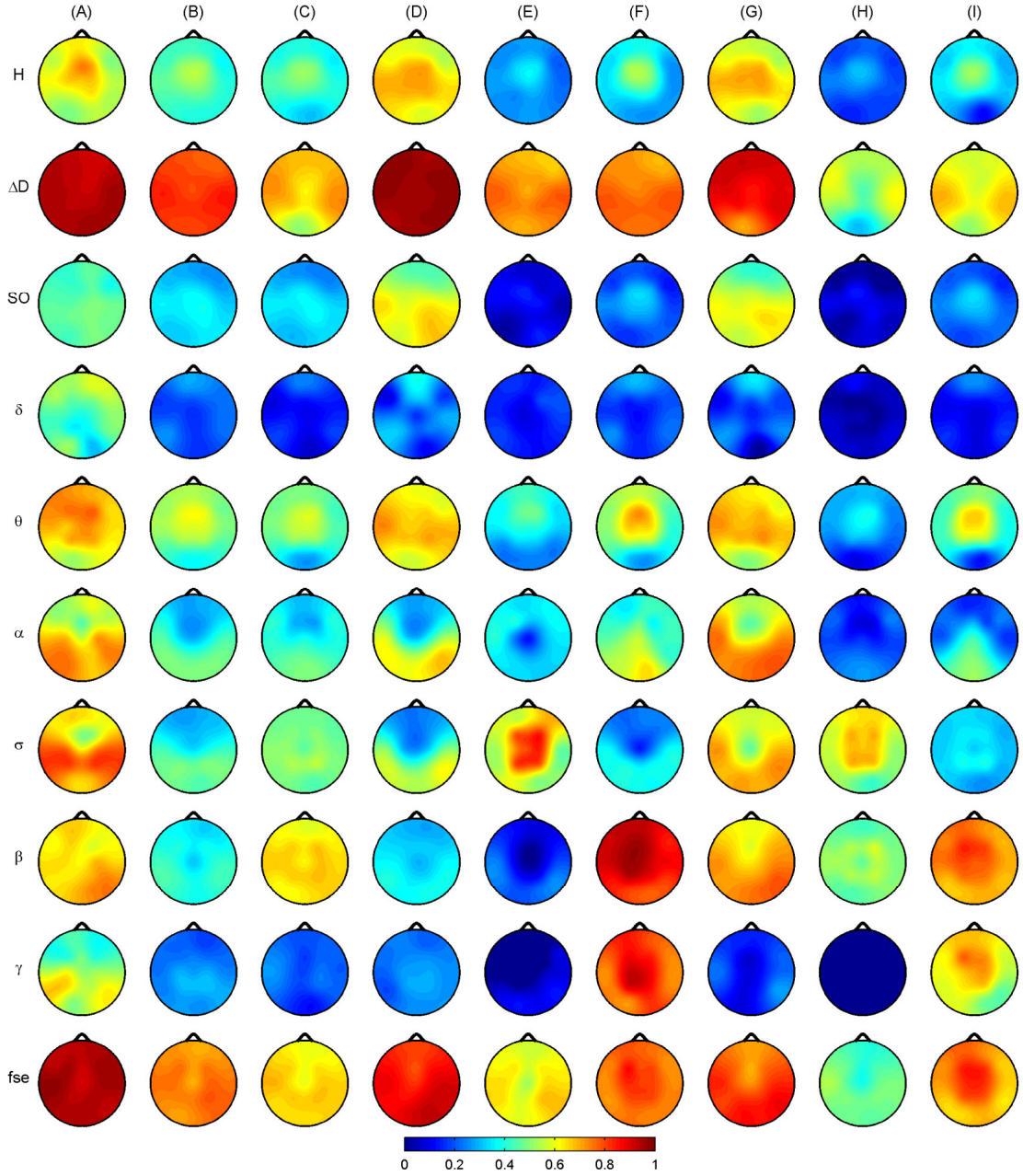

Figure 7.11. Sleep stage classification results obtained using a support vector machine classifier with a linear kernel function both at individual and group levels. (A) Maximal $\hat{K}$ values taken across subjects. (B) Averaged individual $\hat{K}$ values. (C) Group-level $\hat{K}$ values. (D) Individual conditional $\hat{K}$ values averaged across subjects for sleep stage NREM4. (E) Individual conditional $\hat{K}$ values averaged across subjects for sleep stage NREM2. (F) Individual conditional $\hat{K}$ values averaged across subjects for REM sleep. (G) Group-level conditional $\hat{K}$ for NREM4 sleep. (H) Group-level conditional $\hat{K}$ for sleep stage NREM2. (I) Group-level conditional $\hat{K}$ for REM sleep. Relative band powers are denoted by the labels of the corresponding frequency bands.

DOI:10.15774/PPKE.ITK.2010.008

C.6. Support vector machine with a radial basis kernel function

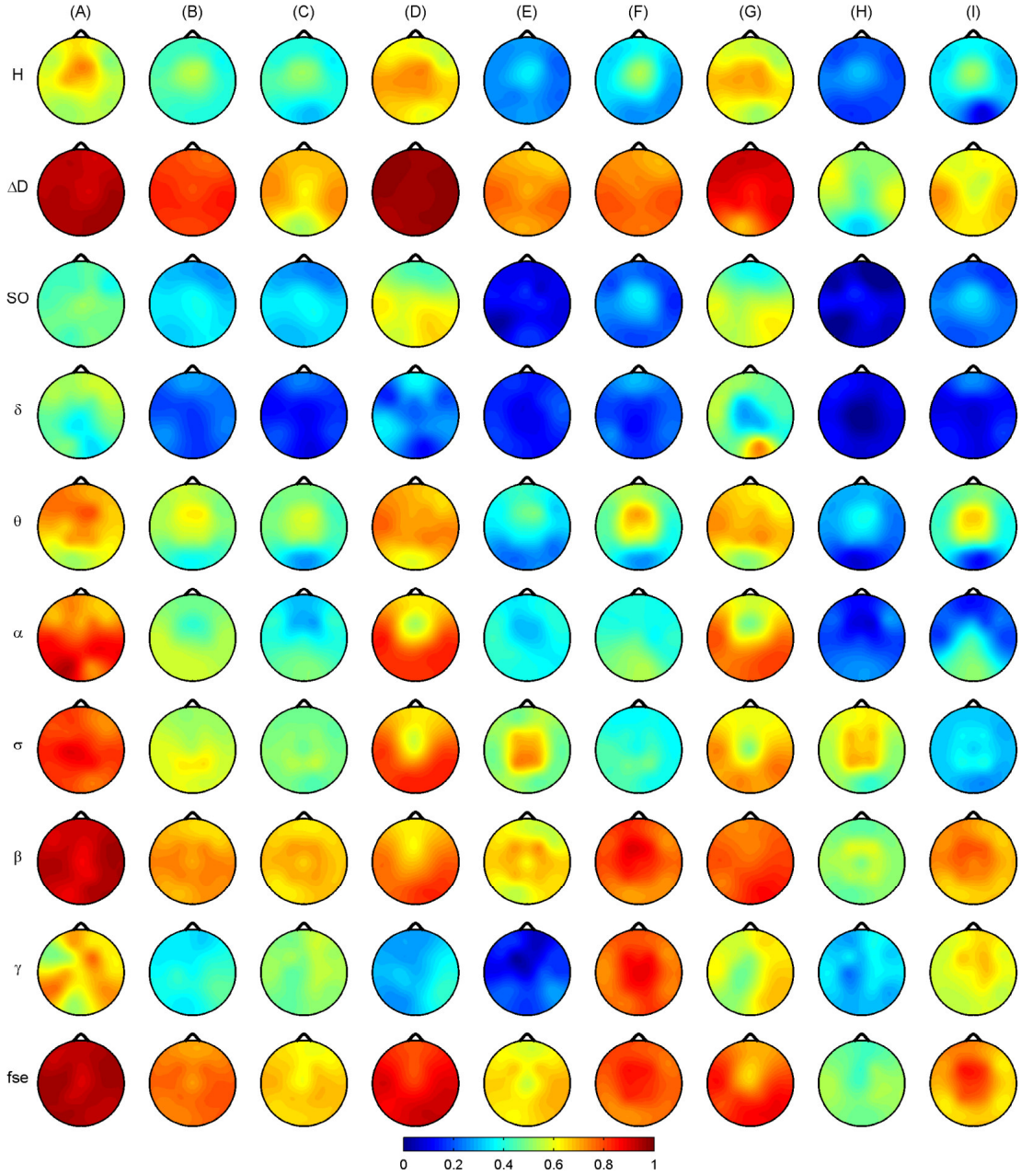

Figure 7.12. Sleep stage classification results obtained using a support vector machine classifier with a radial basis kernel function both at individual and group levels. (A) Maximal $\hat{K}$ values taken across subjects. (B) Averaged individual $\hat{K}$ values. (C) Group-level $\hat{K}$ values. (D) Individual conditional $\hat{K}$ values averaged across subjects for sleep stage NREM4. (E) Individual conditional $\hat{K}$ values averaged across subjects for sleep stage NREM2. (F) Individual conditional $\hat{K}$ values averaged across subjects for REM sleep. (G) Group-level conditional $\hat{K}$ for NREM4 sleep. (H) Group-level conditional $\hat{K}$ for sleep stage NREM2. (I) Group-level conditional $\hat{K}$ for REM sleep. Relative band powers are denoted by the labels of the corresponding frequency bands.

DOI:10.15774/PPKE.ITK.2010.008

D. Combination of measures

D.1. Combination of three measures

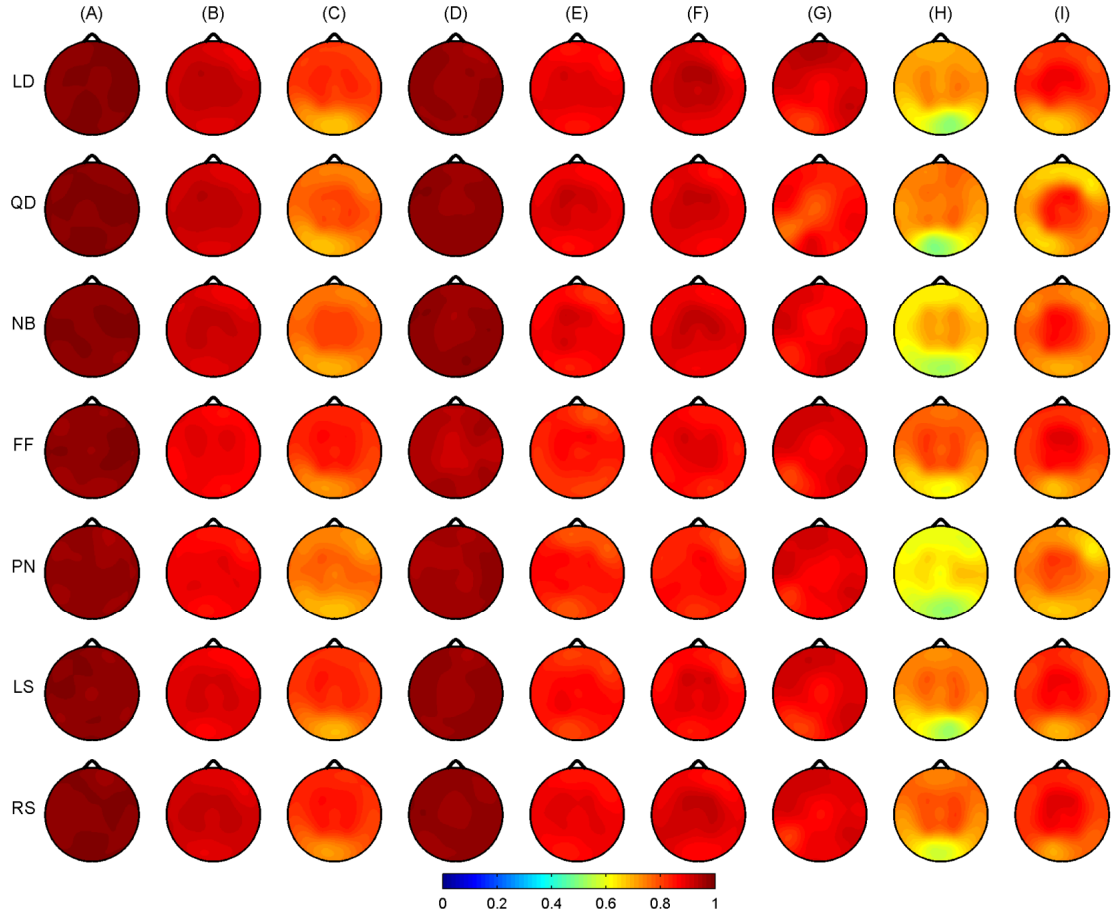

Figure 7.13. $\hat{K}$ values achieved by combination of three best measures in particular channels. Rows present results for different classifiers. Meaning of the column labels is as follows. (A) Maximal $\hat{K}$ values taken across subjects. (B) Averaged individual $\hat{K}$ values. (C) Group-level $\hat{K}$ values. (D) Individual conditional $\hat{K}$ values averaged across subjects for sleep stage NREM4. (E) Individual conditional $\hat{K}$ values averaged across subjects for sleep stage NREM2. (F) Individual conditional $\hat{K}$ values averaged across subjects for REM sleep. (G) Group-level conditional $\hat{K}$ for NREM4 sleep. (H) Group-level conditional $\hat{K}$ for sleep stage NREM2. (I) Group-level conditional $\hat{K}$ for REM sleep.

DOI:10.15774/PPKE.ITK.2010.008

D.2. Combination of four measures

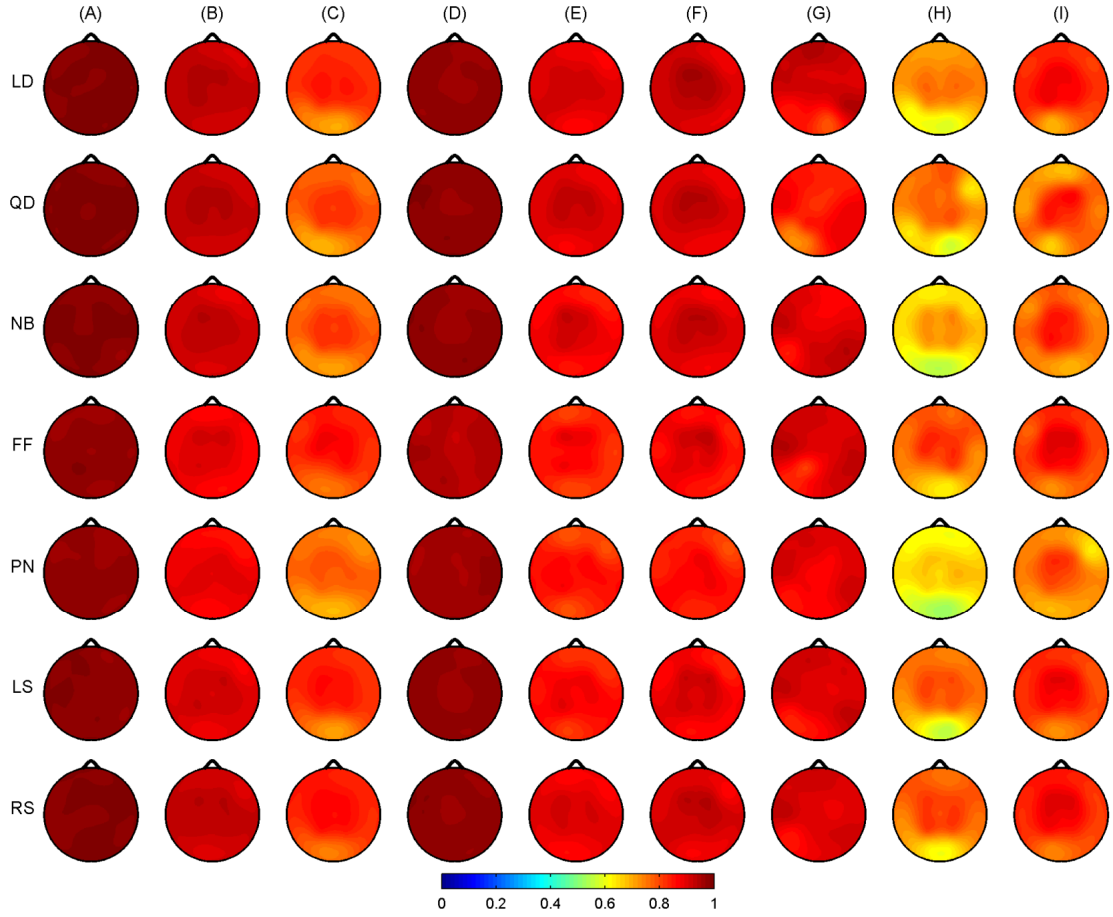

Figure 7.14. $\hat{K}$ *values achieved by combination of four best measures in particular channels. Rows present results for different classifiers. Meaning of the column labels is as follows. (A) Maximal* $\hat{K}$ *values taken across subjects. (B) Averaged individual* $\hat{K}$ *values. (C) Group-level* $\hat{K}$ *values. (D) Individual conditional* $\hat{K}$ *values averaged across subjects for sleep stage NREM4. (E) Individual conditional* $\hat{K}$ *values averaged across subjects for sleep stage NREM2. (F) Individual conditional* $\hat{K}$ *values averaged across subjects for REM sleep. (G) Group-level conditional* $\hat{K}$ *for NREM4 sleep. (H) Group-level conditional* $\hat{K}$ *for sleep stage NREM2. (I) Group-level conditional* $\hat{K}$ *for REM sleep.*

DOI:10.15774/PPKE.ITK.2010.008

E. Individual-level channel and measure selection results

E.1. Overall results

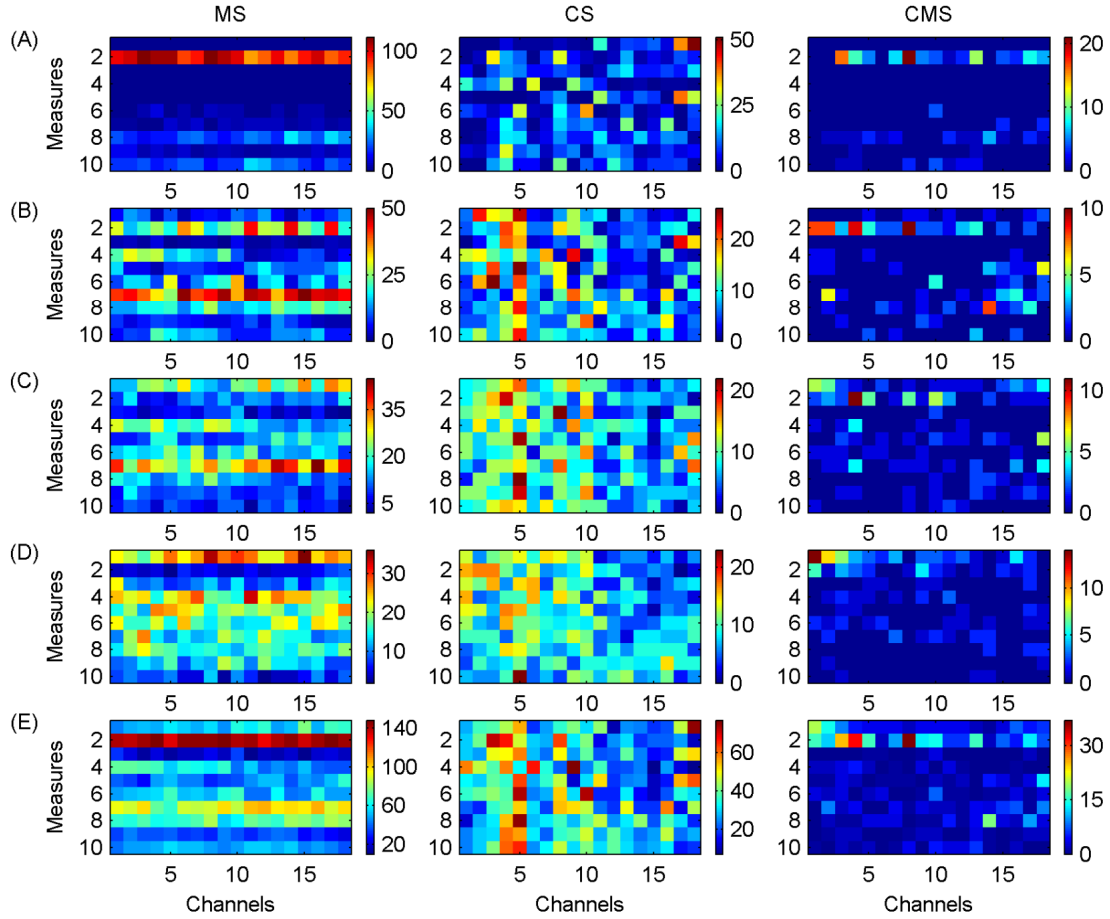

Figure 7.15. Individual-level feature selection results. Number of cases (subjects x paradigms) when particular measures were selected as the best measures in single channels (MS), particular channels were selected as the best channels considering particular measures (CS) and when particular channel x measure combinations were selected as the best features according to the obtained $\hat{K}$ values. (A)-(D) denote cases when particular measures, channels and channel x measure combination were found to be the 1st, 2nd, 3rd and 4th best features, respectively. (E) stands for sums of cases presented in rows (A)-(D). The order of the measures is H, ΔD, P_{SO}, P_{δ}, P_{θ}, P_{α}, P_{σ}, P_{β}, P_{γ}, f_{se}, while the order of the channels is as follows: Fp2, F8, T4, T6, O2, Fp1, F7, T3, T5, O1, F4, C4, P4, F3, C3, P3, Fz, Cz.

DOI:10.15774/PPKE.ITK.2010.008

E.2. Measure selection results

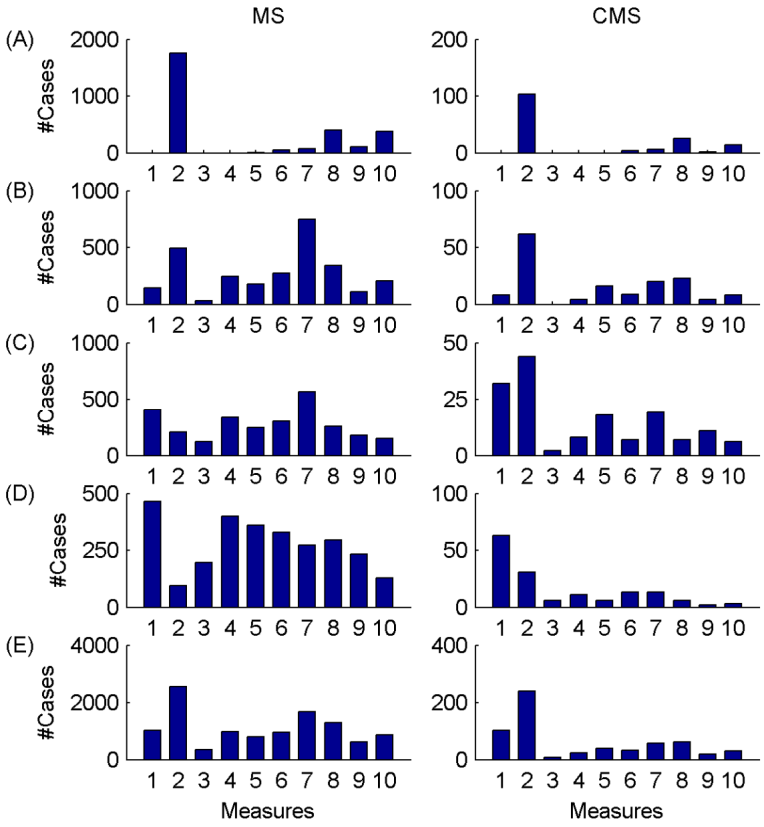

Figure 7.16. Individual-level results. Number of cases (subjects x paradigms x channels) when particular measures (MS) and channel x measure combinations (CMS) were selected as the best features. (A)-(D) denote cases when particular measures and channel x measure combinations were found to be the 1st, 2nd, 3rd and 4th best features, respectively. Row (E) stands for sums of cases presented in rows (A)-(D). The order of the measures is as follows: H, ΔD, P_{SO}, P_{δ}, P_{θ}, P_{α}, P_{σ}, P_{β}, P_{γ}, f_{se}. Bars can be considered as sums across the columns of corresponding subplots in Figure 7.15.

DOI:10.15774/PPKE.ITK.2010.008

E.3. Channel selection results

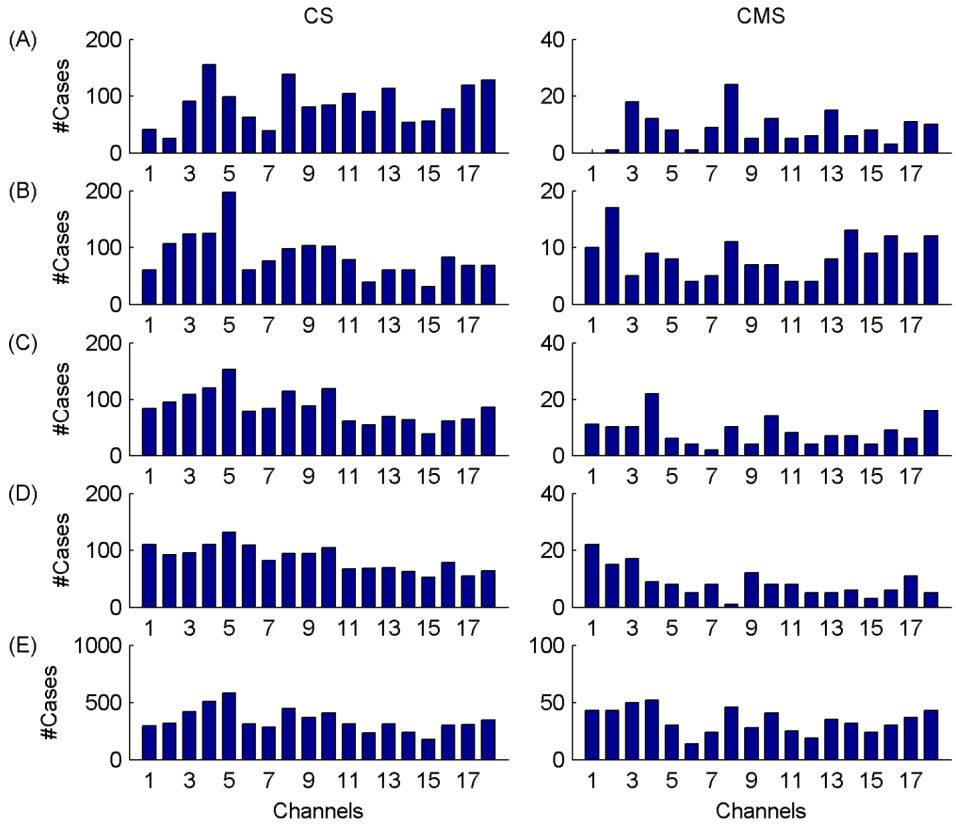

Figure 7.17. Individual-level results. Number of cases (subjects x paradigms x measures) when particular channels (CS) and channel x measure combinations (CMS) were selected as the best features. (A)-(D) denote cases when particular channels and channel x measure combinations were found to be the 1st, 2nd, 3rd and 4th best features, respectively. Row (E) stands for sums of cases presented in rows (A)-(D). The order of the channels is as follows: Fp2, F8, T4, T6, O2, Fp1, F7, T3, T5, O1, F4, C4, P4, F3, C3, P3, Fz, Cz. Bars can be considered as sums across the rows of corresponding subplots in Figure 7.15.

DOI:10.15774/PPKE.ITK.2010.008

BIBLIOGRAPHY

The author's journal publications related to the dissertation

[1] **B. Weiss**, Z. Clemens, R. Bódizs, Z. Vágó, and P. Halász, "Spatio-temporal analysis of monofractal and multifractal properties of the human sleep EEG," *Journal of Neuroscience Methods*, vol. 185, no. 1, pp. 116-24, Dec 2009.

[2] **B. Weiss**, Z. Clemens, R. Bódizs, and P. Halász, "Comparison of fractal and power spectral EEG features: effects of topography and sleep stages," *submitted*.

[3] **B. Weiss**, Z. Clemens, R. Bódizs, and P. Halász, "Gender-related differences of fractal and power spectral EEG features in young adults: effects of topography and sleep stages," *submitted*.

[4] **B. Weiss**, Z. Clemens, R. Bódizs, and P. Halász, "A comparison of classification methods for sleep staging by combination of fractal and power spectral features of EEG signals recorded at different topographic locations," *submitted*.

The author's conference publications related to the dissertation

[5] **B. Weiss**, Z. Clemens, R. Bódizs, P. Halász, and T. Roska, "Topographic distribution of temporal self-similarity properties of human sleep EEG recordings," in *Frontiers in Systems Neuroscience. Conference Abstract: 12th Meeting of the Hungarian Neuroscience Society*, Budapest, Hungary: Frontiers in Systems Neuroscience, 2009.

The author's other journal and conference publications

[6] Z. Clemens, **B. Weiss**, A. Szucs, L. Eross, G. Rásonyi, and P. Halász, "Phase coupling between rhythmic slow activity and gamma characterizes mesiotemporal rapid-eye-movement sleep in humans.," *Neuroscience,* vol. 163, pp. 388-96, Sep 2009.

[7] **B. Weiss**, Y. C. Tang, and F. R. Tang, "Fractal properties of epileptic field potentials recorded from the CA1 area of the hippocampus in the mouse model of temporal lobe epilepsy," presented at *28th International Epilepsy Congress*, Budapest, Hungary, 2009.

[8] **B. Weiss**, I. Ulbert, and L. Erőss, "Fractal properties of epileptic local field potentials recorded from different layers of the frontal cortex using a chronically implanted laminar microelectrode in humans," in *4th International IEEE EMBS Conference on Neural Engineering*, Antalya, Turkey, 2009, pp. 498-501.

[9] **B. Weiss**, Z. Vágó, R. Tetzlaff, and T. Roska, "Long-range dependence of long-term continuous intracranial electroencephalograms for detection and prediction of epileptic seizures," in *International Symposium on Nonlinear Theory and its Applications*, Budapest, Hungary, 2008, pp. 704-707.

[10] **B. Weiss**, Z. Vágó, R. Tetzlaff, P. Halász, and T. Roska, "Comparison of self-similar properties of epileptic seizures of mesiotemporal/hippocampal and

DOI:10.15774/PPKE.ITK.2010.008

neocortical origin," in *8th European Congress on Epileptology*, Berlin, Germany, 2008, p. 203.

[11] **B. Weiss**, B. Hegedűs, Z. Vágó, and T. Roska, "Fractal spectra of intracranial electroencephalograms in different types of epilepsy," in *19th International EURASIP Conference Biosignal*, Brno, Czech Republic, 2008, pp. ID 115, 1-5.

[12] L. Gerencsér, C. Matias, Z. Vágó, B. Torma, and **B. Weiss**, "Self-exciting point processes with applications in finance and medicine," in *18th International Symposium on Mathematical Theory of Networks and Systems*, Blacksburg, Virginia, 2008.

[13] **B. Weiss**, Z. Vágó, and T. Roska, "Epileptic seizure prediction and detection based on Hurst parameter estimation," presented at *IX Workshop on Neurobiology of Epilepsy*, Langkawi, Malaysia, 2007.

[14] **B. Weiss**, Z. Vágó, and T. Roska, "Long-range dependence of epileptic seizures," in *3rd International Workshop on Seizure Prediction in Epilepsy*, Freiburg, Germany, 2007, p. 36.

Publications cited in the dissertation

[15] A. Rechtschaffen and A. Kales, *A manual of standardized terminology, techniques and scoring system for sleep stages of human subjects*: Bethesda, Md., U. S. National Institute of Neurological Diseases and Blindness, Neurological Information Network, 1968.

[16] C. Stam, "Nonlinear dynamical analysis of EEG and MEG: review of an emerging field.," *Clin Neurophysiol,* vol. 116, no. 10, pp. 2266-301, Oct 2005.

[17] P. Rapp, A. Albano, T. Schmah, and L. Farwell, "Filtered noise can mimic low-dimensional chaotic attractors.," *Phys Rev E Stat Phys Plasmas Fluids Relat Interdiscip Topics,* vol. 47, no. 4, pp. 2289-2297, Apr 1993.

[18] T. Schreiber and A. Schmitz, "Surrogate time series," *Physica D: Nonlinear Phenomena,* vol. 142, no. 3-4, pp. 346-382, 2000.

[19] R. Cerf, A. Daoudi, M. Ould Hénoune, and E. el Ouasdad, "Episodes of low-dimensional self-organized dynamics from electroencephalographic alpha-signals.," *Biol Cybern,* vol. 77, no. 4, pp. 235-45, Oct 1997.

[20] M. Palus, "Nonlinearity in normal human EEG: cycles, temporal asymmetry, nonstationarity and randomness, not chaos.," *Biol Cybern,* vol. 75, no. 5, pp. 389-96, Nov 1996.

[21] C. Stam, J. Pijn, P. Suffczynski, and F. Lopes da Silva, "Dynamics of the human alpha rhythm: evidence for non-linearity?," *Clin Neurophysiol,* vol. 110, no. 10, pp. 1801-13, Oct 1999.

[22] K. Linkenkaer-Hansen, V. Nikouline, J. Palva, and R. Ilmoniemi, "Long-range temporal correlations and scaling behavior in human brain oscillations.," *J Neurosci,* vol. 21, no. 4, pp. 1370-7, Feb 2001.

[23] P. Bak, C. Tang, and K. Wiesenfeld, "Self-organized criticality.," *Phys Rev A,* vol. 38, no. 1, pp. 364-374, Jul 1988.

[24] P. Bak, *How nature works: the science of self-organized criticality*. Oxford: Oxford University Press, 1997.

[25] A. L. Barabási and H. E. Stanley, *Fractal concepts in surface growth*. Cambridge: Cambridge University Press, 1994.

DOI:10.15774/PPKE.ITK.2010.008

[26] J. B. Bassingthwaighte, L. S. Liebovitch, and B. J. West, *Fractal physiology*. New York: Oxford University Press, 1994.
[27] P. Bak, C. Tang, and K. Wiesenfeld, "Self-organized criticality: An explanation of the 1/f noise.," *Phys Rev Lett,* vol. 59, no. 4, pp. 381-384, Jul 1987.
[28] V. Nikulin and T. Brismar, "Long-range temporal correlations in electroencephalographic oscillations: Relation to topography, frequency band, age and gender.," *Neuroscience,* vol. 130, no. 2, pp. 549-58, 2005.
[29] M. Shadlen and W. Newsome, "The variable discharge of cortical neurons: implications for connectivity, computation, and information coding.," *J Neurosci,* vol. 18, no. 10, pp. 3870-96, May 1998.
[30] Y. Shu, A. Hasenstaub, and D. McCormick, "Turning on and off recurrent balanced cortical activity.," *Nature,* vol. 423, no. 6937, pp. 288-93, May 2003.
[31] J. Beggs and D. Plenz, "Neuronal avalanches in neocortical circuits.," *J Neurosci,* vol. 23, no. 35, pp. 11167-77, Dec 2003.
[32] D. Chialvo and P. Bak, "Learning from mistakes.," *Neuroscience,* vol. 90, no. 4, pp. 1137-48, 1999.
[33] V. G. Kiselev, K. R. Hahn, and D. P. Auer, "Is the brain cortex a fractal?," *Neuroimage,* vol. 20, no. 3, pp. 1765-1774, Nov 2003.
[34] A. Pellionisz, "Neural geometry: towards a fractal model of neurons," in *Models of Brain Function*, R. M. J. Cotterill, Ed. Cambridge, New York and Melbourne: Cambridge University Press, 1989, pp. 453-464.
[35] W. Freeman, M. Holmes, B. Burke, and S. Vanhatalo, "Spatial spectra of scalp EEG and EMG from awake humans.," *Clin Neurophysiol,* vol. 114, no. 6, pp. 1053-68, Jun 2003.
[36] W. Freeman, L. Rogers, M. Holmes, and D. Silbergeld, "Spatial spectral analysis of human electrocorticograms including the alpha and gamma bands.," *J Neurosci Methods,* vol. 95, no. 2, pp. 111-21, Feb 2000.
[37] S. B. Lowen, L. S. Liebovitch, and J. A. White, "Fractal ion-channel behavior generates fractal firing patterns in neuronal models," *Physical review. E, Statistical physics, plasmas, fluids, and related interdisciplinary topics,* vol. 59, no. 5 Pt B, pp. 5970-80, May 1999.
[38] C. D. Lewis, G. L. Gebber, P. D. Larsen, and S. M. Barman, "Long-term correlations in the spike trains of medullary sympathetic neurons," *Journal of Neurophysiology,* vol. 85, no. 4, pp. 1614-22, Apr 2001.
[39] S. Spasic, A. Kalauzi, G. Grbic, L. Martac, and M. Culic, "Fractal analysis of rat brain activity after injury," *Medical & Biological Engineering & Computing,* vol. 43, no. 3, pp. 345-348, May 2005.
[40] J. González, A. Gamundi, R. Rial, M. Nicolau, L. de Vera, and E. Pereda, "Nonlinear, fractal, and spectral analysis of the EEG of lizard, Gallotia galloti.," *Am J Physiol,* vol. 277, no. 1 Pt 2, pp. R86-93, Jul 1999.
[41] B. Weiss. *CerebroLab - EEG visualization and processing toolbox*. [Online]. Available: https://digitus.itk.ppke.hu/~weiss/research/cerebrolab/
[42] H. E. Hurst, "Long Term Storage Capacity of Reservoirs," *Transactions of the American Society of Civil Engineers,* vol. 116, pp. 770-799, 1951.
[43] B. B. Mandelbrot and M. S. Taqqu, "Robust R/S analysis of long-run serial correlation," in *Proceedings of the 42nd Session of the International Statistical Institute*. vol. 48, Book 2 Manila, 1979, pp. 69-104.
[44] V. Kulish, A. Sourin, and O. Sourina, "Human electroencephalograms seen as fractal time series: Mathematical analysis and visualization," *Computers in Biology and Medicine,* vol. 36, no. 3, pp. 291-302, Mar 2006.

DOI:10.15774/PPKE.ITK.2010.008

[45] J. Beran, *Statistics for Long-Memory Processes*, 1st ed. New York: Chapman & Hall/CRC, 1994.

[46] R. Acharya, O. Faust, N. Kannathal, T. Chua, and S. Laxminarayan, "Non-linear analysis of EEG signals at various sleep stages," *Comput. Methods Programs Biomed.,* vol. 80, no. 1, pp. 37-45, Oct 2005.

[47] H. Kantz and T. Schreiber, *Nonlinear time series analysis*, 2nd ed. Cambridge, New York and Melbourne: Cambridge University Press, 2003.

[48] C. K. Peng, S. V. Buldyrev, S. Havlin, M. Simons, H. E. Stanley, and A. L. Goldberger, "Mosaic organization of DNA nucleotides," *Physical Review E,* vol. 49, no. 2, p. 1685, 1994.

[49] C. Peng, S. Havlin, H. Stanley, and A. Goldberger, "Quantification of scaling exponents and crossover phenomena in nonstationary heartbeat time series.," *Chaos,* vol. 5, no. 1, pp. 82-7, 1995.

[50] A. Eke, P. Herman, L. Kocsis, and L. Kozak, "Fractal characterization of complexity in temporal physiological signals.," *Physiol Meas,* vol. 23, no. 1, pp. R1-38, Feb 2002.

[51] T. Higuchi, "Relationship between the fractal dimension and the power law index for a time series: A numerical investigation," *Physica D: Nonlinear Phenomena,* vol. 46, no. 2, pp. 254-264, 1990.

[52] A. Eke, et al., "Physiological time series: distinguishing fractal noises from motions.," *Pflugers Arch,* vol. 439, no. 4, pp. 403-15, Feb 2000.

[53] D. Delignieres, S. Ramdani, L. Lemoine, K. Torre, M. Fortes, and G. Ninot, "Fractal analyses for 'short' time series: A re-assessment of classical methods," *Journal of Mathematical Psychology,* vol. 50, no. 6, pp. 525-544, 2006.

[54] G. Rangarajan and M. Ding, "Integrated approach to the assessment of long range correlation in time series data," *Phys Rev E Stat Phys Plasmas Fluids Relat Interdiscip Topics,* vol. 61, no. 5A, pp. 4991-5001, May 2000.

[55] K. Hu, P. Ivanov, Z. Chen, P. Carpena, and H. Stanley, "Effect of trends on detrended fluctuation analysis.," *Phys Rev E Stat Nonlin Soft Matter Phys,* vol. 64, no. 1 Pt 1, p. 011114, Jul 2001.

[56] Z. Chen, P. Ivanov, K. Hu, and H. Stanley, "Effect of nonstationarities on detrended fluctuation analysis.," *Phys Rev E Stat Nonlin Soft Matter Phys,* vol. 65, no. 4 Pt 1, p. 041107, Apr 2002.

[57] Z. Chen, K. Hu, P. Carpena, P. Bernaola-Galvan, H. Stanley, and P. Ivanov, "Effect of nonlinear filters on detrended fluctuation analysis.," *Phys Rev E Stat Nonlin Soft Matter Phys,* vol. 71, no. 1 Pt 1, p. 011104, Jan 2005.

[58] S. Gudmundsson, T. Runarsson, S. Sigurdsson, G. Eiriksdottir, and K. Johnsen, "Reliability of quantitative EEG features.," *Clin Neurophysiol,* vol. 118, no. 10, pp. 2162-71, Oct 2007.

[59] S. Katsev and I. L'Heureux, "Are Hurst exponents estimated from short or irregular time series meaningful?," *COMPUTERS & GEOSCIENCES,* pp. 1085-1089, NOV 2003 2003.

[60] Y. Shen, E. Olbrich, P. Achermann, and P. F. Meier, "Dimensional complexity and spectral properties of the human sleep EEG," *Clinical Neurophysiology,* vol. 114, no. 2, pp. 199-209, Feb 2003.

[61] A. Rényi, *Probability Theory*. Amsterdam: North Holland, 1971.

[62] J. Fell, J. Röschke, K. Mann, and C. Schäffner, "Discrimination of sleep stages: a comparison between spectral and nonlinear EEG measures.," *Electroencephalogr Clin Neurophysiol,* vol. 98, no. 5, pp. 401-10, May 1996.

DOI:10.15774/PPKE.ITK.2010.008

[63] C. Long, N. Shah, C. Loughlin, J. Spydell, and R. Bedford, "A comparison of EEG determinants of near-awakening from isoflurane and fentanyl anesthesia. Spectral edge, median power frequency, and delta ratio.," *Anesth Analg,* vol. 69, no. 2, pp. 169-73, Aug 1989.

[64] G. Gurman, "Assessment of depth of general anesthesia. Observations on processed EEG and spectral edge frequency.," *Int J Clin Monit Comput,* vol. 11, no. 3, pp. 185-9, Aug 1994.

[65] G. Gurman, S. Fajer, A. Porat, M. Schily, and A. Pearlman, "Use of EEG spectral edge as index of equipotency in a comparison of propofol and isoflurane for maintenance of general anaesthesia.," *Eur J Anaesthesiol,* vol. 11, no. 6, pp. 443-8, Nov 1994.

[66] M. Massimini, R. Huber, F. Ferrarelli, S. Hill, and G. Tononi, "The sleep slow oscillation as a traveling wave.," *The Journal of neuroscience,* vol. 24, no. 31, pp. 6862-70, Aug 2004.

[67] P. Achermann and A. Borbély, "Low-frequency (< 1 Hz) oscillations in the human sleep electroencephalogram.," *Neuroscience,* vol. 81, no. 1, pp. 213-22, Nov 1997.

[68] V. Nikulin and T. Brismar, "Long-range temporal correlations in alpha and beta oscillations: effect of arousal level and test-retest reliability.," *Clin Neurophysiol,* vol. 115, no. 8, pp. 1896-908, Aug 2004.

[69] T. Bojić, A. Vuckovic, and A. Kalauzi, "Modeling EEG fractal dimension changes in wake and drowsy states in humans--a preliminary study.," *J Theor Biol,* vol. 262, no. 2, pp. 214-22, Jan 2010.

[70] K. Linkenkaer-Hansen, V. Nikulin, J. Palva, K. Kaila, and R. Ilmoniemi, "Stimulus-induced change in long-range temporal correlations and scaling behaviour of sensorimotor oscillations.," *Eur J Neurosci,* vol. 19, no. 1, pp. 203-11, Jan 2004.

[71] L. Poupard, R. Sartène, and J. Wallet, "Scaling behavior in beta-wave amplitude modulation and its relationship to alertness.," *Biol Cybern,* vol. 85, no. 1, pp. 19-26, Jul 2001.

[72] J. M. Lee, D. J. Kim, I. Y. Kim, K. S. Park, and S. I. Kim, "Nonlinear-analysis of human sleep EEG using detrended fluctuation analysis," *Medical Engineering & Physics,* vol. 26, no. 9, pp. 773-776, Nov 2004.

[73] S. Leistedt, M. Dumont, N. Coumans, J. Lanquart, F. Jurysta, and P. Linkowski, "The modifications of the long-range temporal correlations of the sleep EEG due to major depressive episode disappear with the status of remission.," *Neuroscience,* vol. 148, no. 3, pp. 782-93, Sep 2007.

[74] S. Leistedt, M. Dumont, J. P. Lanquart, F. Jurysta, and P. Linkowski, "Characterization of the sleep EEG in acutely depressed men using detrended fluctuation analysis," *Clinical Neurophysiology,* vol. 118, no. 4, pp. 940-50, Apr 2007.

[75] Q. L. Ma, X. B. Ning, J. Wang, and C. H. Bian, "A new measure to characterize multifractality of sleep electroencephalogram," *Chinese Science Bulletin,* vol. 51, no. 24, pp. 3059-3064, Dec 2006.

[76] E. Pereda, A. Gamundi, R. Rial, and J. González, "Non-linear behaviour of human EEG: fractal exponent versus correlation dimension in awake and sleep stages.," *Neurosci Lett,* vol. 250, no. 2, pp. 91-4, Jul 1998.

[77] O. Benoit, A. Daurat, and J. Prado, "Slow (0.7-2 Hz) and fast (2-4 Hz) delta components are differently correlated to theta, alpha and beta frequency bands during NREM sleep.," *Clin Neurophysiol,* vol. 111, no. 12, pp. 2103-6, Dec 2000.

DOI:10.15774/PPKE.ITK.2010.008

[78] E. Pereda, A. Gamundi, M. Nicolau, R. Rial, and J. González, "Interhemispheric differences in awake and sleep human EEG: a comparison between non-linear and spectral measures.," *Neurosci Lett,* vol. 263, no. 1, pp. 37-40, Mar 1999.

[79] D. Lin, A. Sharif, and H. Kwan, "Scaling and organization of electroencephalographic background activity and alpha rhythm in healthy young adults.," *Biol Cybern,* vol. 95, no. 5, pp. 401-11, Nov 2006.

[80] T. C. Ferree and R. C. Hwa, "Power-law scaling in human EEG: relation to Fourier power spectrum," *Neurocomputing,* vol. 52-54, pp. 755-761, 2003.

[81] E. Werth, P. Achermann, and A. Borbély, "Brain topography of the human sleep EEG: antero-posterior shifts of spectral power.," *Neuroreport,* vol. 8, no. 1, pp. 123-7, Dec 1996.

[82] L. De Gennaro, M. Ferrara, G. Curcio, and R. Cristiani, "Antero-posterior EEG changes during the wakefulness-sleep transition.," *Clin Neurophysiol,* vol. 112, no. 10, pp. 1901-11, Oct 2001.

[83] E. Werth, P. Achermann, and A. Borbély, "Fronto-occipital EEG power gradients in human sleep.," *J Sleep Res,* vol. 6, no. 2, pp. 102-12, Jun 1997.

[84] O. Jenni, E. van Reen, and M. Carskadon, "Regional differences of the sleep electroencephalogram in adolescents.," *J Sleep Res,* vol. 14, no. 2, pp. 141-7, Jun 2005.

[85] L. De Gennaro, M. Ferrara, G. Curcio, R. Cristiani, and M. Bertini, "Cortical EEG topography of REM onset: the posterior dominance of middle and high frequencies.," *Clin Neurophysiol,* vol. 113, no. 4, pp. 561-70, Apr 2002.

[86] L. Finelli, A. Borbély, and P. Achermann, "Functional topography of the human nonREM sleep electroencephalogram.," *Eur J Neurosci,* vol. 13, no. 12, pp. 2282-90, Jun 2001.

[87] G. Tinguely, L. A. Finelli, H. P. Landolt, A. A. Borbely, and P. Achermann, "Functional EEG topography in sleep and waking: state-dependent and state-independent features," *Neuroimage,* vol. 32, no. 1, pp. 283-92, Aug 1 2006.

[88] S. Happe, P. Anderer, G. Gruber, G. Klösch, B. Saletu, and J. Zeitlhofer, "Scalp topography of the spontaneous K-complex and of delta-waves in human sleep.," *Brain Topogr,* vol. 15, no. 1, pp. 43-9, 2002.

[89] P. Halasz, "K-complex, a reactive EEG graphoelement of NREM sleep: an old chap in a new garment," *SLEEP MEDICINE REVIEWS,* vol. 9, no. 5, pp. 391-412, OCT 2005 2005.

[90] L. De Gennaro and M. Ferrara, "Sleep spindles: an overview," *SLEEP MEDICINE REVIEWS,* vol. 7, no. 5, pp. 423-440, OCT 2003 2003.

[91] E. Werth, P. Achermann, D. Dijk, and A. Borbély, "Spindle frequency activity in the sleep EEG: individual differences and topographic distribution.," *Electroencephalogr Clin Neurophysiol,* vol. 103, no. 5, pp. 535-42, Nov 1997.

[92] J. Zeitlhofer, G. Gruber, P. Anderer, S. Asenbaum, P. Schimicek, and B. Saletu, "Topographic distribution of sleep spindles in young healthy subjects.," *J Sleep Res,* vol. 6, no. 3, pp. 149-55, Sep 1997.

[93] A. Yasoshima, et al., "Potential distribution of vertex sharp wave and saw-toothed wave on the scalp.," *Electroencephalogr Clin Neurophysiol,* vol. 58, no. 1, pp. 73-6, Jul 1984.

[94] M. Sekimoto, M. Kato, N. Kajimura, T. Watanabe, K. Takahashi, and T. Okuma, "Asymmetric interhemispheric delta waves during all-night sleep in humans.," *Clin Neurophysiol,* vol. 111, no. 5, pp. 924-8, May 2000.

DOI:10.15774/PPKE.ITK.2010.008

[95] C. Roth, P. Achermann, and A. Borbély, "Frequency and state specific hemispheric asymmetries in the human sleep EEG.," *Neurosci Lett,* vol. 271, no. 3, pp. 139-42, Aug 1999.

[96] T. Kobayashi, S. Madokoro, K. Misaki, J. Murayama, H. Nakagawa, and Y. Wada, "Interhemispheric differences of the correlation dimension in a human sleep electroencephalogram.," *Psychiatry Clin Neurosci,* vol. 56, no. 3, pp. 265-6, Jun 2002.

[97] P. Achermann and A. Borbély, "Coherence analysis of the human sleep electroencephalogram.," *Neuroscience,* vol. 85, no. 4, pp. 1195-208, Aug 1998.

[98] R. Ferri, F. Rundo, O. Bruni, M. Terzano, and C. Stam, "Regional scalp EEG slow-wave synchronization during sleep cyclic alternating pattern A1 subtypes.," *Neurosci Lett,* vol. 404, no. 3, pp. 352-7, Sep 2006.

[99] M. Kamiński, K. Blinowska, and W. Szclenberger, "Topographic analysis of coherence and propagation of EEG activity during sleep and wakefulness.," *Electroencephalogr Clin Neurophysiol,* vol. 102, no. 3, pp. 216-27, Mar 1997.

[100] S. Hu, M. Stead, Q. Dai, and G. Worrell, "On the Recording Reference Contribution to EEG Correlation, Phase Synchorony, and Coherence.," *IEEE Trans Syst Man Cybern B Cybern,* Jan 2010.

[101] M. Essl and P. Rappelsberger, "EEG coherence and reference signals: experimental results and mathematical explanations.," *Med Biol Eng Comput,* vol. 36, no. 4, pp. 399-406, Jul 1998.

[102] V. Vyazovskiy, P. Achermann, A. Borbély, and I. Tobler, "Interhemispheric coherence of the sleep electroencephalogram in mice with congenital callosal dysgenesis.," *Neuroscience,* vol. 124, no. 2, pp. 481-8, 2004.

[103] V. Vyazovskiy and I. Tobler, "Regional differences in NREM sleep slow-wave activity in mice with congenital callosal dysgenesis.," *J Sleep Res,* vol. 14, no. 3, pp. 299-304, Sep 2005.

[104] D. Dijk, D. Beersma, and G. Bloem, "Sex differences in the sleep EEG of young adults: visual scoring and spectral analysis.," *Sleep,* vol. 12, no. 6, pp. 500-7, Dec 1989.

[105] J. Carrier, S. Land, D. Buysse, D. Kupfer, and T. Monk, "The effects of age and gender on sleep EEG power spectral density in the middle years of life (ages 20-60 years old)." *Psychophysiology,* vol. 38, no. 2, pp. 232-42, Mar 2001.

[106] F. Latta, R. Leproult, E. Tasali, E. Hofmann, and E. Van Cauter, "Sex differences in delta and alpha EEG activities in healthy older adults.," *Sleep,* vol. 28, no. 12, pp. 1525-34, Dec 2005.

[107] B. Shaywitz, et al., "Sex differences in the functional organization of the brain for language.," *Nature,* vol. 373, no. 6515, pp. 607-9, Feb 1995.

[108] A. Kaiser, S. Haller, S. Schmitz, and C. Nitsch, "On sex/gender related similarities and differences in fMRI language research.," *Brain Res Rev,* vol. 61, no. 2, pp. 49-59, Oct 2009.

[109] E. Huupponen, S. Himanen, A. Värri, J. Hasan, M. Lehtokangas, and J. Saarinen, "A study on gender and age differences in sleep spindles.," *Neuropsychobiology,* vol. 45, no. 2, pp. 99-105, 2002.

[110] K. Linkenkaer-Hansen, et al., "Genetic contributions to long-range temporal correlations in ongoing oscillations.," *J Neurosci,* vol. 27, no. 50, pp. 13882-9, Dec 2007.

[111] T. Nguyen-Ky, P. Wen, and Y. Li, "Theoretical basis for identification of different anesthetic states based on routinely recorded EEG during operation.," *Comput Biol Med,* vol. 39, no. 1, pp. 40-5, Jan 2009.

DOI:10.15774/PPKE.ITK.2010.008

[112] C. Lin, et al., "Development of wireless brain computer interface with embedded multitask scheduling and its application on real-time driver's drowsiness detection and warning.," *IEEE Trans Biomed Eng,* vol. 55, no. 5, pp. 1582-91, May 2008.
[113] B. H. Jansen and B. M. Dawant, "Knowledge-based approach to sleep EEG analysis-a feasibility study," *Biomedical Engineering, IEEE Transactions on,* vol. 36, no. 5, pp. 510-518, 1989.
[114] J. C. Principe, S. K. Gala, and T. G. Chang, "Sleep staging automaton based on the theory of evidence," *Biomedical Engineering, IEEE Transactions on,* vol. 36, no. 5, pp. 503-509, 1989.
[115] S. Kubicki and W. Herrmann, "The future of computer-assisted investigation of the polysomnogram: sleep microstructure.," *J Clin Neurophysiol,* vol. 13, no. 4, pp. 285-94, Jul 1996.
[116] K. Susmáková and A. Krakovská, "Discrimination ability of individual measures used in sleep stages classification.," *Artif Intell Med,* vol. 44, no. 3, pp. 261-77, Nov 2008.
[117] L. Molinari, G. Dumermuth, and B. Lange, "EEG-based multivariate statistical analysis of sleep stages.," *Neuropsychobiology,* vol. 11, no. 2, pp. 140-8, 1984.
[118] N. Schaltenbrand, et al., "Sleep stage scoring using the neural network model: comparison between visual and automatic analysis in normal subjects and patients.," *Sleep,* vol. 19, no. 1, pp. 26-35, Jan 1996.
[119] N. Schaltenbrand, R. Lengelle, and J. Macher, "Neural network model: application to automatic analysis of human sleep.," *Comput Biomed Res,* vol. 26, no. 2, pp. 157-71, Apr 1993.
[120] C. Robert, C. Guilpin, and A. Limoge, "Review of neural network applications in sleep research.," *J Neurosci Methods,* vol. 79, no. 2, pp. 187-93, Feb 1998.
[121] L. Ray, S. Fogel, C. Smith, and K. Peters, "Validating an automated sleep spindle detection algorithm using an individualized approach.," *J Sleep Res,* Feb 2010.
[122] A. Da Rosa, B. Kemp, T. Paiva, F. Lopes da Silva, and H. Kamphuisen, "A model-based detector of vertex waves and K complexes in sleep electroencephalogram.," *Electroencephalogr Clin Neurophysiol,* vol. 78, no. 1, pp. 71-9, Jan 1991.
[123] C. Richard and R. Lengelle, "Joint time and time-frequency optimal detection of K-complexes in sleep EEG.," *Comput Biomed Res,* vol. 31, no. 3, pp. 209-29, Jun 1998.
[124] G. Hatzilabrou, N. Greenberg, R. Sclabassi, T. Carroll, R. Guthrie, and M. Scher, "A comparison of conventional and matched filtering techniques for rapid eye movement detection of the newborn.," *IEEE Trans Biomed Eng,* vol. 41, no. 10, pp. 990-5, Oct 1994.
[125] J. Smith, W. Funke, W. Yeo, and R. Ambuehl, "Detection of human sleep EEG waveforms.," *Electroencephalogr Clin Neurophysiol,* vol. 38, no. 4, pp. 435-7, Apr 1975.
[126] M. Jobert, E. Poiseau, P. Jähnig, H. Schulz, and S. Kubicki, "Pattern recognition by matched filtering: an analysis of sleep spindle and K-complex density under the influence of lormetazepam and zopiclone.," *Neuropsychobiology,* vol. 26, no. 1-2, pp. 100-7, 1992.
[127] W. Martin, L. Johnson, S. Viglione, P. Naitoh, R. Joseph, and J. Moses, "Pattern recognition of EEG-EOG as a technique for all-night sleep stage scoring.," *Electroencephalogr Clin Neurophysiol,* vol. 32, no. 4, pp. 417-27, Apr 1972.
[128] J. Gaillard and R. Tissot, "Principles of automatic analysis of sleep records with a hybrid system.," *Comput Biomed Res,* vol. 6, no. 1, pp. 1-13, Feb 1973.

DOI:10.15774/PPKE.ITK.2010.008

[129] H. Park, J. Oh, D. Jeong, and K. Park, "Automated sleep stage scoring using hybrid rule- and case-based reasoning.," *Comput Biomed Res,* vol. 33, no. 5, pp. 330-49, Oct 2000.

[130] C. Iber, S. Ancoli-Israel, A. Chesson, and S. F. Quan, *The AASM manual for the scoring of sleep and associated events: rules, terminology, and technical specification*. Westchester, IL: American Academy of Sleep Medicine, 2007.

[131] C.-C. Chang and C.-J. Lin, "LIBSVM : a library for support vector machines," 2001.

[132] R. O. Duda, P. E. Hart, and D. G. Stork, *Pattern classification*, 2nd ed. New York: John Willey & Sons, Inc., 2001.

[133] P. Melin and O. Castillo, *Modelling, Simulation and Control of Non-linear Dynamical Systems: An Intelligent Approach Using Soft Computing and Fractal Theory*. London: Taylor & Francis, Inc., 2002.

[134] A. Kandel, *Fuzzy expert systems*. Boca Raton, FL: CRC Press, Inc., 1992.

[135] J. Landis and G. Koch, "The measurement of observer agreement for categorical data.," *Biometrics,* vol. 33, no. 1, pp. 159-74, Mar 1977.

[136] P. Couto, "Assessing the accuracy of spatial simulation models," *Ecological Modelling,* vol. 167, no. 1-2, pp. 181-198, 2003.

[137] R. G. Congalton and K. Green, *Assessing the Accuracy of Remotely Sensed Data: Principles and Practices*, 2nd ed. Boca Raton: CRC Press, 2008.

[138] M. Dash and H. Liu, "Feature selection for classification," *Intelligent Data Analysis,* vol. 1, no. 1-4, pp. 131-156, 1997.

[139] I. Guyon, Andr\, \#233, and Elisseeff, "An introduction to variable and feature selection," *J. Mach. Learn. Res.,* vol. 3, pp. 1157-1182, 2003.

[140] L. De Gennaro, M. Ferrara, F. Vecchio, G. Curcio, and M. Bertini, "An electroencephalographic fingerprint of human sleep.," *Neuroimage,* vol. 26, no. 1, pp. 114-22, May 2005.

[141] L. Finelli, P. Achermann, and A. Borbély, "Individual 'fingerprints' in human sleep EEG topography.," *Neuropsychopharmacology,* vol. 25, no. 5 Suppl, pp. S57-62, Nov 2001.

[142] D. Garrett, D. Peterson, C. Anderson, and M. Thaut, "Comparison of linear, nonlinear, and feature selection methods for EEG signal classification.," *IEEE Trans Neural Syst Rehabil Eng,* vol. 11, no. 2, pp. 141-4, Jun 2003.

[143] T. Hori, et al., "Proposed supplements and amendments to 'A Manual of Standardized Terminology, Techniques and Scoring System for Sleep Stages of Human Subjects', the Rechtschaffen & Kales (1968) standard," *Psychiatry and Clinical Neurosciences,* vol. 55, no. 3, pp. 305-310, Jun 2001.

[144] H. Danker-Hopfe, et al., "Interrater reliability between scorers from eight European sleep laboratories in subjects with different sleep disorders.," *J Sleep Res,* vol. 13, no. 1, pp. 63-9, Mar 2004.

[145] S. Himanen and J. Hasan, "Limitations of Rechtschaffen and Kales.," *Sleep Med Rev,* vol. 4, no. 2, pp. 149-167, Apr 2000.

[146] C. Bédard, H. Kröger, and A. Destexhe, "Does the 1/f Frequency Scaling of Brain Signals Reflect Self-Organized Critical States?," *Physical Review Letters,* vol. 97, no. 11, p. 118102, 2006.

[147] P. A. Robinson, C. J. Rennie, and D. L. Rowe, "Dynamics of large-scale brain activity in normal arousal states and epileptic seizures," *Physical Review E,* vol. 65, no. 4, p. 041924, 2002.

DOI:10.15774/PPKE.ITK.2010.008

[148] P. A. Robinson, C. J. Rennie, J. J. Wright, H. Bahramali, E. Gordon, and D. L. Rowe, "Prediction of electroencephalographic spectra from neurophysiology," *Physical Review E,* vol. 63, no. 2, p. 021903, 2001.

[149] L. Parrino, M. Boselli, M. Spaggiari, A. Smerieri, and M. Terzano, "Cyclic alternating pattern (CAP) in normal sleep: polysomnographic parameters in different age groups.," *Electroencephalogr. Clin. Neurophysiol.,* vol. 107, no. 6, pp. 439-50, Dec 1998.

[150] M. Terzano, L. Parrino, and M. Spaggiari, "The cyclic alternating pattern sequences in the dynamic organization of sleep.," *Electroencephalogr. Clin. Neurophysiol.,* vol. 69, no. 5, pp. 437-47, May 1988.

[151] M. Terzano, D. Mancia, M. Salati, G. Costani, A. Decembrino, and L. Parrino, "The cyclic alternating pattern as a physiologic component of normal NREM sleep.," *Sleep,* vol. 8, no. 2, pp. 137-45, 1985.

[152] C. E. Elger, "Future trends in epileptology," *Curr Opin Neurol,* vol. 14, no. 2, pp. 185-6, Apr 2001.

[153] F. Mormann, R. Andrzejak, C. Elger, and K. Lehnertz, "Seizure prediction: the long and winding road.," *Brain,* vol. 130, no. Pt 2, pp. 314-33, Feb 2007.